

Dissertation
submitted to the
Combined Faculties for the Natural Sciences
and for Mathematics
of the Ruperto-Carola University of
Heidelberg, Germany
for the degree of
Doctor of Natural Sciences

Put forward by
Oscar Esquivel
born in Mexico City, México
Oral examination: 12. November 2008

Aspects of wave mechanics of gravitating systems

Referees: Prof. Dr. Burkhard Fuchs
Dr. Frank van den Bosch

Abstrakt.

Diese Arbeit erforscht die Jeans Instabilität einer Galaxienscheibe in einem dynamisch reagierenden Dunkle-Materie-Halo. Auf kleinen Skalen wird die Instabilität unterdrückt, wenn der Index Q_T der Toomre Instabilität grösser ist als ein bestimmter Grenzwert, aber auf grösseren Skalen tritt die Jeans Instabilität beständig ein. Trotzdem wurde unter Verwendung eines selbstkonsistenten 'disk-halo' Modell gezeigt, dass dies auf Skalen passiert die grösser als das System selbst sind, so dass es als ein nomineller Effekt betrachtet werden kann. Es folgt eine genaue Berechnung der Kraft der dynamischen Reibung in einer Plummer- oder Hernquist-Sphäre, die sich durch ein unendliches homogenes Sternsystem bewegt. Unter Verwendung einer Methode mechanischer Schwingung, erhalten wir Chandrasekhar's Reibungskraftgesetz mit einem modifizierten Coulomblogarithmus, der von der Form der Störung abhängt. Wir erweitern diese Analyse auf anisotrope Geschwindigkeitsverteilungen der Feldsterne. Wir zeigen leicht verwendbare Formeln der Kräfte der dynamischen Reibung, angewandt auf einen Punkt-massensatellit für den Fall wenn das Geschwindigkeitsellipsoid abgeflacht und gestreckt ist (für verschiedene Werte der effektiven Geschwindigkeitsdispersion σ_{eff}) unter Bestimmung der Anisotropie des Systems.

Abstract.

The Jeans instability of a galactic disk embedded in a dynamically responsive dark-matter halo is investigated in this work. On small scales the instability is suppressed, if the Toomre stability index Q_T is higher than a certain threshold, but on large scales the Jeans instability sets invariably in. However, using a simple self-consistent disk-halo model it is demonstrated that this occurs on scales which are much larger than the system so that this is indeed only a nominal effect. Also, a rigorous calculation of the dynamical friction (DF) force exerted on a Plummer and a Hernquist sphere moving through an infinite homogenous system of field stars is presented. By using a wave-mechanical treatment, we recover Chandrasekhar's drag force law with a modified Coulomb logarithm that depends on the exact shape of the perturber. We then extend this mode analysis to anisotropic velocity distributions of the field stars. We present easy-to-use handy formulae of the DF force exerted on a point-mass satellite for the cases when the velocity ellipsoid is either oblate or prolate for different values of the effective velocity dispersion σ_{eff} determining the anisotropy of the host system.

Contents

1	Introduction	1
2	On the stability of a galactic disk	4
2.1	The role of rotation	5
2.2	On the stability of the shearing sheet	7
3	An astrophysical disk embedded in a responsive dark-matter halo	17
3.1	Response of the halo	18
3.2	Stability of the disk	23
3.3	Discussion and Conclusions	25
4	Dynamical friction	30
4.1	The geometry of the two-body approximation	31
4.2	The net dynamical drag	36
4.3	The Coulomb logarithm.	39
5	Density profiles	40
5.1	The Hernquist profile	41
5.2	The Plummer sphere	44
6	Dynamical friction force exerted on spherical bodies	47
6.1	A wave-mechanical treatment	48
6.2	Potentials of the perturbing bodies	49
6.3	Dynamical friction	52
6.4	Discussion and Conclusions	60
7	The role of an anisotropic velocity distribution in DF	64
7.1	The effective velocity dispersion	65
7.2	The dynamical drag	69
7.2.1	First case: $\sigma_v = \sigma_w \neq \sigma_u$	69
7.2.2	Second case: $\sigma_v \neq \sigma_u = \sigma_w$	71

7.3	Discussion and Conclusions	74
7.4	The role of a <i>missaligned</i> velocity ellipsoid	80
7.4.1	First case: $\sigma_v = \sigma_w \neq \sigma_u$	80
7.4.2	Second case: $\sigma_v \neq \sigma_w = \sigma_u$	84
7.5	Discussion and Conclusions	87
8	Conclusions	98

Chapter 1

Introduction

Since its discovery more than one and a half centuries ago [Ros50], the structure of spiral galaxies has remained to some extent unexplained due mainly to the constant use of oversimplifications held by earlier observers. The diversity among spirals is considerably: there are large lenticular galaxies, normal spirals such as our own Galaxy and M31, and dwarf magellanic-type galaxies, all of which can have a bar or not. The common way of studying how the presence of a sudden perturbation affects the stability of these systems two effects are usually taken into account: the Jeans mass and the phase-space density.

The random velocities of their constituents define the Jeans mass, preventing the collapse of the perturbations on small scales. This means that for the same random velocities, smaller densities must necessarily be correlated to larger Jeans masses. In the other case, models with a higher phase-space density will result in a more compact, denser central region, thus being similar to the effect described by the Jeans mass. The Jeans mass is related to the Jeans length which defines the boundary between the gravitational collapse and the stability of the system. It has been constantly argued that in galactic disks, the Jeans length is usually larger than the radial extent of the disk, making this one safely stable.

On the basis of that argument, the continuing increase of our knowledge about galactic systems and the ingredients that compose them has shaped the way in which the theorists work culminating with the discovery in the 60's of dark matter haloes surrounding these spiral configurations. Since inclusion of the dark-matter component complicates considerably the modeling of astrophysical systems, to this day, most of the study on the stability and dynamical evolution of self-gravitating astrophysical configurations, for instance a galactic disk, has been carried out with the use of numerical cal-

culations.

However, the role a dark-matter halo could have on the stability of the disk had not yet been established on theoretical grounds. Recent numerical simulations hinted at the fact that the halo supports small perturbations in the disk to grow although no analytical study had corroborated this effect. We start our work in chapter 2 by looking through Toomre’s original work [Too64] in detail and establishing the role played by rotation and random motion of the particles in the disk. Using a formal approach, which consists of solving both the collisionless Boltzmann equation that determines the distribution function of the stars in phase space and the Poisson equation which takes into account the self-gravity of the disk, we consider the orbits of the stars in the epicyclic approximation and extend in chapter 3 the current study of the stability of the disk by placing it inside a responsive dark-matter halo.

Also, other dynamical phenomena are important in the evolution of galactic systems. In this context, the process of dynamical friction (DF) is one of the most classical and fundamental problems encountered in the description of the evolution of almost all astrophysical systems. From the critical momentum exchange in a protoplanet-protoplanetary disk set up, passing through the problem of satellites in galaxies to galaxies in large clusters, proper understanding of DF is a prerequisite to more ambitious attempts at constructing physically justified models.

Chandrasekhar’s classical formula of DF [Cha43] has been extensively applied to many different situations with relative success even if as originally derived the formula has a lot of caveats. This treatment considers various oversimplifications of real astrophysical systems such as the inclusion of an infinite homogenous distribution of background stars with an isotropic velocity distribution, and, moreover, the extension of the perturbing body is not considered. In chapter 4 we follow Chandrasekhar’s original work in detail.

With mathematical rigor we calculate in chapter 6 the DF force exerted on several extended bodies following the existing mode analysis developed by Marochnik [Mar68] and Kalnajs [19772]. The collisionless Boltzmann equation is solved self-consistently with the use of Poisson equation. A brief description of the different density profiles is given in chapter 5.

Another concern for the theorists that model the evolution of satellites under the effect of DF is the role played by an anisotropic velocity (and mass) distribution of the host system. In chapter 7 we extend the mode

analysis used in chapter 6 to include an anisotropic velocity distribution of the background particles in the unperturbed distribution function. We show that the contribution from the anisotropic distribution is taken into account by considering an effective velocity dispersion. The precise form of the velocity ellipsoid is determined by the components of the velocity dispersion. Several cases are studied: whether the velocity ellipsoid is prolate or oblate the particle is considered to travel at different angles through the ellipsoid. The value of the force with the inclusion of the anisotropic distribution tends to be bigger than its corresponding value when an isotropic velocity distribution is considered. The conclusions are given in chapter 8.

Chapter 2

On the stability of a galactic disk

As said in chapter one, the complexity of the spiral structure of some galaxies made it evident since the beginning that some *fundamental* equations were necessary in order to deal with both the stellar and gas components. First derived by Maxwell, the first application of the moments of the Boltzmann equation (which can be simply understood as the equation of continuity in phase space) to stellar–dynamical problems is due to Jeans [Jea19]. The suggestion given by him about the stability of such systems failed because he envisaged a galaxy to be a uniformly–rotating, pressure-supported gaseous configuration; in that way oversimplifying the more physical situation of a mixture of gas and stars in which the stability is due to the rotation of both components and/or due to the motion of the stars. However, a major contribution of his study was to give an order of magnitude estimate for the boundary that defines stable from instable regions known as *the Jeans length*

$$\lambda_J \equiv \frac{2\pi}{k_J} = \sqrt{\frac{\pi}{G\rho_0}}\sigma, \quad (2.1)$$

where k_J is the wavelength of the perturbation, G is the gravitational constant, ρ_0 is the density of the system, and σ is the radial velocity dispersion of the stars. In the case of gaseous systems, for example, Eq. (2.1) tells us that a cloud that is smaller than its Jeans length will not have sufficient gravity to overcome the repulsive gas pressure forces and condense to form a star, whereas a cloud that is larger than its Jeans length will collapse. In the context of a differentially–rotating disk of gravitating matter, Toomre [Too64] was the first to point out that Coriolis or centrifugal forces stemming from the disk’s rotation were not on their own sufficient to overcome gravitational collapse due to the presence of a small axisymmetric perturbation and that

is the action of the random motion of its constituent particles that provides the *stabilizing pressure* required for the equilibrium of the system. In order to aim at understanding the evolution of a disk surrounded by a dark-matter halo we need first to pay attention to the work done by Toomre, which we outline in this chapter.

2.1 The role of rotation

In this section we discuss the importance of the inclusion of the random motions of the stars, by first considering rotation as the sole stabilizing effect against a small disturbance. Let us follow then the treatment made by Toomre [Too64] in his work, we consider an infinitely-thin differentially-rotating disk where both centrifugal and gravitational forces are in equilibrium. In the presence of a sudden change in the disk structure, for instance a contraction, Coriolis or centrifugal forces will respond to the small perturbation trying to damp the resulting excess of gravitational attraction. Using polar coordinates (r, θ, z) such the plane $z = 0$ coincides with the midplane of the disk, the line $r = 0$ denotes the disk's axis of rotation, and the direction of rotation is given by θ , we can denote unperturbed quantities for the surface density of the disk as μ_0 , its angular velocity as Ω_0 , its radial extension r_0 , and the potential as $\Phi_0(r, z)$. Then we cast the governing Jeans equations in a corotating frame (following Toomre) for the disturbances of the radial $u_1(r, \theta, z)$ and circumferential $v_1(r, \theta, z)$ velocity components, the surface density $\mu_1(r, \theta, z)$ and potential $\Phi_1(r, \theta, z)$ as

$$\frac{\partial u_1}{\partial t} + \Omega_0 \frac{\partial u_1}{\partial \theta} - 2\Omega_0 v_1 - \frac{\partial \Phi_1}{\partial r} = 0, \quad (2.2)$$

$$\frac{\partial v_1}{\partial t} + \Omega_0 \frac{\partial v_1}{\partial \theta} - 2B u_1 - \frac{1}{r} \frac{\partial \Phi_1}{\partial \theta} = 0, \quad (2.3)$$

$$\frac{\partial \mu_1}{\partial t} + \Omega_0 \frac{\partial \mu_1}{\partial \theta} - \frac{1}{r} \frac{\partial}{\partial r} (r \mu_0 u_1) + \frac{\mu_0}{r} \frac{\partial v_1}{\partial \theta} = 0, \quad (2.4)$$

and

$$\nabla^2 \Phi_1 = -4\pi G \mu_1 \delta(z), \quad (2.5)$$

where B is Oort's second constant

$$B = A - \Omega_0, \quad (2.6)$$

and is related to the first one via

$$A = -\frac{1}{2} r_0 \left(\frac{d\Omega}{dr} \right)_{r_0}. \quad (2.7)$$

The set of Eqs. (2.2), (2.3), (2.4), and (2.5) has been linearized, *i. e.*, second-order terms have been dismissed and Poisson equation for the gravity–mass pair of the disk (2.5) has to fulfill Dirac’s delta function $\delta(z)$. The potential is assumed to be axisymmetric, and so it is its associated perturbation. Non–axisymmetric, spiral–like perturbations have been taken into account in the theoretical study made by Fuchs [Fuc01]. However, to gain insight into the stability on physical grounds it suffices to consider only axisymmetric perturbations. Therefore, we take into account perturbations of the type

$$u_1, v_1, \mu_1 = u_A, v_A, \mu_A \times \exp^{i(kr_0 + \omega t)}, \quad (2.8)$$

where the u_A, v_A, μ_A denote constants and the local wavelength $2\pi/k$ is assumed to be much shorter than the disk extension, *i. e.* $kr_0 \gg 1$. For Poisson’s equation we also have

$$\Phi_1 = \Phi_A \times \exp^{i(kr_0 + \omega t)}, \quad (2.9)$$

while

$$\Delta \Phi_1 = 0, \quad (2.10)$$

must hold for $z \neq 0$; this is achieved by

$$\Phi_1 = \Phi_A \times \exp^{i(kr_0 + \omega t) - |kz|}. \quad (2.11)$$

The next step is to integrate Eq. (2.5) over an interval $(-\epsilon, \epsilon)$ and then to take the limit $\epsilon \rightarrow 0$, thus arriving at

$$\lim_{\epsilon \rightarrow 0} \int_{-\epsilon}^{\epsilon} dz \nabla \Phi_1 = \lim_{\epsilon \rightarrow 0} \left. \frac{\partial \Phi_1}{\partial z} \right|_{-\epsilon}^{\epsilon} = 4\pi G \mu_1, \quad (2.12)$$

but we also have

$$\lim_{\epsilon \rightarrow 0} \left. \frac{\partial \Phi_1}{\partial z} \right|_{-\epsilon}^{\epsilon} = -2|k| \Phi_A \exp^{i(kr_0 + \omega t)}, \quad (2.13)$$

and so the constants Φ_A and μ_A are related to each other through

$$-2|k| \Phi_A = 4\pi G \mu_A. \quad (2.14)$$

Solving for Φ_1 we then get

$$\Phi_1 = -\frac{2\pi G \mu_A}{|k|} \exp^{i(kr_0 + \omega t) - |kz|}, \quad (2.15)$$

and the corresponding force

$$\frac{\partial \Phi_1}{\partial r} = 2\pi G \mu_A \exp^{i(kr_0 + \omega t) - |kz|}. \quad (2.16)$$

Table 2.1: Local parameters of the Milky Way

Σ_d	$38 M_\odot/pc^2$	(Holmberg & Flynn [HF04])
σ_d	40 km/s	(Jahreiß & Wielen [JW97])
κ	$\sqrt{2} \cdot 220$ km/s/8.5 kpc	(flat rotation curve)
λ_{crit}	4.8 kpc	

Putting Eqs. (2.15), (2.16), and (2.8) into Eqs. (2.2), (2.3), (2.4), and (2.5), we get after some algebra the next condition for the local wavenumber k and the oscillatory frequency w ,

$$2\pi G\mu_0 k = \kappa^2 - w^2, \quad (2.17)$$

where κ is the epicyclic frequency

$$\kappa = \sqrt{-4\Omega_0 B}. \quad (2.18)$$

The above dispersion Eq. (2.17) defines a line ($w^2 = 0$) that divides exponentially unstable modes ($w^2 < 0$) which occur when the local wavenumbers exceed a certain critical value

$$k_{\text{crit}} = \frac{\kappa^2}{2\pi G\mu_0}, \quad (2.19)$$

and stable perturbances ($w^2 \geq 0$) which take place otherwise. In effect, for most plausible models for spiral galaxies the critical wavelength associated to Eq. (2.19),

$$\lambda_{\text{crit}} = \frac{2\pi}{k_{\text{crit}}} = \frac{4\pi^2 G\mu}{\kappa^2} \quad (2.20)$$

happens to be of the order of the radial scale length of the system, thus implying that the rotation of the disk cannot alone stabilize the disk against small-scale perturbations. For the sake of the discussion we can calculate this critical wavelength using typical values assigned to our own Milky Way listed in Table 1. Due to this short wave length, rotation could only stabilize the disk of the Milky Way at large scales, giving place recently to ideas pointing the possible role of disks in the formation of massive clusters of stars in our galaxy [EL08]. In the next section we briefly discuss what happens to the stability of a galactic disk when the root-mean-square random velocities of its constituent stars cannot longer be ignored.

2.2 On the stability of the shearing sheet

The treatment developed in Toomre's original paper would have to be modified was it to be applied to stellar disks whose thicknesses are not negli-

gible, which is the case of isolated galaxies whose scale-lengths are considerably bigger than those of spiral galaxies [FCT08, and references therein], although from a practical point of view, the basic argument that it is the inclusion of the *random* motion of the stars which stabilizes the system remains applicable [ZMKS08]. Moreover, the simpler theory of a self-gravitating, infinitely-thin shearing sheet has successfully reproduced the dynamical evolution of a galactic-disk system, accounting for the spiral arms ([Fuc04]; [GL65]; [JT66]), and we continue here under its assumptions.

The trajectories of the particles in the disk will be derived from the constraint imposed by the Lagrangian

$$L = \frac{1}{2}(\dot{r}^2 + r\dot{\theta}^2) - \Phi(r, \theta, z), \quad (2.21)$$

where $\Phi(r, \theta, z)$ denotes the disk's gravitational potential. In this scenario (see Fig. 2.1) polar coordinates can safely be rectified to pseudo-Cartesian coordinates and the differential rotation is accounted for by a linear shear flow. Therefore for spatial coordinates (x, y) defined by

$$x = r - r_0 \quad \text{and} \quad y = r_0(\theta - \Omega_0 t), \quad (2.22)$$

where r_0 is the distance between the center of the disk and the center of the patch, y points in the direction of rotation and the mean angular velocity of the patch around the galactic center is

$$\Omega_0 = \left[\frac{1}{r_0} \left(\frac{d\Phi}{dr} \right)_{r_0} \right]^{\frac{1}{2}}, \quad (2.23)$$

we can make use of the epicyclic approximation [Lin59], which considers that the radius of the epicyclic orbits is perturbed. This remains a valid approach as long as the amplitude of the radial oscillation is small compared with the mean radius, *i. e.*

$$|x| \ll r_0 \quad \text{and} \quad |\dot{x}|, |\dot{y}| \ll \Omega_0 r_0. \quad (2.24)$$

We can then make a Taylor expansion of Eq. (2.21) around x ; thus obtaining

$$\begin{aligned} L \approx \frac{1}{2}(\dot{x}^2 + (r_0^2 + 2r_0x + x^2)(\Omega_0^2 + 2\Omega_0\frac{\dot{y}}{r_0} + \frac{\dot{y}^2}{r_0^2})) \\ - \Phi(r_0) - \Phi(r_0)'x - \frac{1}{2}\Phi(r_0)''x^2. \end{aligned} \quad (2.25)$$

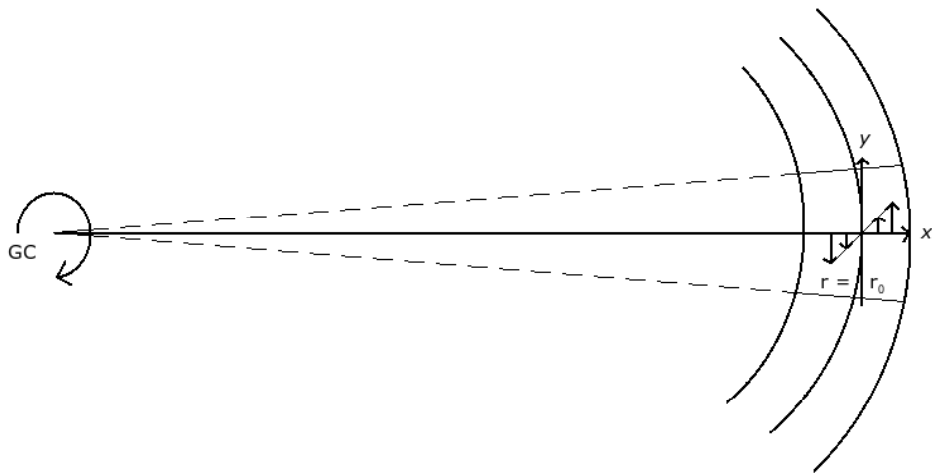


Figure 2.1: A patch of a galactic disk in the shearing sheet model. Due to the small dimension of the region considered the uniform shear can be approximated by considering rectangular coordinates in the Eulerian frame of reference.

We can also rearrange terms by considering appropriate substitutions

$$\Phi(r_0)' = r_0\Omega_0^2 \quad \text{and} \quad \Phi(r_0)''x = \Omega_0^2 - 4AB, \quad (2.26)$$

where we have made use of Oort's constants (Eqs. (2.6), (2.7)). The final version of the Lagrangian will have the form

$$L = \frac{1}{2}[r_0^2\Omega_0^2 - \Phi(r_0) + \dot{x}^2 + \dot{y}^2 + 4\Omega_0x\dot{y} + 4A\Omega_0x^2]. \quad (2.27)$$

The first-order equations of motion can thus be derived by substituting expression (2.27) into the Euler-Lagrange equation, in this way getting

$$\ddot{x} = 2\Omega_0\dot{y} + 4A\Omega_0x \quad (2.28)$$

$$\ddot{y} = -2\Omega_0\dot{x}. \quad (2.29)$$

In epicyclic theory, it is customary to accept solutions of the form $x, y = x, y(\Omega, \kappa, \cos(\kappa t), \sin(\kappa t))$ ([FFT79]; [Van75]), where κ is the epicyclic frequency (Eq. (2.18)) and the trigonometric terms describe the oscillation of disk stars around the mean motion with frequency κ . Therefore, for spatial coordinates (x, y) there are corresponding velocity components (u, v) , respectively given by

$$u = \dot{x} \quad \text{and} \quad v = \dot{y} + 2Ax. \quad (2.30)$$

The Hamiltonian of the system can readily be obtained from the Lagrangian (Eq. (2.27)) via

$$H = \dot{x}p_x + \dot{y}p_y - L, \quad (2.31)$$

to be expressed as

$$H = \frac{1}{2} \left(u^2 + \frac{\kappa^2}{4B^2} v^2 \right) + \frac{A}{2B} (p_y - \Omega_0 r_0)^2 - \frac{1}{2} \Omega_0 r_0^2. \quad (2.32)$$

It is advantageous to consider from now on action variables, defined as

$$J_1 = \frac{1}{2\pi} \oint p_x dx = \frac{1}{2\kappa} \left(u^2 + \frac{\kappa^2}{4B^2} v^2 \right) \quad (2.33)$$

and

$$J_2 = \frac{1}{2\pi} \oint p_y dy = \frac{\partial L}{\partial \dot{y}} = \Omega_0 r_0 + 2\Omega_0 x + \dot{y}. \quad (2.34)$$

Since the actual motion is not involved in this integration, these generalized momenta are constants of motion, the first being the radial action and the

second associated to the angular momentum. The Hamiltonian takes now the form

$$H = \kappa J_1 + \frac{A}{2B}(J_2 - \Omega_0 r_0)^2 - \frac{1}{2}\Omega_0^2 r_0^2. \quad (2.35)$$

To the momenta J_1, J_2 correspond conjugate generalized coordinates w_1, w_2 , named ‘‘angle–coordinates’’, whose dynamics is dictated by Hamilton’s equations

$$\dot{w}_1 = \frac{\partial H}{\partial J_1} = \frac{\kappa J_1}{J_1} = \kappa = \Omega_1 \quad (2.36)$$

and

$$\dot{w}_2 = \frac{\partial H}{\partial J_2} = \frac{A}{B}(J_2 - \Omega_0 r_0). \quad (2.37)$$

Equations (2.29) can then be solved in terms of angle-action coordinates

$$x = \frac{J_2 - \Omega_0 r_0}{-2B} + \sqrt{\frac{2J_1}{\kappa}} \sin w_1, \quad (2.38)$$

$$y = w_2 - \frac{\sqrt{2\kappa J_1}}{2B} \cos w_2 \quad (2.39)$$

Their associated velocity variables read

$$u = \sqrt{2\kappa J_1} \cos w_1, \quad (2.40)$$

$$v = \frac{2B}{\kappa} \sqrt{2\kappa J_1} \sin w_1. \quad (2.41)$$

We are now in the position to carry out a linear perturbation analysis to study the stability of a disk whose Hamiltonian is assumed to be composed of an axisymmetric part H_0 , and a small axisymmetric perturbation Φ_1 . The governing equation describing the dynamical response of the ensemble of disk stars, having an unperturbed distribution function f_0 , due to a small perturbation f_1 in the distribution function is the Boltzmann equation, which has the general form

$$\frac{\partial f}{\partial t} + [f, H] = 0, \quad (2.42)$$

where the square brackets are the Poisson brackets expressed as

$$[f, H] = \frac{\partial f}{\partial w_1} \frac{\partial H}{\partial J_1} + \frac{\partial f}{\partial w_2} \frac{\partial H}{\partial J_2}, \quad (2.43)$$

because terms $\partial H/\partial w_1$ and $\partial H/\partial w_2$ are zero due to the form of Eq.(2.35). The choice of a small perturbation f_1 could seem to be an imposed oversimplification in this treatment, however, spiral arms are most of the time

considered to be only minor disturbances of galactic disks. Eq. (2.42) can be cast in the form of

$$\frac{\partial f_0}{\partial t} + \frac{\partial f_1}{\partial t} + [f_0, H_0] + [f_0, \Phi_1] + [f_1, H_0] = 0. \quad (2.44)$$

Since we are interested in the linear evolution of the system in the presence of a perturbation, we can dispose of second-order terms, retaining only a linearized Boltzmann equation

$$\frac{\partial f_1}{\partial t} + [f_0, \Phi_1] + [f_1, H_0] = 0. \quad (2.45)$$

Assuming that the velocity dispersion is relatively small, we next consider an unperturbed Maxwellian distribution for the disk particles

$$f_0 = \frac{-\kappa}{B} \frac{\Sigma_0}{4\pi\sigma^2} \exp\left(\frac{\kappa}{\sigma^2} J_1\right), \quad (2.46)$$

where σ_u^2 denotes the radial velocity dispersion and is related to the circumferential velocity dispersion through

$$\frac{\sigma_v}{\sigma_u} = 4 \frac{B^2}{\kappa^2} \quad (2.47)$$

Because the equations are easier to handle, we transform quantities to Fourier space with respect to the spatial coordinates. The Fourier transform of the potential perturbation is

$$\Phi_{1,\mathbf{k}} = \Phi_{\mathbf{k}} \exp ik_x x. \quad (2.48)$$

The Poisson brackets are then found to be

$$[f_0, \Phi_1] = \frac{\sqrt{2\kappa J_1}}{\sigma_u^2} (ik_x \cos w_1) f_0 \Phi_{1,\mathbf{k}} \quad (2.49)$$

and

$$[f_1, H_0] = \kappa \frac{\partial f_1}{\partial w_1}, \quad (2.50)$$

leading to the linearized Boltzmann equation

$$\frac{\partial f_1}{\partial t} + \frac{\sqrt{2\kappa J_1}}{\sigma_u^2} (ik_x \cos w_1) f_0 \Phi_1 + \kappa \frac{\partial f_1}{\partial w_1} = 0 \quad (2.51)$$

To analyse the behavior of time-dependent disturbances we consider a perturbation of the type

$$f_1(u, v, t) = f_0(u, v) \delta f(u, v) \exp(\omega t), \quad (2.52)$$

where we have introduced a function $\delta f(u, v)$ which comes in handy since we can then split off the unperturbed function f_0 and momentarily deal with the part of the Boltzmann Eq. (2.51) that looks like

$$i\omega\delta f_\omega + \kappa \frac{d\delta f_\omega}{dw_1} + \frac{\sqrt{2\kappa J_1}}{\sigma_u^2} (ik_x \cos w_1) \Phi_{\mathbf{k},\omega} \\ \times \exp \left[ik_x \left(\frac{J_2 - \Omega_0 r_0}{-2B} + \sqrt{\frac{2J_1}{\kappa}} \sin w_1 \right) \right] = 0. \quad (2.53)$$

The standard way of getting a general solution to Eq. (2.53) is to consider first particular solutions that are basically solutions of the homogeneous part of this equation multiplied by a constant C that depends upon the angle variable w_1 , *i. e.* solutions of the form

$$\delta f_\omega = C(w_1) \exp -i \left(\frac{\omega}{\kappa} w_1 \right). \quad (2.54)$$

It is straight forward to find the explicit form of the constant $C(w_1)$ by putting Eq. (2.54) into Boltzmann's equation (2.53),

$$C(w_1) = \frac{i}{\sigma_u^2} \sqrt{\frac{2J_1}{\kappa}} k_x \exp \left(ik_x \frac{J_2 - \Omega_0 r_0}{-2B} \right) \Phi_{\mathbf{k},\omega} \\ \times \int_0^{w_1} dw'_1 \cos w'_1 \exp i \left(\sqrt{\frac{2J_1}{\kappa}} k_x \sin w'_1 + \frac{\omega}{\kappa} w'_1 \right) \quad (2.55)$$

Then the general solution to Eq. (2.53) is found by the sum of the particular solution (Eq. (2.54)) and a solution that is also composed of the solution to the homogeneous part of Eq. (2.53) but multiplied by an integration constant D ,

$$\delta f_\omega = \frac{\Phi_{\mathbf{k},\omega}}{\sigma_u^2} \exp \left(ik_x \frac{J_2 - \Omega_0 r_0}{-2B} \right) \left[D - i \sqrt{\frac{2J_1}{\kappa}} k_x \int_0^{w_1} dw'_1 \cos w'_1 \right. \\ \left. \times \exp i \left(\sqrt{\frac{2J_1}{\kappa}} k_x \sin w'_1 + \frac{\omega}{\kappa} w'_1 \right) \right] \exp -i \left(\frac{\omega}{\kappa} w_1 \right) \quad (2.56)$$

To determine this last constant D , we apply the condition of periodicity,

$$\delta f_\omega(w_1) = f_\omega(w_1 + 2\pi), \quad (2.57)$$

and consider the integral in $f_\omega(w_1 + 2\pi)$ in its alternative form given by the right-hand side of the identity

$$\int_0^{w_1+2\pi} = \int_0^{2\pi} + \int_{2\pi}^{w_1+2\pi}. \quad (2.58)$$

Then by taken appropriate substitutions and solving for D we find

$$D = -\frac{1}{\sqrt{2\kappa J_1}} \frac{\exp -i(\pi\omega/\kappa)}{2i \sin(\pi\omega/\kappa)} [(\exp(2\pi\omega/\kappa) - 1) - i \frac{\omega}{\kappa} \int_0^{2\pi} dw'_1 \exp \left(\sqrt{\frac{2J_1}{\kappa}} \sin w'_1 + \frac{\omega}{\kappa} w'_1 \right)] \quad (2.59)$$

By inserting this expression into Eq. (2.56) and after doing some algebra we arrive at the final result

$$\delta f_\omega = -\frac{\Phi_{\mathbf{k},\omega}}{\sigma_u^2} \exp \left(ik_x \frac{J_2 - \Omega_0 r_0}{-2B} \right) \exp i \left(\sqrt{\frac{2J_1}{\kappa}} k_x \sin w_1 \right) \left[1 - \frac{\omega/\kappa}{2 \sin(\pi\omega/\kappa)} \times \int_{-\pi}^{+\pi} dw'_1 \exp i \left(\frac{\omega}{\kappa} w'_1 - \sqrt{\frac{2J_1}{\kappa}} k_x \sin w'_1 \cos w_1 - \sqrt{\frac{2J_1}{\kappa}} k_x (1 + \cos w'_1) \sin w_1 \right) \right] \quad (2.60)$$

Now, looking again for vanishing (neutral) disturbances $\omega = 0$, we get the perturbed density distribution f_1 by putting Eq. (2.60) into Eq. (2.52)

$$f_1 = \frac{\Sigma_0}{-B} \frac{\Phi_1 \kappa}{4\pi \sigma_u^4} \exp - \left(\frac{\kappa J_1}{\sigma_u^2} \right) \exp ik_x \left(\frac{J_2 - \Omega_0 r_0}{-2B} - \sqrt{\frac{2J_1}{\kappa}} \sin w_1 \right) \times \left[1 - \frac{1}{2\pi} \int_{-\pi}^{+\pi} dw'_1 \exp -i \left(\sqrt{\frac{2J_1}{\kappa}} k_x \{ \sin w'_1 \cos w_1 + (1 + \cos w'_1) \sin w_1 \} \right) \right] \quad (2.61)$$

where we have taken the explicit form of the equilibrium distribution function f_0 (Eq. (2.46)) and used the limit of $(\omega/\kappa)/\sin(\pi\omega/\kappa) = 1/\pi$ as $\omega \rightarrow 0$. The trigonometric terms that appear in the exponential function inside the square brackets can be rearranged and we consider the Bessel function of the first kind in its integral form

$$\frac{1}{2\pi} \int_{-\pi}^{+\pi} dw'_1 \exp -i \left(\sqrt{\frac{2J_1}{\kappa}} k_x \sin(w'_1 + w_1) \right) = J \left(\sqrt{\frac{2J_1}{\kappa}} k_x \right) \quad (2.62)$$

In order to calculate the disk response to the perturbation given by Eq. (2.61) we return to (x,y,u,v) coordinates via Eqs. (2.39), (2.41), and integrate over (u,v)

$$\Sigma_1 = -2B \int_0^\infty dJ_1 \int_0^{2\pi} dw_1 f_1, \quad (2.63)$$

noting that $dudv = -2BdJ_1dw_1$. Integration over dw_1 follows in a straightforward manner, and with the use of Eq. (2.62) we can express the disk

response as

$$\Sigma_1 = -\kappa \frac{\Sigma_0}{\sigma_u^4} \Phi_1 e^{(i\omega t + k_x x)} \int_0^\infty dJ_1 \exp -i \left(\sqrt{\frac{\kappa J_1}{\sigma_u^2}} \right) \left[1 - J_0^2 \left(\sqrt{\frac{2J_1}{\kappa}} k_x \right) \right] \quad (2.64)$$

The first of the two integrals over dJ_1 is trivial; the second is recognized with the help of a list of integrals to be a modified Bessel function of first kind I_0 , and so the final expression for the disk response will read

$$\Sigma_1 = -\frac{\Sigma_0}{\sigma_u^2} \Phi_1 e^{k_x x} \left[1 - I_0 \left(\frac{\sigma_u^2}{\kappa^2} k_x^2 \right) \right]. \quad (2.65)$$

The radial perturbation of the potential has a simple form (cf. Eq. (2.15))

$$\Phi_1 = -\frac{2\pi G \mu_A}{k_x} \exp^{i(k_x x + \omega t)}, \quad (2.66)$$

which we introduce into Eq. (2.65) with the condition $\omega \rightarrow 0$. Following Toomre we express the result as

$$\frac{|k_x| \sigma_u^2}{2\pi G \Sigma_0} = 1 - \exp \left(-\frac{\sigma_u^2}{\kappa^2} k_x^2 \right) I_0 \left(\frac{\sigma_u^2}{\kappa^2} k_x^2 \right). \quad (2.67)$$

It is easy to see that we recover Eq. (2.19) by considering $\sigma_u \rightarrow 0$ while keeping both k_x and κ finite. In the other limiting case, that is to say when $(\sigma_u^2 k_x^2 / \kappa^2)$ tends to infinity, Eq. (2.67) will be approximated by

$$k_x \approx \frac{2\pi G \Sigma_0}{\sigma_u^2}, \quad (2.68)$$

We illustrate the behaviour of Eq. (2.67) for the complete range of wavelengths in terms of its critical value λ_{crit} (Eq. (2.20)) in Fig. (2.2). Figure (2.2) shows the neutral stability curve which divides the region where the perturbances will remain *bounded* at all times and the *unbounded* region. It is worth-mentioning however, that the perturbations will not exponentially with time if the root-mean-square radial velocities of the disk stars exceed

$$\sigma_{u,\text{min}} = \sqrt{0.2857} \frac{\kappa}{\alpha_{\text{crit}}}, \quad (2.69)$$

where $\alpha_{\text{crit}} = 1/\lambda_{\text{crit}}$.

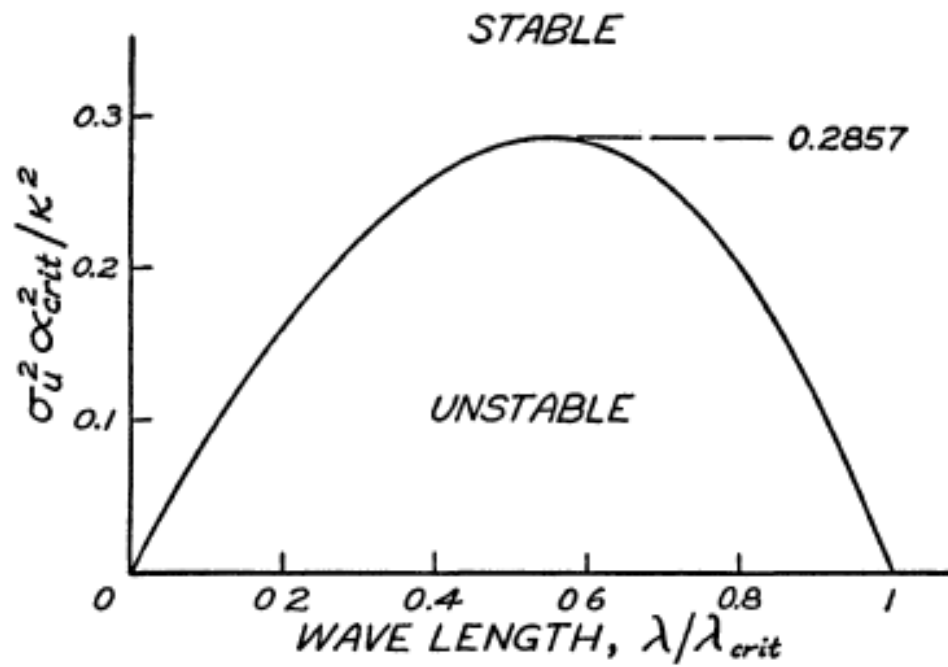


Figure 2.2: Figure 5 of [Too64] showing the neutral stability curve which divides the region where the perturbances will remain *bounded* at all times and the *unbounded* region.

Chapter 3

An astrophysical disk embedded in a responsive dark-matter halo

Instabilities of gravity perturbations, such as those produced by a spontaneous disturbance, seriously affect the evolution of astrophysical disks. While being an unsolved problem still, the formation of protoplanets might be due to rapidly disk instabilities, where formation of clumps of gas in a marginally gravitationally-unstable disk leads to contraction to planetary densities ([Bos97]; [Bos03]). Also, the classical Jeans instability of gravity perturbations is present in a local treatment of the kinetic stability of a gaseous disk that describes the fine-scale spiral structure present in Saturn's rings ([GG03]; [PS91]), and unstable modes may be crucial in driving mass accretion onto central massive black holes [Too77]. Contrary to gravitationally unstable scenarios which appear to successfully reproduce some of the above mentioned situations, it is the dynamical response of a dark-matter halo that is of crucial importance for the stability of a galactic disk in order to match the local disk properties. This latter case has been modeled with the use of numerical calculations in a number of situations starting with the pionnering work of [OP73] where a non-axisymmetric perturbation (a bar) was damped by the inclusion of the halo's gravitational potential. However, Athanassoula showed that due to the exchange of angular momentum within the system it is the bar that grows stronger if it is embedded in a responsive rather than a static halo potential ([Ath03]; [Ath02]).

More recently, more elaborated models have emerged considering not only the stellar but also the gaseous-disk component, both within the framework of classical Newtonian dynamics (CND) and modified Newtonian dynamics [MOND, cf. TC08], and references therein), with basically the same result

that the bar grows stronger in the presence of a dark-halo in the case of CND. On the other hand, scarce improvement on the subject has been made analytically and one can highlight the work of Fuchs ([Fuc04];[FA05]) which verifies the above-mentioned results.

In this chapter we study the dynamical stability of a self-gravitating disk surrounded by a responsive dark-matter halo by extending the work done by Toomre for a stellar disk described in the previous chapter and by considering the formalism derived by Fuchs [Fuc04] who investigated the interaction of the shearing sheet with a live dark halo. We describe in detail the work done in [EF07b].

3.1 Response of the halo

In this section we follow the analysis that is strictly due to Fuchs [Fuc04], but we apply it to the simpler case of a radial perturbation in the disk. In this scenario, the changes of the distribution function of disk-halo particles in phase space will be dictated by a linearized Boltzmann equation that has a general form

$$\frac{\partial f_1}{\partial t} + \sum_{i=1}^3 v_i \frac{\partial f_1}{\partial x_i} - \frac{\partial \Phi_0}{\partial x_i} \frac{\partial f_1}{\partial v_i} - \frac{\partial \Phi_1}{\partial x_i} \frac{\partial f_0}{\partial v_i} = 0, \quad (3.1)$$

where the sum is considered over spatial coordinates (x,y,z) and their corresponding velocity components (u,v,w) with v lying along the direction of galactic rotation. This time the terms denoting the unperturbed potential Φ_0 and the zeroth-order distribution function of the system f_0 in Eq. (3.1), as well as their respective associated perturbed terms f_1 , Φ_1 will comprise both the disk and the halo contributions

$$f_0 = f_{d0} + f_{h0}, f_1 = f_{d1} + f_{h1}, \Phi_0 = \Phi_{d0} + \Phi_{h0} \text{ and } \Phi_1 = \Phi_{d1} + \Phi_{h1}. \quad (3.2)$$

We can immediately neglect the force terms $-\partial \Phi_{d0}/\partial x$, $-\partial \Phi_{h0}/\partial x$ since we are assuming a homogeneous background of particles. In the context of the shearing sheet particles follow straight-line orbits. Due to the fact that Eq. (3.1) is a linear partial differential equation, we can analyse the evolution, for the moment, of the distribution of the disk stars and the halo particles separately. We start by writing explicitly the Boltzmann equation for the

halo particles

$$\begin{aligned} & \frac{\partial f_{h1}}{\partial t} + u \frac{\partial f_{h1}}{\partial x} + v \frac{\partial f_{h1}}{\partial y} + \\ & w \frac{\partial f_{h1}}{\partial z} - \frac{\partial(\Phi_{d1} + \Phi_{h1})}{\partial x} \frac{\partial f_{h0}}{\partial u} - \\ & \frac{\partial(\Phi_{d1} + \Phi_{h1})}{\partial y} \frac{\partial f_{h0}}{\partial v} - \frac{\partial(\Phi_{d1} + \Phi_{h1})}{\partial z} \frac{\partial f_{h0}}{\partial w} = 0, \end{aligned} \quad (3.3)$$

and recognizing that the part of it that describes the halo response to a perturbation in the halo

$$\begin{aligned} & \frac{\partial f_{h1}}{\partial t} + u \frac{\partial f_{h1}}{\partial x} + v \frac{\partial f_{h1}}{\partial y} + w \frac{\partial f_{h1}}{\partial z} \\ & - \frac{\partial \Phi_{h1}}{\partial x} \frac{\partial f_{h0}}{\partial u} - \frac{\partial \Phi_{h1}}{\partial y} \frac{\partial f_{h0}}{\partial v} - \frac{\partial \Phi_{h1}}{\partial z} \frac{\partial f_{h0}}{\partial w} = 0, \end{aligned} \quad (3.4)$$

just describes the Jeans collapse of the halo as was pointed out by Fuchs ([Fuc04]). The instability regime sets in for wave-lengths larger than the Jeans length (Eq. (2.1)), however, typical values for dark-matter haloes assign them large Jeans lengths, of the order of their extension, thus making this result of little importance for the dynamics of the system under consideration and we disregard it. We now move to the part of Eq. (3.3) that includes the halo response to a perturbation in the disk,

$$\begin{aligned} & \frac{\partial f_{h1}}{\partial t} + u \frac{\partial f_{h1}}{\partial x} + v \frac{\partial f_{h1}}{\partial y} + w \frac{\partial f_{h1}}{\partial z} \\ & - \frac{\partial \Phi_{d1}}{\partial x} \frac{\partial f_{h0}}{\partial u} - \frac{\partial \Phi_{d1}}{\partial y} \frac{\partial f_{h0}}{\partial v} - \frac{\partial \Phi_{d1}}{\partial z} \frac{\partial f_{h0}}{\partial w} = 0. \end{aligned} \quad (3.5)$$

Similarly as in section (2.1), a radial perturbation for the disk potential (cf. Eq. (2.9)) is Fourier transform

$$\begin{aligned} \Phi_{d1} &= \int_{-\infty}^{+\infty} dx \Phi_{d\omega, \mathbf{k}_x} \exp [i(k_x x + \omega t) - |k_x z|] \\ &= \int_{-\infty}^{+\infty} dx \int_{-\infty}^{+\infty} dz \Phi_{d\omega, \mathbf{k}} \exp [i(k_x x + \omega t) + k_z z]. \end{aligned} \quad (3.6)$$

To find the *full* perturbed Fourier component $\Phi_{d\omega, \mathbf{k}}$ in terms of the disk component $\Phi_{d\omega, \mathbf{k}_x}$, Fourier coefficients are considered

$$\Phi_{d\omega, \mathbf{k}} = \frac{1}{2\pi} \int_{-\infty}^{+\infty} dz \Phi_{d\omega, \mathbf{k}_x} \exp -[i(k_z z + \omega t) - |k_x z|] = \frac{1}{\pi} \frac{k_x}{k_x^2 + k_z^2} \Phi_{d\omega, \mathbf{k}_x}. \quad (3.7)$$

The perturbation of the distribution function is also Fourier transformed

$$f_{h1} = \int_{-\infty}^{+\infty} d^3k f_{h\omega,\mathbf{k}} \exp i[(\mathbf{k}, \mathbf{x}) + \omega t]. \quad (3.8)$$

A major step in finding a solution to the Boltzmann equation is taken by introducing orthogonal coordinates (ξ, η, ζ) and aligning ξ with the wave vector \mathbf{k} . This will considerably ease the calculations at no loss of generality. Eqs. (3.7), (3.8) will have a dependence on the term $e^{ik\xi}$ and Eq. (3.5) will have the form

$$i\omega f_{h\omega,\mathbf{k}} + vik f_{h\omega,\mathbf{k}} - ik\Phi_{d\omega,\mathbf{k}} \frac{\partial f_{h0}}{\partial v} = 0, \quad (3.9)$$

where v is the velocity component parallel to the ξ -axis. Eq. (3.9) has been integrated over the velocity components perpendicular to v . Adopting Gaussian distribution function for the sea particles,

$$f_{h0} = \frac{\rho_b}{\sqrt{2\pi}\sigma_h} \exp -\frac{v^2}{2\sigma_h^2}, \quad (3.10)$$

where σ_h^2 denotes the velocity dispersion of the halo particles and ρ_b their matter density, we can solve Eq. (3.9),

$$f_{h\omega,\mathbf{k}} = -k\Phi_{d\omega,\mathbf{k}} \frac{v}{\sigma_h^2} \frac{e^{i\omega t}}{\omega + kv} \frac{\rho_b}{\sqrt{2\pi}\sigma_h} \exp -\frac{v^2}{2\sigma_h^2}. \quad (3.11)$$

The Fourier term of the density perturbation is just obtained from Eq. (3.11) by integrating over v -space,

$$\rho_{h\omega,\mathbf{k}} = -\Phi_{d\omega,\mathbf{k}} \frac{\rho_b}{\sqrt{2\pi}\sigma_h^3} e^{i\omega t} \int_{-\infty}^{+\infty} dv \frac{v \exp -\frac{v^2}{2\sigma_h^2}}{\frac{\omega}{k} + v}. \quad (3.12)$$

From now on we split off the term $e^{i\omega t}$ for practical reasons. To be self-consistent, Eq. (3.12) must obey Poisson's equation

$$\nabla^2 \Phi_1 = -4\pi G \rho_1, \quad (3.13)$$

whose representation in Fourier terms is

$$k^2 \Phi_{h\omega,\mathbf{k}} = 4\pi G \rho_{h\omega,\mathbf{k}}. \quad (3.14)$$

Finally, we are able to explicitly relate the response of the halo due to perturbances in the disk; inserting Eq. (3.12) into Eq. (3.14) gives

$$\Phi_{h\omega,\mathbf{k}} = \Phi_{d\omega,\mathbf{k}} \frac{4\pi G \rho_b}{\sqrt{2\pi}\sigma_h^3} \frac{1}{k^2} \int_{-\infty}^{+\infty} dv \frac{v \exp -\frac{v^2}{2\sigma_h^2}}{\frac{\omega}{k} + v}. \quad (3.15)$$

This equation has a singularity at $v = \omega/k$, and the usual technique of Landau's "rule around the poles" is applied in order to circumvent this apparent break-down of the formula. The basic idea is to extend the integral to the imaginary plane to be able to get the contribution of the pole [cf. Keg98]. But first we calculate the real part of Eq. (3.15) by evaluating the principal value integral that will give the contribution of the **non-resonant** particles

$$\begin{aligned} I &= \text{P} \int_{-\infty}^{+\infty} dv \frac{v}{\frac{\omega}{k} + v} \exp -\frac{v^2}{2\sigma_h^2} \\ &= \sqrt{2}\sigma_h \int_{-\infty}^{+\infty} d\eta \frac{\eta}{\eta - \eta_0} \exp -\eta^2, \end{aligned} \quad (3.16)$$

where $\eta = v/\sqrt{2}\sigma_h$ and $\eta_0 = -\omega/k$. Now with the substitution $\xi = \eta - \eta_0$, the integral can be easily calculated by integrating by parts

$$\begin{aligned} &\text{P} \int_{-\infty}^{+\infty} d\xi \frac{\xi + \eta_0}{\xi} \exp -(\xi + \eta_0)^2 \\ &= \sqrt{2\pi}\sigma_h \left[1 + \frac{\eta_0}{\sqrt{\pi}} \text{P} \int_{-\infty}^{+\infty} d\xi \frac{\exp -(\xi^2 + 2\xi\eta_0 + \eta_0^2)}{\xi} \right], \end{aligned} \quad (3.17)$$

where we have employed $\int_{-\infty}^{+\infty} d\xi e^{-(\xi+\eta_0)^2} = \sqrt{\pi}$. Next we observe that

$$\begin{aligned} &e^{-\eta_0^2} \text{P} \int_{-\infty}^{+\infty} d\xi (\cosh 2\eta_0\xi - \sinh 2\eta_0\xi) \frac{e^{-\xi^2}}{\xi} \\ &= -e^{-\eta_0^2} \text{P} \int_{-\infty}^{+\infty} 2 \int_0^{\eta_0} \cosh 2x\xi e^{-\xi^2} d\xi, \end{aligned} \quad (3.18)$$

and use formula (3.546) of [GR00] we perform the integral over ξ

$$\int_{-\infty}^{+\infty} d\xi \cosh 2x\xi e^{-\xi^2} d\xi = \sqrt{\pi} e^{x^2}. \quad (3.19)$$

The perform the integral over x

$$\int_0^{\eta_0} e^{x^2} = e^{\eta_0^2} F(\eta_0) = i\sqrt{\pi}(1 - \text{erfc}(-i\eta_0)) = -i\sqrt{\pi}\text{erf}(\eta_0). \quad (3.20)$$

So we finally find the contribution of the principal value of Eq. (3.15)

$$\Phi_{h\omega, \mathbf{k}}^{nr} = \Phi_{d\omega, \mathbf{k}} \frac{4\pi G \rho_b}{\sigma_h^2} \frac{1}{k^2} \left[1 - i\sqrt{\frac{\pi}{2}} \frac{\omega}{k\sigma_h} \text{erf} \left(\frac{-i\omega}{\sqrt{2}k\sigma_h} \right) \exp \left(\frac{-\omega^2}{2k^2\sigma_h^2} \right) \right]. \quad (3.21)$$

Following Kegel [Keg98], Landau's rule ($\eta_0 = -\omega_r/k - i\omega_i/k$, with $\omega_i < 0$, $\eta_{0i} > 0$, $t_i < 0$) will give the extra term (cf. Eq. (3.17))

$$\sqrt{2\pi}\sigma_h \left[1 + \frac{\eta_0}{\sqrt{\pi}} \text{P} \int_{-\infty}^{+\infty} d\xi \frac{\exp -(\xi^2 + 2\xi\eta_0 + \eta_0^2)}{\xi} + \frac{\eta_0}{\sqrt{\pi}} e^{-\eta_0^2} i\pi \right]. \quad (3.22)$$

And so for the particles in resonance in Eq. (3.15) we have

$$\Phi_{h\omega, \mathbf{k}}^{res} = \Phi_{d\omega, \mathbf{k}} \frac{4\pi G \rho_b}{\sigma_h^2} \frac{1}{k^2} \left[1 - i\sqrt{\frac{\pi}{2}} \frac{\omega}{k\sigma_h} \exp\left(\frac{-\omega^2}{2k^2\sigma_h^2}\right) \right]. \quad (3.23)$$

By comparison we see that this last equation does not contain the error function due to extra term $e^{-\eta_0^2}$ in Eq. (3.22) which makes vanish the error function in Eq. (3.20).

Now we can calculate the disk response by solving the part of Boltzmann Eq. (3.3)

$$\begin{aligned} & \frac{\partial f_{d1}}{\partial t} + u \frac{\partial f_{d1}}{\partial x} + v \frac{\partial f_{d1}}{\partial y} \\ & + w \frac{\partial f_{d1}}{\partial z} - \frac{\partial(\Phi_{d1} + \Phi_{h1})}{\partial x} \frac{\partial f_{d0}}{\partial u} \\ & - \frac{\partial(\Phi_{d1} + \Phi_{h1})}{\partial y} \frac{\partial f_{d0}}{\partial v} - \frac{\partial(\Phi_{d1} + \Phi_{h1})}{\partial z} \frac{\partial f_{d0}}{\partial w} = 0. \end{aligned} \quad (3.24)$$

Due to the fact that for the distribution function of disk stars there is a delta-function dependence on the vertical components (z, w), we can integrate Eq. (3.24) with respect to them, leaving a Boltzmann equation for the midplane ($z = 0$),

$$\begin{aligned} & \frac{\partial f_{d1}}{\partial t} + u \frac{\partial f_{d1}}{\partial x} + v \frac{\partial f_{d1}}{\partial y} \\ & - \frac{\partial(\Phi_{d1} + \Phi_{h1})}{\partial x} \frac{\partial f_{d0}}{\partial u} \\ & - \frac{\partial(\Phi_{d1} + \Phi_{h1})}{\partial y} \frac{\partial f_{d0}}{\partial v} \\ & = 0. \end{aligned} \quad (3.25)$$

Eqs. (3.24),(3.25) have also to be considered at the midplane, so we bring

them in the form

$$\begin{aligned}\Phi_{h\omega, \mathbf{k}_x}^{nr}(z=0) &= \int_{-\infty}^{+\infty} dk_z \frac{k_x}{(k_x^2 + k_z^2)^2} \Phi_{d\omega, \mathbf{k}_x} \frac{4G\rho_b}{\sigma_h^2} \frac{1}{k^2} \\ &\times \left[1 - i\sqrt{\frac{\pi}{2}} \frac{\omega}{k\sigma_h} \operatorname{erf}\left(\frac{-i\omega}{\sqrt{2}k\sigma_h}\right) \exp\left(\frac{-\omega^2}{2k^2\sigma_h^2}\right) \right],\end{aligned}\quad (3.26)$$

and

$$\begin{aligned}\Phi_{h\omega, \mathbf{k}_x}^{res}(z=0) &= - \int_{-\infty}^{+\infty} dk_z \frac{k_x}{(k_x^2 + k_z^2)^2} \Phi_{d\omega, \mathbf{k}_x} \frac{4\pi G\rho_b}{\sqrt{2\pi}\sigma_h^3} \frac{i\omega}{k} \\ &\times \left[1 - i\sqrt{\frac{\pi}{2}} \frac{\omega}{k\sigma_h} \operatorname{erf}\left(\frac{-i\omega}{\sqrt{2}k\sigma_h}\right) \exp\left(\frac{-\omega^2}{2k^2\sigma_h^2}\right) \right].\end{aligned}\quad (3.27)$$

Following Fuchs we formally express the contributions of both the real and imaginary parts in a function Υ

$$\Phi_{h\omega, \mathbf{k}_x}(z=0) = \Upsilon(\omega, k_x) \Phi_{d\omega, \mathbf{k}_x}. \quad (3.28)$$

3.2 Stability of the disk

In this section we study the stability of the disk and in particular we are interested in neutral stable solutions to the set of Eqs. (2.65), (3.25), (3.28) that describe the influence the halo has on the disk's stability. Thereby taking the limit $\omega \rightarrow 0$, we find the contribution from the real part of the potential's perturbation

$$\Phi_{h\mathbf{k}_x}^{res}(z=0) = \int_{-\infty}^{+\infty} dk_z \frac{k_x}{(k_x^2 + k_z^2)^2} \Phi_{d\mathbf{k}_x} \frac{4G\rho_b}{\sigma_h^2}. \quad (3.29)$$

The contribution from its imaginary part is zero

$$\Phi_{h\mathbf{k}_x}^{res}(z=0) = 0, \quad (3.30)$$

which is evident since the phase velocity of the perturbation is zero ($\omega/k=0$). Due to the symmetry in k_z , we integrate Eq. (3.29),

$$\begin{aligned}\Phi_{h\mathbf{k}_x}(z=0) &= \Phi_{d\mathbf{k}_x} \frac{4G\rho_b}{\sigma_h^2} k_x 2 \left[\frac{2k_x}{4k_x^2(k_x^2 + k_z^2)} \Big|_0^\infty + \frac{2}{4k_x^2} \int_0^\infty \frac{dk_x}{k_x^2 + k_z^2} \right] \\ &= \Phi_{d\mathbf{k}_x} \frac{4G\rho_b}{\sigma_h^2} \frac{1}{k_x^2} \left[\arctan\left(\frac{k_z}{k_x}\right) \right]_0^\infty \\ &= \frac{2\pi G\rho_b}{\sigma_h^2} \frac{1}{k_x^2} \Phi_{d\mathbf{k}_x}.\end{aligned}\quad (3.31)$$

By comparison with the formal solution (Eq. (3.28)), we distinguish the function Υ

$$\Upsilon(\omega = 0, k_x) = \frac{2\pi G \rho_b}{\sigma_h^2} \frac{1}{k_x^2}. \quad (3.32)$$

The total induced perturbation in the disk is the linear superposition of the halo and disk isolated contributions

$$\Phi_{\mathbf{k}} \rightarrow \Phi_{d\mathbf{k}} + \Phi_{h\mathbf{k}} \propto \Phi_{d\mathbf{k}}, \quad (3.33)$$

which is proportional to the disk perturbation. Due to this convenient condition, we can insert

$$\Phi_{d\mathbf{k}} = (1 + \Upsilon)\Phi_{d\mathbf{k}} \quad (3.34)$$

into the right-hand side of Toomre's stability Eq. (2.67). First we rewrite its argument here using Eqs. (2.20), as

$$\begin{aligned} \frac{k_x \sigma_u^2}{2\pi G \Sigma_0} &= \frac{\sigma_u^2 k_{\text{crit}}^2}{\kappa^2} \left(\frac{\kappa^2}{2\pi G \Sigma_d} \right)^2 \frac{\kappa^2 k_x}{2\pi G \Sigma_d} \\ &= \frac{\sigma_u^2}{\kappa^2} k_{\text{crit}}^2 \frac{2\pi G \Sigma_d}{\kappa^2} k_x \\ &= \frac{\sigma_u^2}{\kappa^2} k_{\text{crit}}^2 \frac{\lambda_{\text{crit}}}{\lambda} \\ &= \left(\frac{3.36}{2\pi} \right)^2 Q_{\text{T}}^2 \frac{\lambda_{\text{crit}}}{\lambda}. \end{aligned} \quad (3.35)$$

Eq. (2.67) then takes the form

$$\left(\frac{3.36}{2\pi} \right)^2 Q_{\text{T}}^2 = \left[1 - \exp \left(- \frac{(3.36/2\pi)^2 Q_{\text{T}}^2}{(\lambda/\lambda_{\text{crit}})^2} \right) \cdot \text{I}_0 \left(\frac{(3.36/2\pi)^2 Q_{\text{T}}^2}{(\lambda/\lambda_{\text{crit}})^2} \right) \right] \frac{\lambda}{\lambda_{\text{crit}}}. \quad (3.36)$$

Accordingly, we rewrite the function Υ (Eq. (3.32)),

$$\begin{aligned} \Upsilon &= \frac{2G \rho_b}{\sigma_h^2} \frac{1}{k_x^2} \\ &= \frac{2G \rho_b}{\sigma_h^2} \frac{\lambda^2}{4\pi^2} \frac{(2\pi G \Sigma_d)^2}{\kappa^4} \frac{4\pi^2}{\lambda_{\text{crit}}^2} \\ &= \frac{2G \rho_b}{\sigma_h^2} \frac{(2\pi G \Sigma_d)^2}{\kappa^4} \left(\frac{\lambda}{\lambda_{\text{crit}}} \right)^2. \end{aligned} \quad (3.37)$$

And we insert it into Eq. (3.36),

$$\begin{aligned} \alpha Q_{\text{T}}^2 &= \left[1 - \exp \left(- \frac{\alpha Q_{\text{T}}^2}{(\lambda/\lambda_{\text{crit}})^2} \right) \cdot \text{I}_0 \left(\frac{\alpha Q_{\text{T}}^2}{(\lambda/\lambda_{\text{crit}})^2} \right) \right] \frac{\lambda}{\lambda_{\text{crit}}} \\ &\quad \times \left(1 + \beta \left(\frac{\lambda}{\lambda_{\text{crit}}} \right)^2 \right), \end{aligned} \quad (3.38)$$

Table 3.1: Local parameters of the Milky Way

Σ_d	$38 M_\odot/\text{pc}^2$	Holmberg & Flynn [HF04]
σ_d	40 km/s	Jahreiß & Wielen [JW97]
κ	$\sqrt{2} \cdot 220 \text{ km/s}/8.5 \text{ kpc}$	flat rotation curve
ρ_h	$0.01 M_\odot/\text{pc}^3$	Bahcall & Soneira [BS80]
σ_h	$220 \text{ km/s}/\sqrt{2}$	isothermal sphere
λ_{crit}	4.8 kpc	
λ_J	39 kpc	$\beta = 0.0078$

where $\alpha = (3.36/2\pi)^2 = 0.286$, and $\beta = (2\pi G\rho_h/\sigma_h^2)(2\pi G\Sigma_d)^2/\kappa^4$.

3.3 Discussion and Conclusions

Due to the linear treatment we have carried out, we have managed to extend Toomre’s stability Eq. (2.67) by inserting the function Υ that comprises the parameter β which explicitly describes the effect the halo has on the stability of the disk. As a partial check on Eq. (3.38) we see that for the case $\beta \rightarrow 0$, there is correspondingly a neutral stable line ($\omega \rightarrow 0$) that divides perturbations that are unbound ($\omega < 0$) and will grow with time and a region of stable perturbances ($\omega \geq 0$) in this way reproducing Eq. (2.67). The most interesting case though, occurs when we consider finite values of β . One thing natural to explore is to check on the stability of our own Milky Way. First, we extend Table (2.1) by including the most accepted value for the matter density in the halo (ρ_h) and the isotropic velocity dispersion of the halo particles according to the isothermal sphere (σ_h). The parameters given in Table (3.1) imply $Q_T = 2.8$ and $\beta = 0.0057$, respectively. Next, the behaviour of Eq. (3.38) is shown in Fig.(3.1) for different values of β , including for reference Toomre’s case ($\beta \rightarrow 0$). We see that the solutions of Eq. (3.38) always turn upwards, becoming unbound and growing exponentially at all times. This behaviour bears resemblance to the Jeans collapse of the halo component. Its Jeans length is given by $\lambda_J = \pi\sigma_h/G\rho_h$ or

$$\frac{\lambda_J}{\lambda_{\text{crit}}} = \frac{1}{\sqrt{2\beta}}. \quad (3.39)$$

Therefore the stabilizing effect provided by the inclusion of the velocity dispersion components of both the halo as well as the disk particles is valid only at small scales. However, even if we include in our estimate the cold interstellar gas with a local surface density of $4M_\odot/\text{pc}^2$ [Dam93] and assume a velocity dispersion of the interstellar gas of $\sigma_g = 5 \text{ km/s}$, which leads to

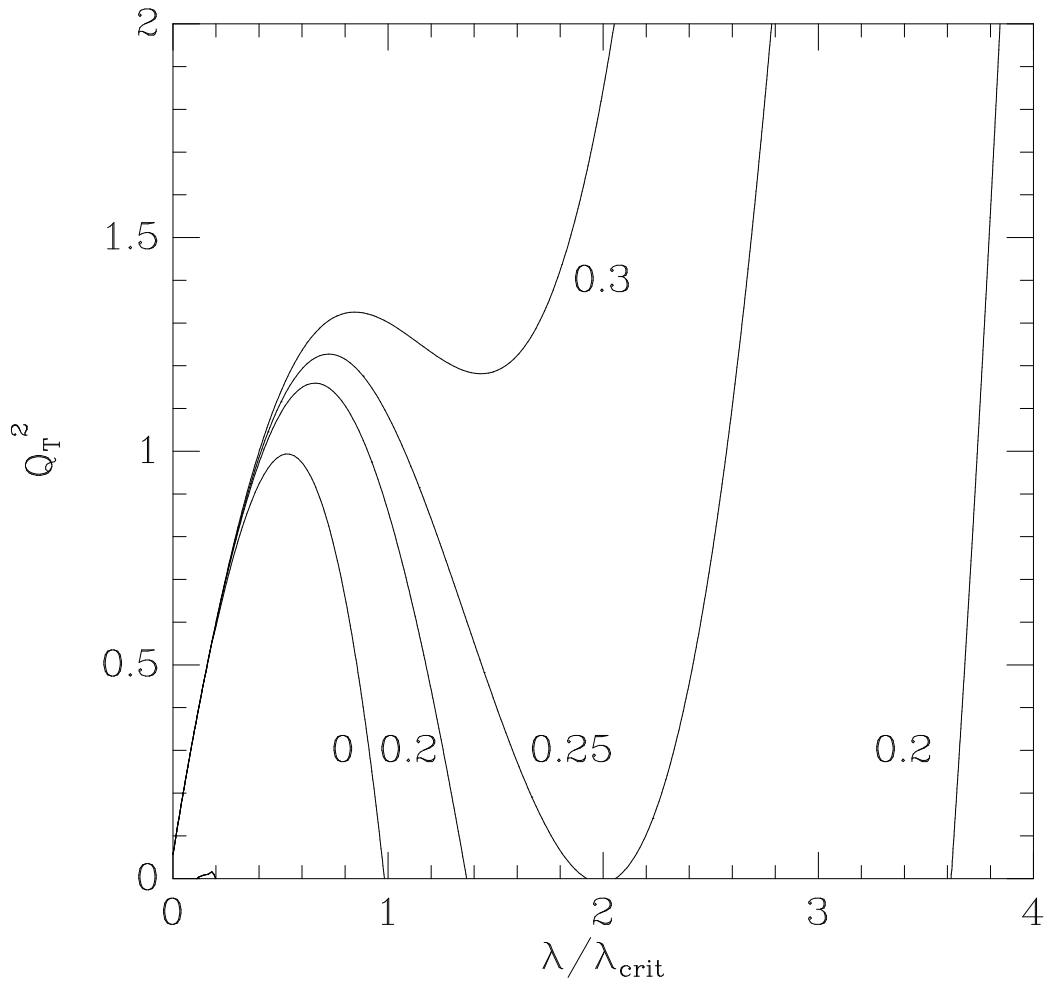


Figure 3.1: Separation of stable from unstable perturbations of a self-gravitating disk embedded in a live dark halo. Q_T denotes the usual Toomre stability index and λ is the wavelength of the perturbation measured in units of λ_{crit} . Unstable perturbations are located in the parameter space below the dividing lines. Lines are shown for values of the β parameter, which describes the dynamical responsiveness of the dark halo, $\beta = 0, 0.2, 0.25,$ and 0.3 , respectively.

a reduced mass weighted effective velocity dispersion of the combined stellar and gaseous disks, the parameter values change to $Q_{\text{T}} = 2.2$ and $\beta = 0.0078$, respectively. Equation (3.39) implies that $\lambda_{\text{J}} = 8 \lambda_{\text{crit}} = 39$ kpc. Thus the Milky Way disk and halo system seems to be very stable.

In order to explore in what range the β -parameter of spiral galaxies is to be expected, we consider the model of a Mestel disk with the surface density $\Sigma_{\text{d}} = \Sigma_0 R^{-1}$ embedded in a singular isothermal sphere representing the dark halo with the density distribution $\rho_{\text{h}} = \rho_0 R^{-2}$. The rotation curve of the model galaxy is given by

$$v_{\text{c}}^2(R) = v_{\text{d}}^2(R) + v_{\text{h}}^2(R) \quad (3.40)$$

with the disk contribution $v_{\text{d}}^2(R) = 2\pi G \Sigma_{\text{d}} R = \text{const.}$ and the halo contribution $v_{\text{h}}^2(R) = 4\pi G \rho_{\text{h}} R^2 = \text{const.}$ [BT87]. Assuming isotropic velocity dispersions of the dark matter particles it follows from the radial Jeans equation,

$$\frac{1}{\rho_{\text{h}}} \frac{d\rho_{\text{h}}\sigma_{\text{h}}^2}{dR} = -\frac{v_{\text{c}}^2}{R}, \quad (3.41)$$

that their velocity dispersion is given by

$$\sigma_{\text{h}}^2 = \frac{1}{2}(v_{\text{d}}^2 + v_{\text{h}}^2), \quad (3.42)$$

because the particles are bound by both the gravitational disk and halo potentials. We find then

$$\beta = \frac{v_{\text{h}}^2}{R^2} \frac{1}{v_{\text{d}}^2 + v_{\text{h}}^2} \frac{R^2}{4} \frac{v_{\text{d}}^4}{(v_{\text{d}}^2 + v_{\text{h}}^2)^2} = \frac{1}{4} \frac{v_{\text{h}}^2 v_{\text{d}}^4}{(v_{\text{d}}^2 + v_{\text{h}}^2)^3}, \quad (3.43)$$

which implies the maximal value

$$\beta \leq \beta_{\text{max}}(v_{\text{d}}^2 = 2v_{\text{h}}^2) = 0.037. \quad (3.44)$$

This means that in realistic halo models its density cannot be increased, on one hand, and the velocity dispersion of the halo particles lowered, on the other hand, indiscriminately, because the halo model has to stay in radial hydrostatic equilibrium. Equation (3.44) implies $\lambda_{\text{J}} = 3.7 \lambda_{\text{crit}}$. In order to ensure stability at smaller wave lengths the Toomre stability index must be larger than $Q_{\text{T}} \geq 1.02$. We conclude from this discussion that embedded galactic disks are not prone to Jeans instabilities, provided their Toomre stability index is a few percent higher than $Q_{\text{T}} = 1$.

As a second example the dynamics of the low surface brightness galaxy F568-1 is analysed. After observing its rotation curve, De Blok et al. [dMR01] have constructed several concurring mass models for the galaxy, which all fit the rotation curve equally well. Using the parameters of the models with isothermal haloes and with either a ‘realistic’ M/L -ratio of the disk or a ‘maximum-disk’ we have solved numerically the radial Jeans equation (3.41) for the dark matter particles,

$$\sigma_{\text{h}}^2(R) = \frac{1}{\rho_{\text{h}}(R)} \int_R^{\infty} dR \frac{\rho_{\text{h}}(R)v_{\text{c}}^2}{R}. \quad (3.45)$$

The resulting β -parameters of both models are shown in Fig. 3.2. As can be seen from Fig. 3.2 the β -parameters are of the same small order of magnitude as in the Milky Way or the simple disk – halo model described above. We conclude from this discussion that embedded galactic disks are not prone to Jeans instabilities, provided their Toomre stability index is a few percent higher than $Q_{\text{T}} = 1$. From a practical point of view the destabilizing effect of the surrounding dark halo on the Jeans instability of the embedded galactic disks seems to be negligible.

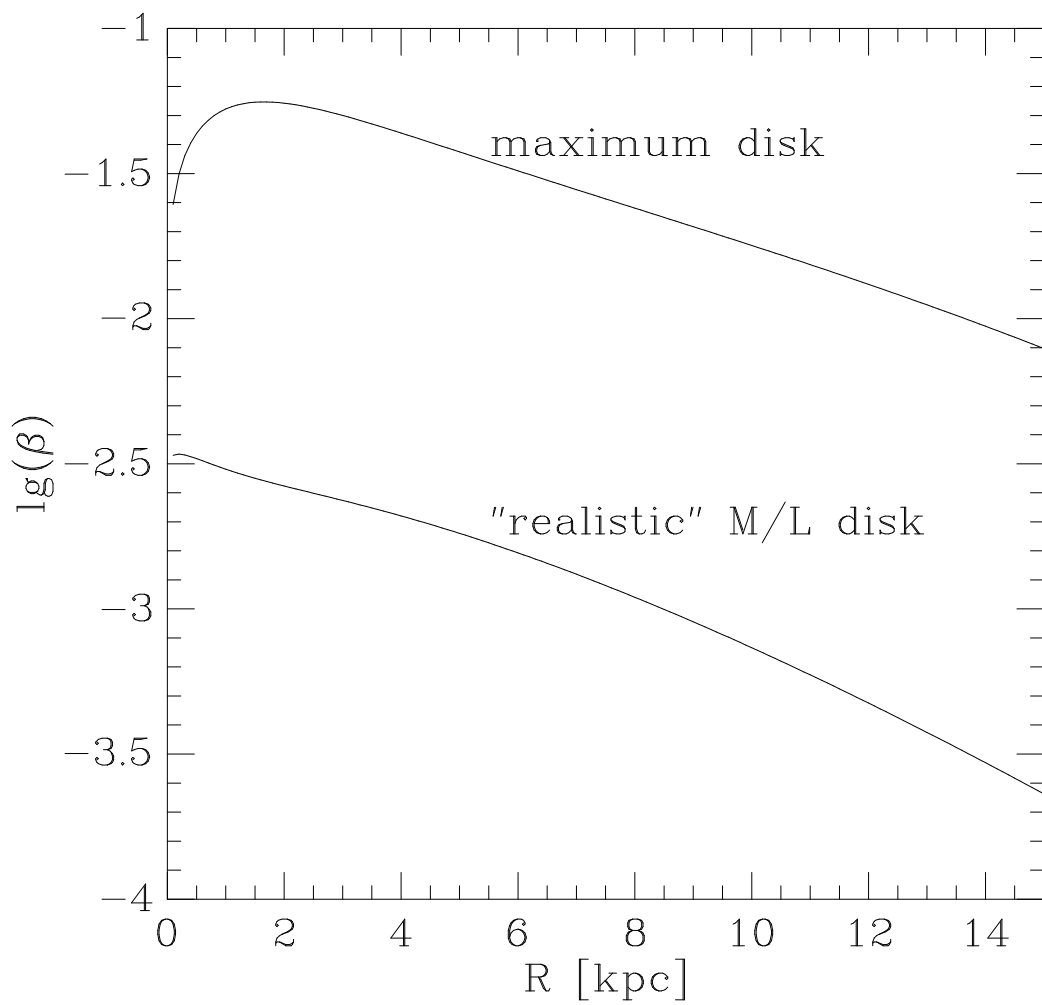


Figure 3.2: β -parameters of mass models of the low surface brightness galaxy F568-1.

Chapter 4

Dynamical friction

Chandrasekhar's formula of DF [Cha43] has become a cornerstone of theoretical physics and nowadays continues to be included in studies of the evolution of many different astrophysical systems. This original work was selected as part of a collection of fundamental papers published during the XX century, and was reprinted in the centennial issue of ApJ [Abt99].

The phenomenon is that of a moving star that is entering a system composed of stars (Fig. (4.1)). Due to the gravitational interaction with the surrounding matter, the star will exchange linear momentum and kinetic energy with the background particles. The value of the drag will depend on the velocity of the body and on the square of the body's mass, which can be intuitively inferred since the wake created will be proportionate to its mass and therefore in its direction of motion the star will be decelerated by this quadratic term.

Inspired by the existing physical theories of Brownian motion of gaseous systems, Chandrasekhar was convinced that the diffusion equation of the background stars in phase space, related to the discrete increments in the mean square velocity of the background stars, should be compensated for by a dynamical friction term associated to the deceleration of the test particle in order to leave the Maxwellian distribution unchanged. Such a conservative stochastic process is expected on quite general grounds, one of these being the fact that the effect the test star has on the overall characteristics of the system can be regarded as a small perturbation to the equilibrium state. To explicitly find the fluctuations in the decelerating force, Chandrasekhar idealized the stellar encounters between the stars as an independent two-body problem, and considered that the stars are homogeneously distributed and possess a Maxwellian velocity distribution function. In this chapter we rewrite Chandrasekhar's original treatment of the effect, and the following

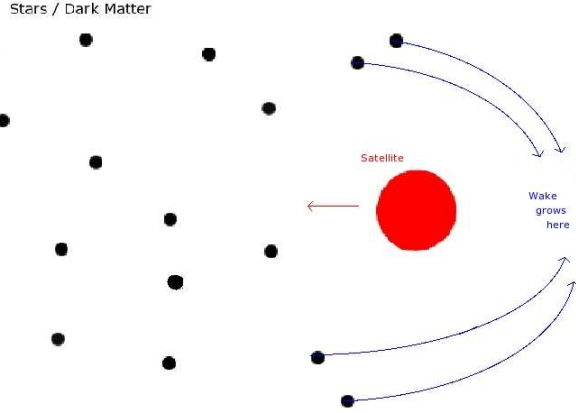


Figure 4.1: Sketch depicting the dynamical friction exerted on the massive moving body. As the body moves through the system, a wake will form behind it pulling it back, and as result the body will be decelerated.

work is strictly due to the work presented in ([Cha42] ; [Cha43]).

4.1 The geometry of the two-body approximation

Let us consider the motion of a *field* star of mass m_1 that is moving at velocity \mathbf{v}_1 , in an chosen fixed frame of reference, and the motion of a *test* star of mass m_2 moving at velocity \mathbf{v}_2 ; their respective equations of motion satisfy the condition

$$m_1 \frac{d\mathbf{v}_1}{dt} + m_2 \frac{d\mathbf{v}_2}{dt} = 0. \quad (4.1)$$

The situation is depicted in Fig. (4.2). \mathbf{V} represents the relative velocity $\mathbf{V} = \mathbf{v}_2 - \mathbf{v}_1$ between the stars. It can also be seen that θ defines the angle between the vectors \mathbf{v}_1 and \mathbf{v}_2 , and δ the angle between the center of gravity vector \mathbf{V}_g and the vector \mathbf{v}_2 . If we define an orbital plane containing the deflection of the relative velocity vector \mathbf{V}' and a *fundamental* plane comprising the the vectors \mathbf{v}_1 , \mathbf{v}_2 , then Θ denotes the angle between these two planes, which can be seen directly from Fig. (4.3). In Fig. (4.2), $\pi - 2\psi$ is the angle of deflection that suffers the relative velocity \mathbf{V} in the orbital plane after the encounter. Eq. (4.1) implies that the motion of the center of

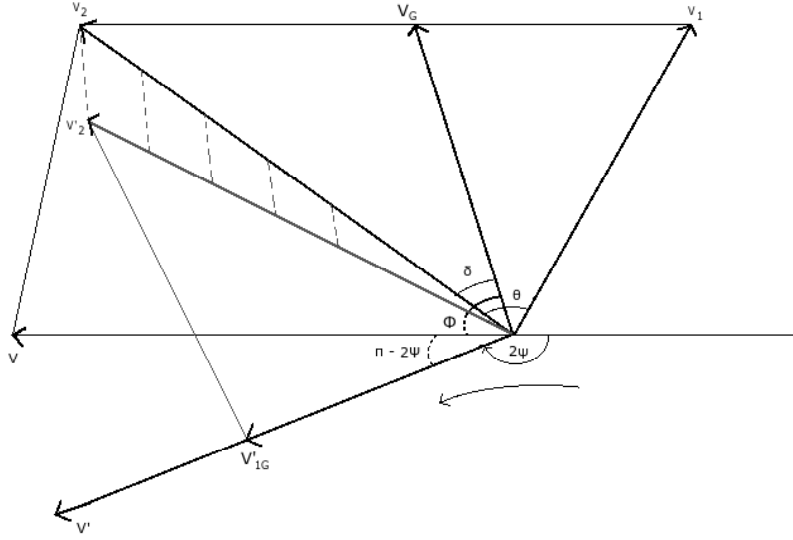


Figure 4.2: Illustration showing two-body hyperbolic, Keplerian encounters.

gravity

$$m_1 \mathbf{v}_1 + m_2 \mathbf{v}_2 = (m_1 + m_2) \mathbf{V}_g, \quad (4.2)$$

is constant at all times. Their relative motion can be cast in the form of

$$\frac{d\mathbf{V}}{dt} = G(m_1 + m_2) \nabla \frac{1}{r}, \quad (4.3)$$

where $\mathbf{r} = \mathbf{r}_1 - \mathbf{r}_2$ is their relative position vector.

Now, considering polar coordinates (r, θ) , the Lagrangian function will look like

$$L = \frac{1}{2}(\dot{\mathbf{r}}^2 + r^2 \dot{\theta}^2) + \frac{G}{r}(m_1 + m_2), \quad (4.4)$$

and their corresponding Lagrangian equations are

$$\ddot{\mathbf{r}} = \mathbf{r} \dot{\theta}^2 - \frac{G}{r^2}(m_1 + m_2), \quad (4.5)$$

and

$$\frac{d}{dt}(r^2 \dot{\theta}) = 0. \quad (4.6)$$

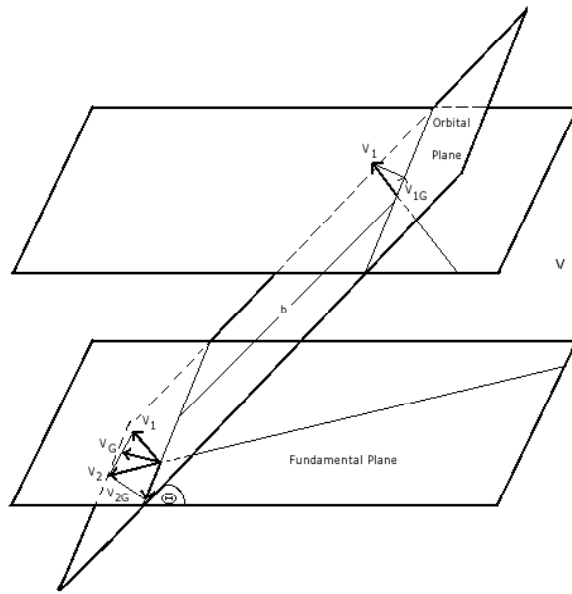


Figure 4.3: Illustration that shows the fundamental and orbital planes as well as the angle Θ and the impact parameter b .

First, we can identify Eq. (4.6) as the usual expression for the conservation of angular momentum

$$l = \mathbf{r}^2 \dot{\theta} = \text{constant}, \quad (4.7)$$

and we use it to rewrite Eq. (4.5) as

$$\frac{d^2(1/r)}{d\theta^2} = -\frac{1}{r} + \frac{G}{l^2}(m_1 + m_2). \quad (4.8)$$

The solution to Eq. (4.8) is conveniently written in terms of a cosine function

$$\frac{1}{r} = \frac{1}{r_0} \cos(\theta + \theta_0) + \frac{G}{l^2}(m_1 + m_2), \quad (4.9)$$

with r_0 and θ_0 are the constants of integration. Eq. (4.9) can be conveniently expressed if we consider the direction of minimum r as the origin of the angle θ , thus obtaining

$$r = \frac{l^2}{G(m_1 + m_2)} \frac{1}{1 + e \cos \theta}, \quad (4.10)$$

where e is the eccentricity of the trajectory,

$$e = \frac{r_a - r_p}{r_a + r_p}, \quad (4.11)$$

defined by the farthest distance of approach r_a (apoapsis) and the closest distance r_p (periapsis). Solutions of the form of Eq. (4.10) will dictate parabolic orbits if $e = 1$ and hyperbolic trajectories if $e > 1$.

As for the conservation of energy, we write it at the point $r = r_p$, as

$$\frac{1}{2} \frac{1}{r_p^2} (r_p^2 \dot{\theta})^2 - \frac{G}{r_p} (m_1 + m_2) = \frac{1}{2} V^2, \quad (4.12)$$

we then introduce the explicit form of r_p by noting that $r = r_p$ for the case $\cos \theta = 1$ in Eq. (4.10), and solve for the eccentricity e ,

$$e^2 = 1 + \frac{b^2 V^4}{G^2 (m_1 + m_2)^2}, \quad (4.13)$$

where we have expressed the angular momentum in terms of the impact parameter, $l = bV$.

The angle 2ψ between the asymptotes of the relative orbit is readily obtain from Eq. (4.10), since $r \rightarrow \infty$ for

$$\theta = \cos^{-1} \left(-\frac{1}{e} \right), \quad (4.14)$$

but the angle we are looking for is $\pi - 2\psi$ (see Fig. (4.2)), or

$$\begin{aligned}\cos \psi &= \frac{1}{e} \\ &= \frac{1}{\sqrt{1 + \frac{b^2 V^4}{G^2(m_1+m_2)^2}}}. \end{aligned} \quad (4.15)$$

The *true* deflection suffered by the test star, *i. e.* the deflection in a fixed frame of reference, can be formally written as

$$\cos(\pi - 2\Psi) = \frac{\mathbf{v}_2 \cdot \mathbf{v}'_2}{v_2 v'_2} \quad (4.16)$$

but in the reference frame in which the center of gravity is at rest, where the velocity of the star before $\mathbf{v}_{2\mathbf{g}}$, and after the encounter $\mathbf{v}'_{2\mathbf{g}}$ are related to \mathbf{v}_2 through

$$\mathbf{v}_{2\mathbf{g}} = \mathbf{v}_2 - \mathbf{V} \quad \text{and} \quad \mathbf{v}'_{2\mathbf{g}} = \mathbf{v}'_2 - \mathbf{V}, \quad (4.17)$$

or using Eq. (4.2), via

$$\mathbf{v}_{2\mathbf{g}} = \frac{m_1}{m_1 + m_2} \mathbf{V}; \quad \mathbf{v}'_{2\mathbf{g}} = \frac{m_1}{m_1 + m_2} \mathbf{V}' \quad (4.18)$$

so that the deflection can be expressed, after some rearrangement of terms, as

$$v_2 v'_2 \cos(\pi - 2\Psi) = \mathbf{v}_2 \cdot \mathbf{v}'_{2\mathbf{g}} + \mathbf{v}_2 \cdot \mathbf{V}_{\mathbf{g}}. \quad (4.19)$$

From Fig. (4.2) the direction cosines of \mathbf{v}_2 with respect to \mathbf{V} , to a direction in the orbital plane perpendicular to \mathbf{V} , and to a direction perpendicular to the orbital plane are

$$\cos(\Phi - \delta) \quad , \quad -\sin(\Phi - \delta) \cos \Theta \quad , \quad \text{and} \quad \sin(\Phi - \delta) \sin \Theta. \quad (4.20)$$

Due to the fact that $\mathbf{v}'_{2\mathbf{g}}$ lies in the same direction as \mathbf{V}' , the direction cosines with respect to the same three directions are

$$\cos(\pi - 2\psi) \quad , \quad \sin(\pi - 2\psi) \quad , \quad \text{and} \quad 0. \quad (4.21)$$

Therefore we have

$$\begin{aligned}\mathbf{v}_2 \cdot \mathbf{v}'_{2\mathbf{g}} &= v_2 \cdot v'_{2g} [\cos(\pi - 2\psi) \cos(\Phi - \delta) - \sin(\pi - 2\psi) \sin(\Phi - \delta) \cos \Theta] \\ &+ V_g \cos \delta, \end{aligned} \quad (4.22)$$

which can be rewritten by using Eq. (4.18), as

$$\begin{aligned}\cos 2\Psi &= \frac{1}{(m_1 + m_2)^2 v'_2} [2m_1(v_2 - v_1 \cos \theta) \cos^2 \psi \\ &+ 2m_1 v_1 \sin \theta \cos \Theta \sin \psi \cos \psi - (m_1 + m_2)v_2]. \end{aligned} \quad (4.23)$$

Since the change in the velocity parallel to and perpendicular to the original direction of the test star are (cf. Fig. (4.2)),

$$\Delta v_{\parallel} = v'_2 \cos(\pi - 2\Psi) \quad \text{and} \quad \Delta v_{\perp} = v'_2 \sin 2\Psi, \quad (4.24)$$

we are now able to express the velocity components explicitly in terms of their direction cosine. Inserting Eq. (4.23) into Eq. (4.24) we get

$$\Delta v_{\parallel} = -\frac{2m_1}{m_1 + m_2} [(v_2 - v_1 \cos \theta) \cos \psi + v_1 \sin \theta \cos \Theta \sin \psi] \cos \psi, \quad (4.25)$$

and also

$$\begin{aligned} \Delta v_{\perp} = & -\frac{2m_1}{m_1 + m_2} [v_1^2 + v_2^2 - 2v_1 v_2 \cos \theta - \{(v_2 - v_1 \cos \theta) \cos \psi \\ & + v_1 \sin \theta \cos \Theta \sin \psi\}^2]^{1/2} \cos \psi. \end{aligned} \quad (4.26)$$

This last equation could be comparable to the parallel component (Eq. (4.25)) for an isolated two-body encounter, however, as more and more such isolated encounters with different parameters are summed up, Eq. (4.26) vanishes identically.

4.2 The net dynamical drag

In order to formally obtain the net change the test star's velocity experiences we need to integrate Eq. (4.25) over the several parameters involved in the encounters, namely the angles (θ, δ, Θ) , the impact parameter b (cf. Fig. (4.3)), and the velocity of the background stars v_1 ; the intervals of integration encompass all possible parameter combinations. The net velocity change during a time Δt is

$$v_{\parallel} = \Delta t \int_0^{\infty} dv_1 \int_0^{\pi} d\theta \int_0^{2\pi} d\delta \int_0^{infy} \int_0^{2\pi} \frac{d\Theta}{2\pi} [2\pi N(v_1, \theta, \delta) V b \Delta v_{\parallel}]. \quad (4.27)$$

The integration over Θ is trivial. To make the integration over the impact parameter b , we need to introduce Eq. (4.15) into the equation,

$$\begin{aligned} v_{\parallel} = & -\frac{4\pi m_1}{m_1 + m_2} \Delta t \int_0^{\infty} dv_1 \int_0^{\pi} d\theta \int_0^{2\pi} d\delta \int_0^{\infty} N(v_1, \theta, \delta) \\ & \times V(v_2 - v_1 \cos \theta) \frac{b}{1 + \frac{b^2 V^4}{G^2(m_1 + m_2)^2}}. \end{aligned} \quad (4.28)$$

We can immediately see that the integration over b diverges; the problem is avoided by considering a finite, maximum impact parameter b_{max} as the end of the range of integration. The resulting integration will include the famous, so-called *Coulomb logarithm* $\log(1 + CV^4)$, where $C = b_{max}^2/G^2(m_1 + m_2)^2$ and which we will discuss in further detail in the next section. We thus obtain

$$v_{\parallel} = -2\pi m_1(m_1 + m_2)G^2\Delta t \int_0^{\infty} dv_1 \int_0^{\pi} d\theta \int_0^{2\pi} d\delta \int_0^{\infty} N(v_1, \theta, \delta) \times \frac{1}{V^3}(v_2 - v_1 \cos \theta) \log(1 + CV^4). \quad (4.29)$$

To continue with the integration, the simplest distribution of the velocities of the background stars is considered, *i. e.* a spherical distribution

$$N(v_1, \theta, \delta) = N(v_1) \frac{1}{4\pi} \sin \theta, \quad (4.30)$$

and the result of the integration over δ reads

$$v_{\parallel} = -\pi m_1(m_1 + m_2)G^2\Delta t \int_0^{\infty} dv_1 \int_0^{\pi} d\theta N(v_1) \times \frac{\sin \theta}{V^3}(v_2 - v_1 \cos \theta) \log(1 + CV^4). \quad (4.31)$$

Since θ is the angle between the vectors \mathbf{v}_1 and \mathbf{v}_2 , the natural way to carry out the integration is to change this variable for the relative velocity \mathbf{V} , or by taking

$$V^2 = v_1^2 + v_2^2 - 2v_1v_2 \cos \theta, \quad (4.32)$$

we obtain

$$VdV = v_1v_2 \sin \theta d\theta, \quad (4.33)$$

and

$$v_2 - v_1 \cos \theta = \frac{1}{2v_2}(V^2 + v_2^2 - v_1^2). \quad (4.34)$$

Substituting Eqs. (4.33) and (4.34) into Eq. (4.31) and integrating by parts, we get

$$v_{\parallel} = -\frac{\pi}{2}m_1(m_1 + m_2)\frac{G^2}{v_2^2} \int_0^{\infty} dv_1 N(v_1) \left\{ \left(V - \frac{v_2^2 - v_1^2}{V} \right) \log(1 + CV^4) \right\} \Big|_{|v_1 - v_2|}^{v_1 + v_2} - 4 \int_{|v_1 - v_2|}^{v_1 + v_2} dV \left(1 - \frac{v_2^2 - v_1^2}{V^2} \right) \frac{CV^4}{1 + CV^4} \Big\} \Delta t. \quad (4.35)$$

Since the assumption is that $CV^4 \gg 1$ (see next section), then the second integral can be easily performed; Eq. (4.35) reduces to

$$v_{\parallel} = -\frac{\pi}{2}m_1(m_1 + m_2)\frac{G^2}{v_2^2}\int_0^{\infty}dv_1N(v_1)\Delta t\left\{\left(V - \frac{v_2^2 - v_1^2}{V}\right)\log(1 + CV^4) - 4\int_{|v_1 - v_2|}^{v_1 + v_2}dV\left(V - \frac{v_2^2 - v_1^2}{V}\right)\right\}_{|v_1 - v_2|}^{v_1 + v_2}. \quad (4.36)$$

The different evaluations of Eq. (4.35) depend on the relative value of the velocities v_1 and v_2 . After keeping the leading terms of Eq. (4.35), it can be seen that for the case $v_1 > v_2$ the contribution to the equation is negligible, and so the case where the test star moves faster than the see stars ($v_2 \geq v_1$), we have

$$v_{\parallel} = -4\pi m_1(m_1 + m_2)\frac{G^2}{v_2^2}\log(\Lambda)\Delta t\int_0^{v_2}N(v_1)dv_1, \quad (4.37)$$

where the Coulomb logarithm now takes the form $\log(\Lambda) = (b_{max}/b_{min})$, which includes the minimum value the impact parameter can have, $b_{min} = Gm/V^2$. To continue further, we need to explicitly write the Maxwellian distribution of velocities for the stars of the system

$$N(v_1) = \frac{2N}{\sqrt{2\pi}\sigma^3}v_1^2\exp\left(-\frac{v_1^2}{2\sigma^2}\right), \quad (4.38)$$

where σ is the isotropic, velocity dispersion of the stars and N is just the spatial density of the stars. Chandrasekhar's classical formula is expressed in terms of the error integral

$$\Phi(x) = \frac{2}{\sqrt{\pi}}\int_0^xe^{-x^2}dx, \quad (4.39)$$

which is inserted into Eq. (4.38) and so we find

$$v_{\parallel} = -4\pi m_1(m_1 + m_2)\frac{G^2}{v_2^2}\log(\Lambda)\Delta t\left[\Phi\left(\frac{v_2}{2\sigma^2}\right) - \frac{v_2}{2\sigma^2}\Phi'\left(\frac{v_2}{2\sigma^2}\right)\right]. \quad (4.40)$$

Technically, the approximation that led to the derivation of Eq. (4.40), which relies upon the background being homogeneous, isotropic, and infinite, is safely valid since the extension and internal evolution of the perturber is not considered. The collisional treatment used by Chandrasekhar in finding this expression for the dynamical drag on a test particle is not the only one way to calculate such effect. Another method based on a more *wave-mechanical*

approach will be discussed in the next chapter, such a method will help us to formally calculate the DF on extended test particles, but first we end this chapter with a brief discussion on the rather *intriguing*, so-far-not-yet completely understood Coulomb logarithm $\log(\Lambda)$

4.3 The Coulomb logarithm.

Although the physical concept behind the DF effect seems simple, Chandrasekhar’s formula has not been fully understood and discrepancies between different numerical and analytical studies are abundant in the literature. As said in the previous section, the inclusion of the Coulomb logarithm was necessary in order to avoid the formula to diverge to infinity. However, assigning appropriate values to both limits b_{min} and b_{max} is not an easy task and depends on the particular situation under consideration. Values in the literature could be found in the range $1 \leq \log(\Lambda) \leq 20$. As for the minimum impact parameter, b_{min} , many have followed White [Whi76] and set this lower cutoff to be of the order of the virial radius of the system, meaning that the relative velocity at infinity is approximated by its root-mean-square (rms) value $\langle V^2 \rangle^{1/2}$. This choice makes apparently more sense than previous choices for b_{min} that considered it to be of the order of the size of the core of the background system, since for a lot of situations the test particle’s internal rms motion is less than the magnitude of the velocity with which it moves through the parent system. However, the choice of the upper cutoff is even trickier, some times it is set as the size of the system $\sim R$ ([JB00]; [HWdZ99]; [JSH95]), but in case there is an important central concentration this is not a good choice since the density at large radius will be much less than, for example, at half the radius of the system. In this case an effective b_{max} must be selected, and some numerical studies have used the Coulomb logarithm as a fitting parameter [VW99], however, this is not correct since the mass distribution of the parent galaxy should be used to determine its value.

In more sophisticated numerical calculations [HFM03] the Coulomb logarithm was set to vary radially in order to match their results and the analytical predictions of Eq. (4.40). Whether the Coulomb logarithm is constant or varies at all scales, it is clear that its value can be regarded as a fine-tuning to the system’s DF formula.

Chapter 5

Density profiles

According to hierarchical cosmologies, large galaxies are the result of the aggregation of smaller subunits. While some substructures may have been entirely destroyed in the course of time (contributing in this way to the field), some of these may have survived until the present day in the form of satellites. Chandrasekhar's Eq. (4.40) was derived considering a point-mass test particle. However, this is a major oversimplification of realistic systems. That is why we mention here some density profiles that we will later consider in order to extend the current analytical treatment of DF.

As said in previous chapters, the dynamical evolution of astrophysical systems is determined by solving the Boltzmann equation that determines the distribution function f of the constituent particles in phase space, and the Poisson equation which allows a self-consistent treatment of the system's gravity. However, it is practically imposible to find an analytical distribution function–density pair, implying that N-body methods are required to explicitly follow the evolution of the distribution function f . Due to the power of the Jeans theorem, which states that the distribution function of a system that is in equilibrium can be expressed in terms of integrals of motion, some analytic steady state models have been obtained. We enumerate here two benchmark density profiles: the Hernquist profile [Her90] and the Plummer sphere [Plu15], which have been extensively used in the literature.

By reference we mention first the associated potential to a point–mass profile

$$\Phi(r) = -\frac{GM}{r}, \quad (5.1)$$

which moves with a keplerian circular velocity

$$v_c = \sqrt{\frac{GM}{r}}. \quad (5.2)$$

5.1 The Hernquist profile

The Hernquist profile has received considerable attention, specially in the study of elliptical galaxies and self-interacting dark matter in isolated galactic haloes. It was originally proposed [Her90], as an alternative to the already existing Jaffe profile for spherical galaxies [Jaf83],

$$\rho_J(r) = \frac{\rho_0 r_J}{4\pi r^2 (r + r_J)^2} \quad (5.3)$$

where r_J is a scale length. Due to its analytical form, the Jaffe profile was widely used in numerical calculations. However, the Jaffe profile presents deviations from the de Vaucouleurs profile [de 48],

$$\log_{10} \left[\frac{I(R)}{I(R_e)} \right] = -3.331 \left[\left(\frac{R}{R_e} \right)^{1/4} - 1 \right], \quad (5.4)$$

which is the most widely used empirical law to describe the surface brightness profiles of elliptical galaxies and bulges. I denotes the surface brightness at the projected radius on the plane of the sky R and at the R_e the effective radius of the isophote enclosing half of the light.

The deviation of the Jaffe profile from the de Vaucouleurs profile (also known as the $R^{1/4}$ law), is evident in limit of small radii ($r \rightarrow 0$), since $\rho_J \sim r^{-2}$ for the first profile while $\rho_{R^{1/4}} \sim r^{-3/4}$ for the second. The Hernquist density profile

$$\rho(r) = \frac{M r_0}{2\pi r} \frac{1}{(r + r_0)^3}, \quad (5.5)$$

where M is the total mass and r_0 is again a scale length, is similar to that described by Eq. (5.3) but its behaviour as $r \rightarrow 0$, $\rho(r) \sim r^{-1}$, follows closer the de Vaucouleurs profile. Figs. (5.1) and (5.2) [Figs. (2) and (3) of Her90, , respectively], illustrate this fact. For a spherical, isotropic model the distribution function that corresponds to Eq. (5.5) depends solely on the total specific energy, $f = f(E)$. In Fig. (5.1) the distribution function is plotted as a function of energy for different values of the scaling factor r_0 , in units such that $G = 1$ and $M = 1$. The distribution function corresponding to the de Vaucouleurs Eq. (5.4) is also shown.

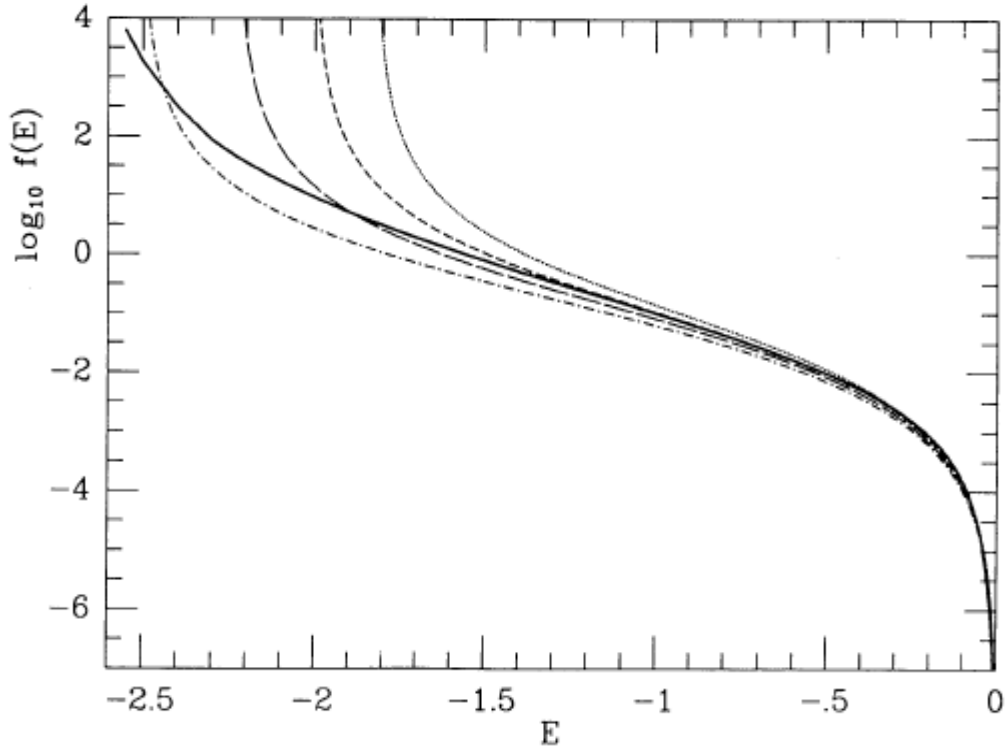


Figure 5.1: Fig 2. of [Her90]. The distribution function for the $R^{1/4}$ law Eq. (5.4), has been numerically integrated and it is shown here (solid curve). Various values of the scaling factor r_0 for the Hernquist model are show: $r_0 = 0.55$ (dotted), $r_0 = 0.5$ (short-dashed), $r_0 = 0.45$, and $r_0 = 0.4$ (dashed-dotted).

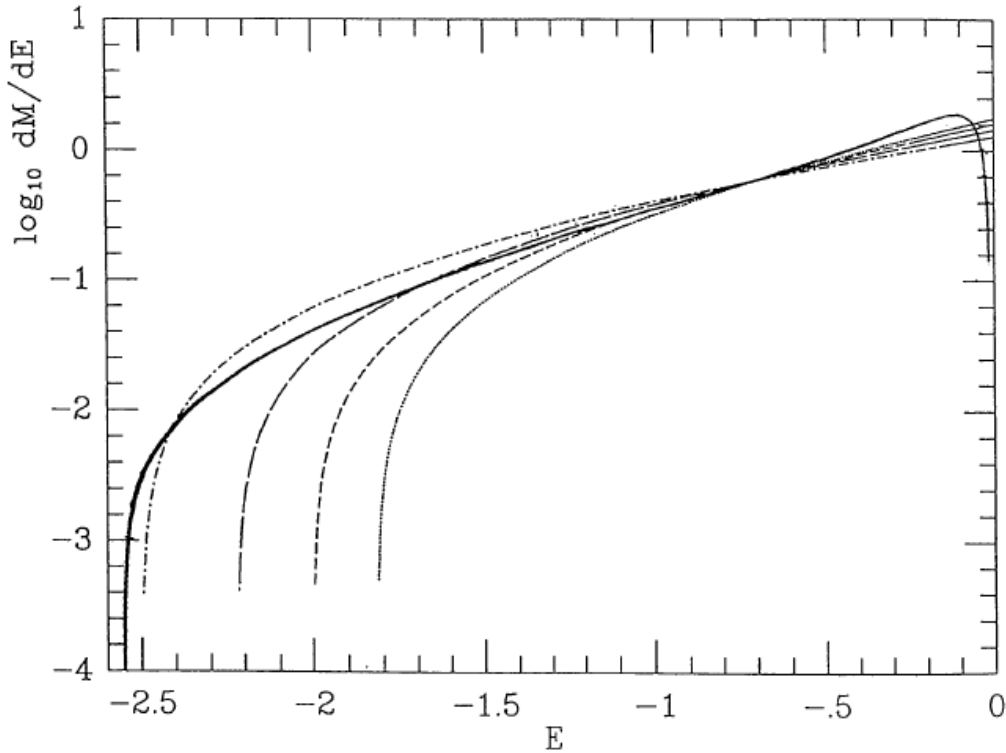


Figure 5.2: Fig. 3 of [Her90]. The differential energy distributions corresponding to the de Vaucouleurs (solid curve) and to the Hernquist profile for the same values for the scale factor considered in Fig. (5.1) are plotted.

Because the unique dependence of the distribution function on energy, Hernquist calculated in a simpler manner, following a standard procedure [cf. Jaf83, for a full description of the method], the differential mass distribution dM/dE , Fig. (5.2). From both figures one can observe that the Hernquist models mimic to a really good extent the behavior of the $R^{1/4}$ law, specially the case $r_0 = 0.45$, for which the distribution function and the differential energy distribution agree to $\sim 35\%$ in the energy range $(-2.0 \leq E \leq -0.03)$. It can be fairly said that the Hernquist profile is a reliable tool at modeling elliptical and bulge systems.

In the dark-matter context, however, the results are apparently not so accurate. Let us consider a general fitting formula [KKBP98], for the cuspy density profile of dark-matter haloes of the form

$$\rho = \frac{C\rho_0}{(r/a)^\gamma [1 + (r/a)^\alpha]^{(\beta-\gamma)/\alpha}}, \quad (5.6)$$

where ρ_0 is the total mass, C is a constant, and a is a scale length. The index γ controls the slope of the inner profile, β that of the outer profile, and α the sharpness of the transition. Depending upon the indices considered, one obtains from Eq. (5.6) different distribution functions. Although we are not interested in this work in the profile dark-matter haloes follow, Eq. (5.6) shows directly that of all possible combinations of indices with the restriction imposed by the observations, only Eq. (5.5) can provide an analytical distribution function-density pair. However, the Hernquist profile arises a special case of Eq. (5.6) in the sense that it falls off as $\rho(r) \sim r^{-4}$ at large radii, contrary to what is found in high-resolution numerical simulations, for example, the NFW profile [NFW97],

$$\rho_{NFW} = \frac{\rho_0}{(r/a)(1+r/a)^2}, \quad (5.7)$$

where a is its scale length, and ρ_0 its total mass, has a more gradual falloff than r^{-4} .

Finally, by integrating Poisson equation (cf. 3.13) the potential associated to Eq. (5.5) has the form

$$\Phi(r) = -\frac{GM}{r+r_0}. \quad (5.8)$$

5.2 The Plummer sphere

The Plummer sphere [Plu15],

$$\rho(r) = \frac{\rho_0}{[1+r^2/r_0^2]^{-5/2}}, \quad (5.9)$$

where ρ_0 is the total density, and r_0 is a scale factor, can be thought of as the profile of an extended body with a central core. Its associated potential is often used in numerical simulations to *soften* gravity at small scales. Although this model is not a good fit to simulate cold-dark-matter (CDM) haloes, this profile is necessary to prevent point particles from scattering too hardly off one another on close approximation, and is commonly used in the study of star clusters. In addition, its very rapid fall off at large radii, $\rho(r) \sim r^{-5}$, makes it natural to impose a truncation radius, as oppose to other models that need somewhat unjustified truncation radii. Usually the factor r_0 is considered to be of the size of the body itself as its potential approaches that of a point mass beyond that radius. The integration of Poisson equation

is best done if we consider the contribution of the density to the potential inside the sphere of radius \bar{r} , and outside of it

$$\begin{aligned}
\Phi &= -\frac{4\pi G}{r} \int_0^r d\bar{r} \frac{\rho_0 \bar{r}^2}{[1 + \bar{r}^2/r_0^2]^{5/2}} - 4\pi G \int_r^\infty d\bar{r} \frac{\rho_0 \bar{r}}{[1 + \bar{r}^2/r_0^2]^{5/2}} \\
&= -\frac{4\pi G}{r} \rho_0 r_0^3 \left[\frac{x^3}{3(1+x^2)^{3/2}} \right]_0^{r/r_0} - 2\pi G \rho_0 r_0^2 \left[-\frac{2/3}{(1+r)^{3/2}} \right]_{r^2/r_0^2}^\infty \\
&= -\frac{4\pi G \rho_0}{3} \frac{r_0^2}{\sqrt{1+r^2/r_0^2}}.
\end{aligned} \tag{5.10}$$

In Fig. (5.3) we plott a comparison between the different analytical models discussed so far, for reference reasons we include the isothermal sphere,

$$\rho(r) = \rho_0 \left(\frac{r_0}{r} \right)^2, \tag{5.11}$$

which corresponds to an unrealistic configuration of infinite radius and mass. Nonetheless, the isothermal sphere has been usually applied to the study of stellar cores with no nuclear burning and star clusters [VB05].

We can conclude that the Plummer sphere is a also convenient choice for testing the impulse approximation against N-body calculations, since it possesses a simple form.

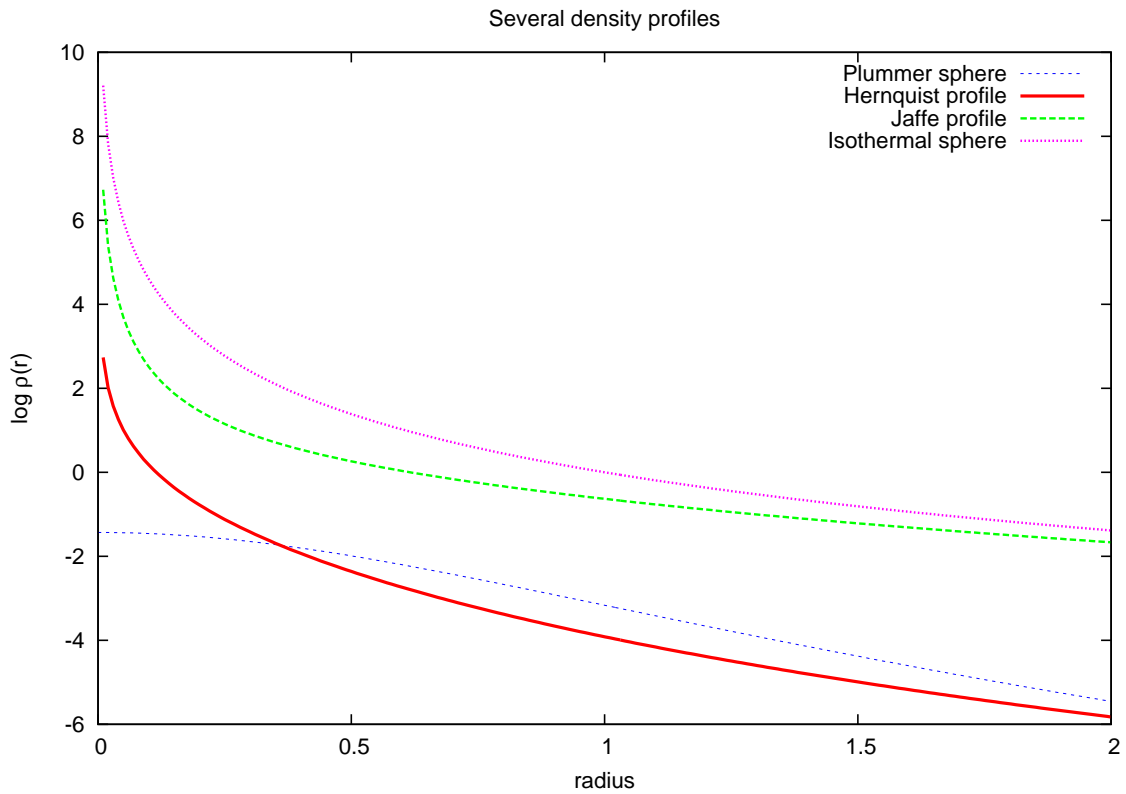


Figure 5.3: Several density profiles as function of radius are plotted. It can be seen the similar behaviour between the Jaffe and Hernquist models. This contrasts with the *soft* behaviour of the Plummer sphere near the center. The isothermal sphere is included for reference. The units are so that $G = M = r_0 = 1$.

Chapter 6

Dynamical friction force exerted on spherical bodies

The applications of Chandrasekhar's formula covered a wide field, ranging from calculations of the DF and diffusion coefficients of the Fokker-Planck equation, which is used to describe the internal dynamics of star clusters, to determinations of the sinking rates of satellite galaxies which are accreted by massive galaxies. Specially this last point has received a lot of attention. However, let us remember that the basic assumptions behind the derivation of Chandrasekhar's Eq. (4.40), are that the stars are distributed homogeneously, that they possess an isothermal Gaussian velocity distribution, that the system they form has infinite extension, and that the extension of the massive test star is not taken into account. These could be regarded as a series of oversimplifications that do not represent realistic physical situations. Concerning the possible inhomogeneity of the self-gravitating system, it has been shown that for such system, whose density falls off radially, the large scales perturbations the test star creates as it moves through it will have a relatively small contribution to the DF exerted on it [cf. CMG99], so we can be confident that the assumption of homogeneity is reliable to first order.

As for the extension of the system, if a finite extension of the system is considered second-order terms will appear and the transfer of angular momentum will play also a role in decelerating the perturber [Ath03]. However, if the test star's orbit decays sufficiently rapid, Eq. (4.40) remains approximately valid. Cora et al. [CVM01] investigated on the effect chaotic orbits for the background stars could have for DF and came to the conclusion that the inclusion of such orbits do not affect significantly the orbital decay of the test star and that the local description given by Eq. (4.40) remains also accurate. Also, Zaritsky & White [ZW88], as well as Bontekoe & Van Albada [Bv87], found that the global responses in a large galaxy which are induced

by the presence of the test star are not dynamically important and that the decay of the orbit of the perturber can be adequately described by Eq. (4.40).

Although Chandrasekhar’s formula seems to work remarkably well in different situations, one major oversimplification is that it does not include the extension of the test particle. In this chapter we investigate the current analytical understanding of DF by including the extension of the perturber.

6.1 A wave-mechanical treatment

In this paper we present a rigorous calculation of the dynamical friction force exerted by an infinite homogenous background on a spherical massive body using the wave-mechanical method of [Mar68] and [19772]. We will present in more detail the work of Esquivel & Fuchs [EF07a]. This approach is topically closely related to studies of the exchange of angular and linear momentum in stellar systems ([LK72]; [Dek76]; [TW84]; [Fuc04]) or in plasmas [Sti62].

We assume an infinite homogenous distribution of field stars on isotropic straight-line orbits. The response of the system of background stars to the perturbation due to a massive perturber is determined by solving the linearized Boltzmann equation

$$\frac{\partial f_1}{\partial t} + \sum_{i=1}^3 v_i \frac{\partial f_1}{\partial x_i} - \frac{\partial \Phi_1}{\partial x_i} \frac{\partial f_0}{\partial v_i} = 0, \quad (6.1)$$

where Φ_1 denotes the gravitational potential of the perturber and f_1 is the induced perturbation of the distribution function of the field stars in phase space. The unperturbed distribution function is described by f_0 .

The solution of the Boltzmann equation is greatly facilitated by considering Fourier transforms of the perturbations of the distribution function and the potential, respectively,

$$f_{\omega, \mathbf{k}} \Phi_{\omega, k} \exp i[\omega t + \mathbf{k} \cdot \mathbf{x}], \quad (6.2)$$

where ω and \mathbf{k} denote the frequency and wave vector of the Fourier components. Without loss of generality the spatial coordinates x_i and the corresponding velocity components v_i can be oriented with one axis parallel to the direction of the wave vector. This treatment bears resemblance to the one described in chapter three where the response of a dark-matter halo to a small perturbation in the disk was tested. The Boltzmann equation (6.1)

takes then the form

$$\omega f_{\omega,\mathbf{k}} + vk f_{\omega,\mathbf{k}} - k\Phi_{\omega,\mathbf{k}} \frac{\partial f_0}{\partial v} = 0 \quad (6.3)$$

with $k = |\mathbf{k}|$ and v denoting the velocity component parallel to \mathbf{k} . Equation (6.3) has been integrated over the two velocity components perpendicular to \mathbf{k} . In the following we assume for the field stars always a Gaussian velocity distribution function, or specifically in eq. (6.3)

$$\frac{\partial f_0}{\partial v} = -\frac{v}{\sigma^2} \frac{n_b}{\sqrt{2\pi}\sigma} e^{-\frac{v^2}{2\sigma^2}}, \quad (6.4)$$

where n_b denotes the spatial density of the field stars. We find then the solution of the Fourier transformed Boltzmann equation

$$f_{\omega,\mathbf{k}} = -\frac{kv}{\omega + kv} \frac{n_b}{\sqrt{2\pi}\sigma^3} e^{-\frac{v^2}{2\sigma^2}} \Phi_{\omega,\mathbf{k}}. \quad (6.5)$$

Integrating Eq. (6.5) over the v -velocity leads to the density distribution of the induced polarization cloud. This has been calculated here without taking into account the self-gravity of the background medium. [Fuc04] has shown that in linear approximation the effects of self-gravity can be described by another linearized Boltzmann equation of the form of Eq. (6.1) where Φ_1 denotes then the gravitational potential of the density perturbation of the background medium. In a self-gravitating system the density perturbations are the sources of the potential perturbations so that the density - potential pair has to fulfill the Poisson equation.

The solution of the combined Boltzmann and Poisson equations describes simply the Jeans collapse of the background medium on scales larger than the Jeans length. In real stellar systems or dark haloes their Jeans length will be always larger than the size of the system, because otherwise the system would have collapsed to smaller sizes. Since the polarization cloud is contained within the system, self-gravity is not important for its dynamics.

6.2 Potentials of the perturbing bodies

For reference reasons we include in our analysis also the potential of a point mass (Eq. (5.1)), which moves with the velocity v_0 along the y -axis,

$$\Phi_1 = -\frac{Gm}{\sqrt{x^2 + (y - v_0 t)^2 + z^2}}. \quad (6.6)$$

Then we calculate its Fourier-Transform,

$$\begin{aligned}
\Phi_{\mathbf{k}} &= -\frac{1}{(2\pi)^3} \int_{-\infty}^{+\infty} dx \int_{-\infty}^{+\infty} dy \int_{-\infty}^{+\infty} dz \frac{Gm}{\sqrt{x^2 + (y - v_0 t)^2 + z^2}} \exp -i[\mathbf{k} \cdot \mathbf{x}] \\
&= -\frac{1}{(2\pi)^3} \int_{-\infty}^{+\infty} dx \int_{-\infty}^{+\infty} dy \int_{-\infty}^{+\infty} dz \frac{Gm}{\sqrt{x^2 + y^2 + z^2}} \exp -i[k_x x + k_y (y + v_0 t) + k_z z] \\
&= -\frac{1}{(2\pi)^3} \int_{-\infty}^{+\infty} d\xi \int_{-\infty}^{+\infty} d\eta \int_{-\infty}^{+\infty} d\zeta \frac{Gm}{\sqrt{\xi^2 + \eta^2 + \zeta^2}} e^{-i|\mathbf{k}|\xi} e^{-ik_y v_0 t} \\
&= -\frac{1}{(2\pi)^3} \int_{-\infty}^{+\infty} d\eta \int_{-\infty}^{+\infty} d\zeta 2Gm K_0(|\mathbf{k}| \sqrt{\eta^2 + \zeta^2}) e^{-ik_y v_0 t}, \tag{6.7}
\end{aligned}$$

where we have used formula (3.754) of Gradshteyn & Ryzhik [GR00] in the last step and where K_0 is a modified Bessel function of the second kind. We further reduce Eq. (6.7) by introducing polar coordinates (r, θ) and using formula (6.561) of the same book we obtain

$$\Phi_{\mathbf{k}} = -\frac{2Gm}{2\pi^2} \frac{1}{k^2} e^{-ik_y v_0 t}. \tag{6.8}$$

Next, we rewrite the potential of the Plummer sphere Eq. (5.10) as

$$\Phi_1 = -\frac{Gm}{\sqrt{r_0^2 + x^2 + (y - v_0 t)^2 + z^2}}, \tag{6.9}$$

which now includes the motion of the perturber along the y -axis. The Fourier transform of a moving Plummer sphere is given by

$$\begin{aligned}
\Phi_{\mathbf{k}} &= -\frac{1}{(2\pi)^3} \int_{-\infty}^{+\infty} dx \int_{-\infty}^{+\infty} dy \int_{-\infty}^{+\infty} dz \frac{Gm}{\sqrt{r_0^2 + x^2 + (y - v_0 t)^2 + z^2}} \exp -i[\mathbf{k} \cdot \mathbf{x}] \\
&= -\frac{1}{(2\pi)^3} \int_{-\infty}^{+\infty} d\eta \int_{-\infty}^{+\infty} d\zeta 2Gm K_0(|\mathbf{k}| \sqrt{r_0^2 + \eta^2 + \zeta^2}) e^{-ik_y v_0 t} \\
&= -\frac{2Gm}{(2\pi)^2} \int_0^{+\infty} dr K_0(|\mathbf{k}| \sqrt{r_0^2 + r^2}) e^{-ik_y v_0 t} \\
&= -\frac{2Gm}{(2\pi)^2} \left\{ \frac{1}{k^2} - r_0^2 \frac{\Gamma(1)}{r_0^2 k^2} + r_0^2 \frac{K_1(r_0 |\mathbf{k}|)}{r_0 |\mathbf{k}|} \right\}, \tag{6.10}
\end{aligned}$$

where $K_1(r_0 |\mathbf{k}|)$ denotes another modified Bessel function the second kind. The final form of the Fourier-Transform will be

$$\Phi_{\mathbf{k}} = -\frac{2Gm}{2\pi^2} \frac{r_0}{k} K_1(k r_0) e^{-ik_y v_0 t}. \tag{6.11}$$

As third example we consider a perturber which has the mass density distribution of a profile, whose gravitational potential is (cf. Eq. (5.8)),

$$\Phi(r) = -\frac{Gm}{r_0 + \sqrt{x^2 + (y - v_0 t)^2 + z^2}}. \quad (6.12)$$

We Fourier-Transform Eq. (6.12),

$$\begin{aligned} \Phi_{\mathbf{k}} &= -\frac{1}{(2\pi)^3} \int_{-\infty}^{+\infty} dx \int_{-\infty}^{+\infty} dy \int_{-\infty}^{+\infty} dz \frac{Gm}{r_0^2 + x^2 + (y - v_0 t)^2 + z^2} \exp -i[\mathbf{k} \cdot \mathbf{x}] \\ &= -\frac{Gm}{(2\pi)^3} \int_0^{2\pi} d\phi \int_0^\pi d\theta \int_0^\infty dr \frac{r^2}{r + r_0} \exp -i[k \cos \phi] \sin \phi \exp -i(k_y v_0 t) \\ &= -\frac{2Gm}{(2\pi)^2} \frac{1}{k} \int_0^\infty dr \frac{r}{r + r_0} \sin(kr) \exp -i(k_y v_0 t) \\ &= -\frac{2Gm}{(2\pi)^2} \frac{1}{k} \left(-\frac{\partial}{\partial k} \right) \int_0^\infty dr \frac{1}{r + r_0} \cos(kr) \exp -i(k_y v_0 t) \\ &= \frac{2Gm}{(2\pi)^2} \frac{1}{k} \frac{\partial}{\partial k} [-\sin(kr_0) \text{si}(kr_0) - \cos(kr_0) \text{ci}(kr_0)] \exp -i(k_y v_0 t), \quad (6.13) \end{aligned}$$

where si and ci denote the sine- and cosine-integrals, respectively and in the last step use of Eq. (3.722) of Grandshteyn & Ryzik [GR00] has been made. After some rearrngment of terms, we write the potential as

$$\Phi_{\mathbf{k}} = -\frac{2Gm}{(2\pi)^2} \frac{1}{k^2} [1 + kr_0 \cos(kr_0) \text{si}(kr_0) - kr_0 \sin(kr_0) \text{ci}(kr_0)] \exp -i(k_y v_0 t). \quad (6.14)$$

As stated in the previous chapter Plummer spheres have constant density cores, whereas numerical simulations of the formation of galactic haloes in cold dark matter cosmology show that dark haloes may have a central density cusp [NFW97]. Thus models of a Plummer or a Hernquist sphere should encompass the range of plausible models for satellite galaxies. The density in both models falls off radially steeper than found in the cold dark matter galaxy cosmogony simulations. The density in both models falls off radially steeper than found in the cold dark matter galaxy cosmogony simulations. This mimics the tidal truncation of satellite galaxies in the gravitational field of their parent galaxies.

6.3 Dynamical friction

In this section we follow the concept of Dekker [Dek76]. The ensemble of stars is accelerated by the moving perturber as

$$\langle \dot{\mathbf{v}} \rangle = - \int_{-\infty}^{+\infty} d^3x \int_{-\infty}^{+\infty} d^3v f(\mathbf{x}, \mathbf{v}) \nabla \Phi_1, \quad (6.15)$$

where f denotes the full distribution function $f = f_0 + f_1$. The contribution from the unperturbed distribution f_0 cancels out, and introducing the Fourier transforms (6.2) we find

$$\begin{aligned} \langle \dot{\mathbf{v}} \rangle = & - \int_{-\infty}^{+\infty} d^3x \int_{-\infty}^{+\infty} d^3v \int_{-\infty}^{+\infty} d^3k i\mathbf{k} \Phi_{\mathbf{k}} \exp i(\omega t + \mathbf{k} \cdot \mathbf{x}) \\ & \times \int_{-\infty}^{+\infty} d^3k' f_{\mathbf{k}'} \exp i(\omega' t + \mathbf{k}' \cdot \mathbf{x}). \end{aligned} \quad (6.16)$$

From symmetry reasons the acceleration vector $\langle \dot{\mathbf{v}} \rangle$ is expected to be oriented along the y -axis.

Then, using the definition of the delta function

$$\int_{-\infty}^{+\infty} d^3x \exp i\mathbf{x} \cdot (\mathbf{k} + \mathbf{k}') = \delta(\mathbf{k} + \mathbf{k}') (2\pi)^3, \quad (6.17)$$

Eq. (6.16) takes the form

$$\langle \dot{\mathbf{v}} \rangle = (2\pi)^3 \int_{-\infty}^{+\infty} d^3v \int_{-\infty}^{+\infty} d^3k i\mathbf{k} \Phi_{-\mathbf{k}} f_{\mathbf{k}'}. \quad (6.18)$$

The best way to find the solution is to express the potential as real components of the type $\Phi : 1/2[(\Phi_{\mathbf{k}} e^{i\omega t}, \Phi_{-\mathbf{k}} e^{-i\omega^* t}) + (\Phi_{\mathbf{k}}^* e^{-i\omega^* t}, \Phi_{-\mathbf{k}} e^{i\omega t})]$, and so with the solution of the Fourier-transformed Boltzmann Eq. (6.5) we will get

$$\Phi_{\mathbf{k}} e^{i\omega t} \Rightarrow - \frac{f_0}{\sigma^2} \frac{vk}{\omega + kv} \Phi_{\mathbf{k}} e^{i\omega t} \quad (6.19)$$

and

$$\Phi_{\mathbf{k}}^* e^{-i\omega^* t} \Rightarrow + \frac{f_0}{\sigma^2} \frac{vk}{-\omega^* - kv} \Phi_{\mathbf{k}}^* e^{-i\omega^* t}. \quad (6.20)$$

With Eqs. (6.19), (6.20) at hand, we bring the force formula in the form of

$$\begin{aligned} \langle \dot{\mathbf{v}} \rangle = & (2\pi)^3 \int_{-\infty}^{+\infty} dv \int_{-\infty}^{+\infty} d^3k i\mathbf{k} \frac{f_0}{\sigma^2} (\Phi_{-\mathbf{k}} e^{-i\omega^* t} + \Phi_{-\mathbf{k}}^* e^{i\omega t}) \\ & \times \frac{1}{4} \left[- \frac{vk}{\omega + kv} \Phi_{\mathbf{k}} e^{i\omega t} - \frac{vk}{-\omega^* - kv} \Phi_{\mathbf{k}}^* e^{-i\omega^* t} \right] \end{aligned} \quad (6.21)$$

In Eq. (6.21) the frequency ω is given according to Eqs. (6.8), (6.11) and (6.14) by $\omega = -k_y v_0 - i\lambda$ ($\omega_r = -k_y v_0$), where we follow Landau's rule, and introduce a negative imaginary part ($\lambda > 0$), which we will let go to zero in the following. We note that $\Phi_{-\mathbf{k}} = \Phi_{\mathbf{k}}^*$ must hold, so that the potential is a real quantity. The sum of the mixed terms $\Phi_{-\mathbf{k}} e^{-i\omega^* t} \Phi_{\mathbf{k}} e^{i\omega t} v / (\omega + kv)$ and $\Phi_{-\mathbf{k}}^* e^{i\omega t} \Phi_{\mathbf{k}}^* e^{-i\omega^* t} v / (\omega^* + kv)$ gives only the real term which is antisymmetric with respect to the integral over k and so this term vanishes. For the remaining two terms we have

$$\Phi_{-\mathbf{k}} e^{-i\omega^* t} \Phi_{\mathbf{k}}^* e^{-i\omega^* t} \frac{v}{\omega^* + kv} = |\Phi_{-\mathbf{k}}|^2 \frac{v e^{-i2\omega^* t}}{\omega^* + kv} = |\Phi_{-\mathbf{k}}|^2 \frac{v e^{2\lambda t}}{\omega^* + kv} \quad (6.22)$$

and

$$\Phi_{-\mathbf{k}}^* e^{i\omega t} \Phi_{\mathbf{k}} e^{i\omega t} \frac{v}{\omega + kv} = |\Phi_{\mathbf{k}}|^2 \frac{v e^{i2\omega t}}{\omega + kv} = |\Phi_{\mathbf{k}}|^2 \frac{v e^{2\lambda t}}{\omega + kv}. \quad (6.23)$$

Proceeding further, we multiply by 1 both equations

$$|\Phi_{-\mathbf{k}}|^2 \frac{v e^{2\lambda t}}{\omega^* + kv} \frac{\omega + kv}{\omega + kv} = |\Phi_{-\mathbf{k}}|^2 \frac{-v(\omega_r - i\lambda + kv)}{(\omega_r + kv)^2 + \lambda^2} \quad (6.24)$$

and

$$|\Phi_{\mathbf{k}}|^2 \frac{v e^{2\lambda t}}{\omega + kv} \frac{\omega^* + kv}{\omega^* + kv} = |\Phi_{\mathbf{k}}|^2 \frac{v(\omega_r + i\lambda + kv)}{(\omega_r + kv)^2 + \lambda^2} \quad (6.25)$$

and since the real part of these equations are antisymmetric with respect to the integral over k , only the imaginary part contribute with the term $2|\Phi_{\mathbf{k}}|^2 e^{2\lambda t} i v \lambda / (\omega_r + kv)^2 + \lambda^2$.

Next we observe that when we let it go to zero, the imaginary part satisfies

$$\lim_{\lambda \rightarrow 0} e^{2\lambda t} \frac{\lambda}{(k_y v_0 - kv)^2 + \lambda^2} = \pi \delta(kv - k_y v_0), \quad (6.26)$$

so that with the use of Eqs. (6.24), (6.25), and (6.26), Eq. (6.21) will look like

$$\begin{aligned} \langle \dot{\mathbf{v}} \rangle &= \frac{(2\pi)^{5/2} n_b}{\sigma^3} \int_{-\infty}^{+\infty} d^3 k \int_{-\infty}^{+\infty} dv |\Phi_{\mathbf{k}}|^2 k^2 e^{-\frac{(k_y v_0)^2}{2k^2 \sigma^2}} 2\pi v \delta(k_y v_0 + kv) \\ &= \frac{(2\pi)^{5/2} \pi n_b}{\sigma^3} \int_{-\infty}^{+\infty} d^3 k |\Phi_{\mathbf{k}}|^2 k_y v_0 e^{-\frac{(k_y v_0)^2}{2k^2 \sigma^2}}. \end{aligned} \quad (6.27)$$

The Fourier transform of any potential with spherical symmetry depends only on $k = |\mathbf{k}|$. Thus it follows immediately from eq. (6.27) that indeed the two acceleration components

$$\langle \dot{v}_x \rangle = \langle \dot{v}_z \rangle = 0 \quad (6.28)$$

as anticipated from symmetry reasons. Only in the direction of motion of the perturber there is a net effect.

We now evaluate the integrals over the wave vector components starting with the potential generated by a point mass. Inserting Eq. (6.8) into Eq. (6.27),

$$\begin{aligned} \langle \dot{v}_y \rangle = & \frac{(2\pi)^{5/2} \pi n_b}{\sigma^3} \int_{-\infty}^{+\infty} dk_x \int_{-\infty}^{+\infty} dk_y \int_{-\infty}^{+\infty} dk_z \frac{4G^2 m^2}{(2\pi)^4} \frac{1}{k^5} \\ & \times (k_x, k_y, k_z) k_y v_0 e^{-\frac{(k_y v_0)^2}{2k^2 \sigma^2}}. \end{aligned} \quad (6.29)$$

Next we introduce polar coordinates (θ, r) , and so we obtain

$$\begin{aligned} \langle \dot{v}_y \rangle = & 2 \frac{G^2 m^2 n_b}{\sqrt{2\pi} \sigma^3} \int_{-\infty}^{+\infty} dk_y k_y^2 v_0 \int_0^{+\infty} dr 2\pi r \\ & \times \frac{1}{\sqrt{k_y^2 + r^2}^5} \exp\left(-\frac{(k_y v_0)^2}{2(k_y^2 + r^2)\sigma^2}\right), \end{aligned} \quad (6.30)$$

and we make an appropriate substitution of variables,

$$x^2 = \frac{1}{k_y^2 + r^2}, \quad 2x dx = -\frac{2r dr}{(k_y^2 + r^2)^2}. \quad (6.31)$$

And we substitute for x ,

$$\begin{aligned} \langle \dot{v}_y \rangle = & -2 \frac{\sqrt{2\pi} G^2 m^2 n_b}{\sigma^3} \int_{-\infty}^{+\infty} dk_y k_y^2 v_0 \int_{1/|k_y|}^0 dx \frac{x}{\sqrt{k_y^2 + r^2}} \\ & \times \exp\left(-\frac{(k_y v_0)^2 x^2}{2\sigma^2}\right). \end{aligned} \quad (6.32)$$

To carry out the integration over x we integrate by parts,

$$\begin{aligned}
\langle \dot{\mathbf{v}}_{\mathbf{y}} \rangle &= 2 \frac{\sqrt{2\pi} G^2 m^2 n_b}{\sigma^3} \int_{-\infty}^{+\infty} dk_y k_y^2 v_0 \left[x \left(-\frac{2\sigma^2}{2k_y^2 v_0^2} \right) \exp \left(-\frac{(k_y v_0)^2 x^2}{2\sigma^2} \right) \right]_0^{1/|k_y|} \\
&\quad - \int_0^{1/|k_y|} dx \left(-\frac{2\sigma^2}{2k_y^2 v_0^2} \right) \exp \left(-\frac{(k_y v_0)^2 x^2}{2\sigma^2} \right) \\
&= -4 \frac{\sqrt{2\pi} G^2 m^2 n_b}{\sigma^3} \left(\frac{\sigma^2}{k_y^2 v_0^2} \right) \int_0^{+\infty} dk_y k_y^2 v_0 \left\{ \left(\frac{1}{|k_y|} \right) \exp \left(-\frac{v_0^2}{2\sigma^2} \right) \right. \\
&\quad \left. - \frac{\sqrt{2}\sigma}{|k_y v_0|} \int_0^{\frac{\sqrt{2}\sigma|k_y|}{|k_y v_0|}} dx e^{-x^2} \right\} \\
&= -4 \frac{\sqrt{2\pi} G^2 m^2 n_b}{v_0 \sigma} \int_0^{+\infty} dk_y \left\{ \frac{1}{|k_y|} \exp \left(-\frac{v_0^2}{2\sigma^2} \right) - \frac{\sqrt{2}\sigma}{|k_y v_0|} \frac{\sqrt{\pi}}{2} \operatorname{erf} \left(\frac{v_0}{\sqrt{2}\sigma} \right) \right\}, \tag{6.33}
\end{aligned}$$

where we erf denotes the usual error function.

Next we observe that

$$\begin{aligned}
\langle \dot{\mathbf{v}}_{\mathbf{y}} \rangle &= 4\sqrt{2\pi} G^2 m^2 n_b \sqrt{\frac{\pi}{2}} \frac{1}{v_0^2} \left[\operatorname{erf} \left(\frac{v_0}{\sqrt{2}\sigma} \right) \right. \\
&\quad \left. - \sqrt{\frac{2}{\pi}} \frac{v_0}{\sigma} \exp \left(-\frac{v_0^2}{2\sigma^2} \right) \right] \int_0^{+\infty} dk_y \frac{1}{k_y}, \tag{6.34}
\end{aligned}$$

the integral over k_y diverges, showing the same behaviour as Chandrasekhar's Eq. (4.40). If we consider then a bit different Coulomb logarithm $\ln(\Lambda)$, we can rewrite Eq. (6.33) as

$$\langle \dot{\mathbf{v}}_{\mathbf{y}} \rangle = \frac{4\pi G^2 m^2 n_b}{v_0^2} \left[\operatorname{erf} \left(\frac{v_0}{\sqrt{2}\sigma} \right) - \frac{2}{\sqrt{\pi}} \frac{v_0}{\sqrt{2}\sigma} \exp \left(-\frac{v_0^2}{2\sigma^2} \right) \right] \ln \left(\frac{k_{y\max}}{k_{y\min}} \right). \tag{6.35}$$

According to Newton's third law the drag force exerted on the perturber is given by $m\dot{v} = -m_b \langle \dot{v}_y \rangle$ where m_b is the mass of a background particle, so that the drag force is anti-parallel to the velocity of the perturber. Therefore the drag experienced by the perturber is

$$\langle \dot{\mathbf{v}} \rangle = -\frac{4\pi G^2 m^2 n_b}{v_0^2} \ln \left(\frac{k_{y,\max}}{k_{y,\min}} \right) \left[\operatorname{erf} \left(\frac{v_0}{\sqrt{2}\sigma} \right) - \frac{2}{\sqrt{\pi}} \frac{v_0}{\sqrt{2}\sigma} \exp \left(-\frac{v_0^2}{2\sigma^2} \right) \right]. \tag{6.36}$$

This result was first obtained in this form by Kalnajs [19772] and is identical to Chandrasekhar's formula (4.40), if $m + m_b \approx m$. The Coulomb logarithm

diverges in the familiar way both on small and large scales, i.e. at k_{\max}^{-1} and k_{\min}^{-1} , respectively.

Now we evaluate the case of the Plummer sphere. We put Eq. (6.11) into Eq. (6.27) and obtain

$$\begin{aligned} \langle \dot{\mathbf{v}}_{\mathbf{y}} \rangle = & \frac{(2\pi)^{5/2}\pi n_b}{\sigma^3} \int_{-\infty}^{+\infty} dk_x \int_{-\infty}^{+\infty} dk_y \int_{-\infty}^{+\infty} dk_z \frac{4G^2 m^2 r_0^2}{(2\pi)^4 k^3} K_1^2(kr_0) \\ & \times (k_x, k_y, k_z) k_y v_0 e^{-\frac{(k_y v_0)^2}{2k^2 \sigma^2}}, \end{aligned} \quad (6.37)$$

we then introduce polar coordinates as done before and we find

$$\begin{aligned} \langle \dot{\mathbf{v}}_{\mathbf{y}} \rangle = & \frac{2G^2 m^2 n_b}{\sqrt{2\pi}\sigma^3} \int_{-\infty}^{+\infty} dk_y k_y^2 v_0 \int_0^{+\infty} dr 2\pi r \frac{r_0^2}{\sqrt{k_y^2 + r^2}^3} K_1^2(kr_0) \\ & \times \exp\left(-\frac{(k_y v_0)^2}{2(k_y^2 + r^2)\sigma^2}\right). \end{aligned} \quad (6.38)$$

The solution of the two remaining integrals is best done by making the transformation of coordinates $k'_y = k_y$, $k' = \sqrt{k_y^2 + r^2} = k$, with $dk'_y dk' = r dk_y dr / \sqrt{k_y^2 + r^2}$. Eq. (6.38) takes the form

$$\begin{aligned} \langle \dot{\mathbf{v}}_{\mathbf{y}} \rangle = & 4\sqrt{2\pi} \frac{G^2 m^2 n_b r_0^2}{\sigma^3} v_0 \int_0^{+\infty} dk_y k_y^2 \int_{k_y}^{+\infty} dk \frac{\sqrt{k_y^2 + r^2}}{\sqrt{k_y^2 + r^2}^3} K_1^2(r_0 \sqrt{k_y^2 + r^2}) \\ & \times \exp\left(-\frac{(k_y v_0)^2}{2(k_y^2 + r^2)\sigma^2}\right). \\ = & 4\sqrt{2\pi} \frac{G^2 m^2 n_b r_0^2}{\sqrt{2\pi}\sigma^3} v_0 \int_0^{+\infty} dk_y k_y^2 \int_{k_y}^{+\infty} dk \frac{1}{k^2} K_1^2(r_0 k) \\ & \times \exp\left(-\frac{(k_y v_0)^2}{2k^2 \sigma^2}\right). \end{aligned} \quad (6.39)$$

One can see that the Bessel function depends only on the variable k ; having this in mind Eq. (6.39) takes a simpler form if we change the limits of integration

$$\begin{aligned} \langle \dot{\mathbf{v}}_{\mathbf{y}} \rangle = & 4\sqrt{2\pi} \frac{G^2 m^2 n_b r_0^2}{\sqrt{2\pi}\sigma^3} v_0 \int_0^{+\infty} dk \frac{1}{k^2} \int_0^k dk_y k_y^2 K_1^2(r_0 k) \\ & \times \exp\left(-\frac{(k_y v_0)^2}{2k^2 \sigma^2}\right), \end{aligned} \quad (6.40)$$

and integrate by parts, obtaining

$$\begin{aligned}
\langle \dot{\mathbf{v}}_y \rangle &= 4 \frac{\sqrt{2\pi} G^2 m^2 n_b}{\sigma^3} v_0 \int_0^{+\infty} dk \left[k_y \left(-\frac{2\sigma^2}{2k^2 v_0^2} \right) \exp \left(-\frac{(k_y v_0)^2}{2k^2 \sigma^2} \right) \right]_0^k \\
&\quad - \int_0^k dk_y \left(-\frac{2\sigma^2}{2k^2 v_0^2} \right) \exp \left(-\frac{(k_y v_0)^2}{2k^2 \sigma^2} \right) K_1^2(r_0 k) \\
&= -\frac{4\sqrt{2\pi} G^2 m^2 n_b}{\sigma^3} \left(\frac{\sigma^2}{k^2 v_0^2} \right) v_0 \int_0^{+\infty} dk \left\{ \exp \left(-\frac{(k_y v_0)^2 k^2}{2k^2 \sigma^2} \right) \right. \\
&\quad \left. - \sqrt{\frac{\pi}{2}} \operatorname{erf} \left(\frac{v_0 k}{\sqrt{2}\sigma k} \right) \right\} K_1^2(r_0 k) \\
&= \frac{4\sqrt{2\pi} G^2 m^2 n_b}{\sigma^3} \left(\frac{\sigma^2}{k^2 v_0} \right) \left\{ \operatorname{erf} \left(\frac{v_0}{\sqrt{2}\sigma} \right) \right. \\
&\quad \left. - \frac{2}{\sqrt{\pi}} \frac{v_0}{\sqrt{2}\sigma} \exp \left(-\frac{v_0^2}{2\sigma^2} \right) \right\} r_0^2 \int_0^{+\infty} dk k K_1^2(r_0 k) \\
&= 4\sqrt{2\pi} G^2 m^2 n_b r_0^2 \sqrt{\frac{\pi}{2}} \frac{1}{v_0^2} \left\{ \operatorname{erf} \left(\frac{v_0}{\sqrt{2}\sigma} \right) \right. \\
&\quad \left. - \sqrt{\frac{2}{\pi}} \frac{v_0}{\sigma} \exp \left(-\frac{v_0^2}{2\sigma^2} \right) \right\} r_0^2 \int_0^{+\infty} dk k K_1^2(r_0 k). \tag{6.41}
\end{aligned}$$

The DF force for exerted on a Plummer sphere has the final form

$$\begin{aligned}
\langle \dot{\mathbf{v}} \rangle &= -\frac{4\pi G^2 m^2 n_b}{v_0^2} \left[\operatorname{erf} \left(\frac{v_0}{\sqrt{2}\sigma} \right) - \frac{2}{\sqrt{\pi}} \frac{v_0}{\sqrt{2}\sigma} \exp \left(-\frac{v_0^2}{2\sigma^2} \right) \right] \\
&\quad \times r_0^2 \int_0^{+\infty} dk k K_1^2(r_0 k). \tag{6.42}
\end{aligned}$$

And we identify the Coulomb logarithm of the dynamical friction force exerted on a Plummer sphere as

$$\ln(\Lambda) = r_0^2 \int_{k_{\min}}^{\infty} dk k K_1^2(r_0 k). \tag{6.43}$$

If the Plummer radius r_0 shrinks to zero, expression (6.44) changes smoothly into the Coulomb logarithm of a point mass, because $\lim_{r_0 \rightarrow 0} r_0 K_1(r_0 k) = k^{-1}$. The integral over the square of the Bessel functions in Eq. (6.44) can be evaluated using formula (5.54) of Gradshteyn & Ryzhik [GR00].

$$\ln(\Lambda) = -\frac{r_0^2 k_{\min}^2}{2} [K_1^2(r_0 k_{\min}) - K_0(r_0 k_{\min}) K_2(r_0 k_{\min})] \tag{6.44}$$

which is approximately

$$\ln(\Lambda) \approx -\frac{1}{2} - \ln(r_0 k_{\min}), \quad (6.45)$$

in the limit of $r_0 k_{\min} \ll 1$. This modified Coulomb logarithm converges on small scales precisely as found by [Whi76], but still diverges on large scales. A natural cut-off will be then the size of the stellar system under consideration.

Finally, as a third example we insert the potential given by Eq. (6.14)

$$\begin{aligned} \langle \dot{\mathbf{v}}_{\mathbf{y}} \rangle &= \frac{(2\pi)^{5/2} n_b}{\sigma^3} \int_{-\infty}^{+\infty} dk_x \int_{-\infty}^{+\infty} dk_y \int_{-\infty}^{+\infty} dk_z \frac{4G^2 m^2}{(2\pi)^4} \frac{1}{k^3} \\ &\times k_y^2 v_0 \left[\frac{1}{k} + r_0 \cos(kr_0) \text{si}(kr_0) - r_0 \sin(kr_0) \text{ci}(kr_0) \right]^2 e^{-\frac{(k_y v_0)^2}{2k^2 \sigma^2}}. \end{aligned} \quad (6.46)$$

Introducing polar coordinates (θ, r) we get Eq. (6.46) into the form

$$\begin{aligned} \langle \dot{\mathbf{v}}_{\mathbf{y}} \rangle &= \frac{2G^2 m^2 n_b}{\sqrt{2\pi} \sigma^3} \int_{-\infty}^{+\infty} dk_y k_y^2 v_0 \int_0^{+\infty} dr 2\pi r \frac{1}{k^3} \left[\frac{1}{k} + r_0 \cos(kr_0) \text{si}(kr_0) \right. \\ &\quad \left. - r_0 \sin(kr_0) \text{ci}(kr_0) \right]^2 \exp\left(-\frac{(k_y v_0)^2}{2\sigma^2(k_y^2 + r^2)}\right) \end{aligned} \quad (6.47)$$

And we use again the transformation $k'_y = k_y$, $k' = \sqrt{k_y^2 + r^2} = k$, with $dk'_y dk' = r dk_y dr / \sqrt{k_y^2 + r^2}$, and the formula will look like

$$\begin{aligned} \langle \dot{\mathbf{v}}_{\mathbf{y}} \rangle &= 2\sqrt{2\pi} \frac{4G^2 m^2 n_b}{\sigma^3} \int_{-\infty}^{+\infty} dk_y k_y^2 v_0 \int_{k_y}^{+\infty} dk \frac{\sqrt{k_y^2 + r^2}}{\sqrt{k_y^2 + r^2}^3} \left[\frac{1}{k} \right. \\ &\quad \left. + r_0 \cos(kr_0) \text{si}(kr_0) - r_0 \sin(kr_0) \text{ci}(kr_0) \right]^2 \exp\left(-\frac{(k_y v_0)^2}{2\sigma^2(k_y^2 + r^2)}\right) \\ &= 4\sqrt{2\pi} \frac{G^2 m^2 n_b r_0^2}{\sqrt{2\pi} \sigma^3} v_0 \int_0^{+\infty} dk_y k_y^2 \int_{k_y}^{+\infty} dk \frac{1}{k^2} \left[\frac{1}{k} \right. \\ &\quad \left. + r_0 \cos(kr_0) \text{si}(kr_0) - r_0 \sin(kr_0) \text{ci}(kr_0) \right]^2 \exp\left(-\frac{(k_y v_0)^2}{2\sigma^2 k^2}\right). \end{aligned} \quad (6.48)$$

Changing the limits of integration we find

$$\begin{aligned} \langle \dot{\mathbf{v}}_{\mathbf{y}} \rangle &= 4\sqrt{2\pi} \frac{G^2 m^2 n_b r_0^2}{\sqrt{2\pi} \sigma^3} v_0 \int_0^{+\infty} dk \frac{1}{k^2} \int_0^k dk_y k_y^2 \left[\frac{1}{k} + r_0 \cos(kr_0) \text{si}(kr_0) \right. \\ &\quad \left. - r_0 \sin(kr_0) \text{ci}(kr_0) \right]^2 \exp\left(-\frac{(k_y v_0)^2}{2k^2 \sigma^2}\right). \end{aligned} \quad (6.49)$$

The solution is found by integrating by parts, thus obtaining

$$\begin{aligned}
\langle \dot{\mathbf{v}}_{\mathbf{y}} \rangle &= 4 \frac{\sqrt{2\pi} G^2 m^2 n_b}{\sigma^3} v_0 \int_0^{+\infty} dk \left[k_y \left(-\frac{2\sigma^2}{2k^2 v_0^2} \right) \exp \left(-\frac{(k_y v_0)^2}{2k^2 \sigma^2} \right) \right]_0^k \\
&\quad - \int_0^k dk_y \left(-\frac{2\sigma^2}{2k^2 v_0^2} \right) \exp \left(-\frac{(k_y v_0)^2}{2k^2 \sigma^2} \right) \left[\frac{1}{k} + r_0 \cos(kr_0) \text{si}(kr_0) \right. \\
&\quad \left. - r_0 \sin(kr_0) \text{ci}(kr_0) \right]^2 \\
&= -\frac{4\sqrt{2\pi} G^2 m^2 n_b}{\sigma^3} \left(\frac{\sigma^2}{k^2 v_0^2} \right) v_0 \int_0^{+\infty} dk \left\{ \exp \left(-\frac{(k_y v_0)^2 k^2}{2k^2 \sigma^2} \right) \right. \\
&\quad \left. - \sqrt{\frac{\pi}{2}} \text{erf} \left(\frac{v_0 k}{\sqrt{2}\sigma k} \right) \right\} \left[\frac{1}{k} + r_0 \cos(kr_0) \text{si}(kr_0) \right. \\
&\quad \left. - r_0 \sin(kr_0) \text{ci}(kr_0) \right]^2 \\
&= \frac{4\sqrt{2\pi} G^2 m^2 n_b}{\sigma^3} \left(\frac{\sigma^2}{k^2 v_0} \right) \left\{ \text{erf} \left(\frac{v_0}{\sqrt{2}\sigma} \right) \right. \\
&\quad \left. - \frac{2}{\sqrt{\pi}} \frac{v_0}{\sqrt{2}\sigma} \exp \left(-\frac{v_0^2}{2\sigma^2} \right) \right\} r_0^2 \int_0^{+\infty} dk \left[\frac{1}{k} + r_0 \cos(kr_0) \text{si}(kr_0) \right. \\
&\quad \left. - r_0 \sin(kr_0) \text{ci}(kr_0) \right]^2 \\
&= 4\sqrt{2\pi} G^2 m^2 n_b r_0^2 \sqrt{\frac{\pi}{2}} \frac{1}{v_0^2} \left\{ \text{erf} \left(\frac{v_0}{\sqrt{2}\sigma} \right) \right. \\
&\quad \left. - \sqrt{\frac{2}{\pi}} \frac{v_0}{\sigma} \exp \left(-\frac{v_0^2}{2\sigma^2} \right) \right\} r_0^2 \int_0^{+\infty} dk \left[\frac{1}{k} + r_0 \cos(kr_0) \text{si}(kr_0) \right. \\
&\quad \left. - r_0 \sin(kr_0) \text{ci}(kr_0) \right]^2 \tag{6.50}
\end{aligned}$$

The drag on a body having a density distribution of a Hernquist profile is

$$\begin{aligned}
\langle \dot{\mathbf{v}} \rangle &= -\frac{4\pi G^2 m^2 n_b}{v_0^2} \left[\text{erf} \left(\frac{v_0}{\sqrt{2}\sigma} \right) - \frac{2}{\sqrt{\pi}} \frac{v_0}{\sqrt{2}\sigma} \exp \left(-\frac{v_0^2}{2\sigma^2} \right) \right] \\
&\quad \times r_0^2 \int_0^{+\infty} dk \left[\frac{1}{k} + r_0 \cos(kr_0) \text{si}(kr_0) - r_0 \sin(kr_0) \text{ci}(kr_0) \right]^2. \tag{6.51}
\end{aligned}$$

Accordingly, we identify its Coulomb logarithm

$$\ln(\Lambda) = r_0^2 \int_{k_{\min}}^{\infty} dk \frac{1}{k} [1 + r_0 k \cos(kr_0) \text{si}(kr_0) - r_0 k \sin(kr_0) \text{ci}(kr_0)]^2. \tag{6.52}$$

Using the asymptotic expansions of the sine- and cosine-integrals (5.2.6) given by Abramowitz & Stegun [AS72] the integrand in expression (6.52)

takes the form

$$\begin{aligned}
& \frac{1}{k} \left[1 - r_0 k \frac{1}{r_0 k} \left(1 - \frac{2}{r_0^2 k^2} \right) \right]^2 \\
& \Rightarrow \frac{1}{k} \left(\frac{2}{r_0^2 k^2} \right)^2 = \frac{4}{r_0^4 k^5} \\
& \Rightarrow \int dk \frac{1}{k^5} \rightarrow 0.
\end{aligned} \tag{6.53}$$

at large k . Thus the Coulomb logarithm converges at small scales. This is expected because, although the density distribution has an inner density cusp, the deflecting mass ‘seen’ by a field star with a small impact parameter scales with square of the impact parameter.

At small wave numbers a Taylor expansion shows that

$$\begin{aligned}
\frac{1}{k} \left[1 + r_0 k \left(1 - \frac{k^2 r_0^2}{2} \right) \left(-\frac{\pi}{2} + r_0 k \right) - r_0 k \left(1 - \ln(r_0 k) - \frac{r_0^2 k^2}{4} \right) \right]^2 & \Rightarrow \frac{1}{k} \rightarrow \infty \\
& \text{which implies} \\
& \int dk \frac{1}{k} = \ln(k) \tag{6.54}
\end{aligned}$$

so the square bracket in expression (6.52) approaches 1 so that we find a logarithmic divergence of the Coulomb logarithm as in the case of the Plummer sphere.

6.4 Discussion and Conclusions

In Fig. (6.1) we illustrate the Coulomb logarithms of the Plummer sphere and a sphere with a Hernquist density distribution according to Eqs. (6.43) and (6.52) as function of $r_0 k_{\min}$. Fig. (6.1) shows clearly that at given mass small sized perturbers experience a stronger dynamical friction force than larger ones. Since the cut-off of the wave number at k_{\min} is determined by the radial extent of the stellar system, which corresponds roughly to one half of the largest subtended wave length $\lambda_{\max} = 2\pi/k_{\min}$, we use actually $r_0/(\lambda_{\max}/4)$ as abscissa in Fig. (6.1). For comparison we have also drawn $-\ln(r_0 k_{\min})$ in Fig. (6.1). The insert shows the cumulative mass distributions of both mass models. The half mass radius of the Hernquist model measured in units of r_0 is about twice as that of the Plummer sphere. Thus for a proper comparison of the drag forces exerted on a Plummer sphere and a sphere with a Hernquist density profile the dashed line in Fig. (6.1) should be stretched by a factor of about 2 towards the right. But it is clear from

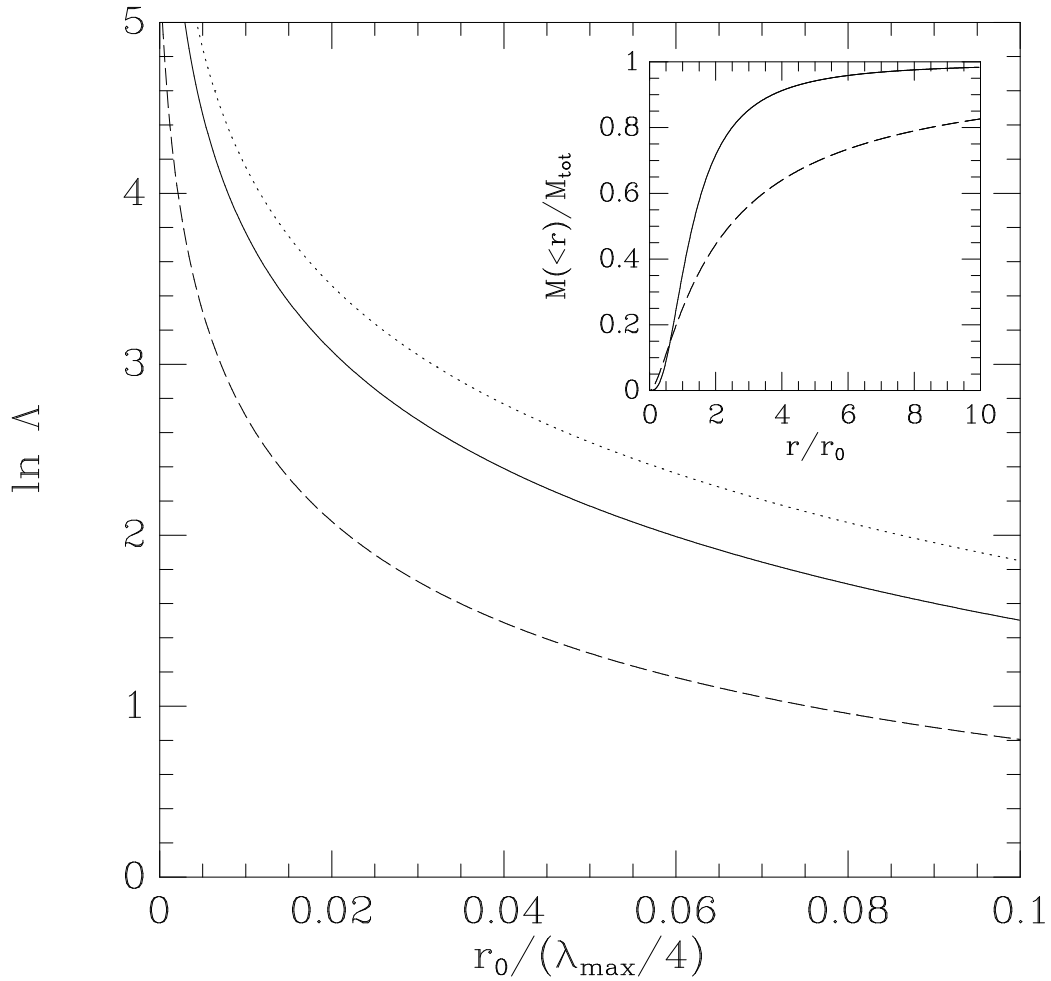


Figure 6.1: Coulomb logarithms of the Plummer sphere (solid line), and a sphere with a Hernquist density profile (dashed line). The dotted line indicates $-\ln(2\pi r_0 / \lambda_{\max})$. r_0 denotes the radial scale lengths of the spheres and λ_{\max} is the upper cut-off of the wavelength of the density perturbations (see text). The inset shows the cumulative mass distributions of the Plummer and Hernquist models.

Fig. (6.1) that the drag force exerted on a Plummer is always larger than the drag on a sphere with a Hernquist density profile. This is to be expected because of its shallower density profile. The logarithm $-\ln(r_0 k_{\min})$, although being the asymptotic expansion of the Coulomb logarithms (6.43) and (6.52) for $r_0 k_{\min} \rightarrow 0$, is not a good approximation at larger $r_0 k_{\min}$. There is a systematic off-set relative to the true Coulomb logarithms which is given explicitly in Eq. (6.45) for the case of the Plummer sphere.

So far we have treated the moving perturbers as rigid bodies. In reality, perturbers can be deformed by tidal fields. One source of the tidal field is the induced polarization cloud itself. However, its effect is expected to be small. The moving perturber induces the polarization cloud in the background medium which reacts back on the perturber. Thus the dynamical friction force and any tidal fields exerted by the polarization cloud is of the order G^2 (cf. Eq. 6.36). The deformation of the perturber can be viewed as mass excesses and deficiencies. The momentum imparted by these ‘extra’ masses to the particles of the background medium will be of the order of G^3 and can be safely considered as a higher order effect.

There is a further effect if the perturbers are gravitationally bound systems themselves like globular clusters or dwarf satellite galaxies. Such objects can and do lose mass due to tidal shocking. This mass loss is primarily driven by tidal shocking due to the shrinking of the tidal radii at the inner pericenters of the orbits of the perturbing objects or by disc shocking when they pass through the galactic disc ([GO97]; [GHO99]). Many studies, which cannot be all enumerated here, have shown that mass loss, which reduces dynamical friction, plays thus an important role for the evolution of the orbits of the satellite galaxies. In order to illustrate the effect of mass loss, on one hand, and the effect of a finite size of the perturber, on the other hand, we show in Fig. (6.2) the variation of the deceleration by dynamical friction exerted on a Plummer sphere as function of the mass m and the radial scale length r_0 . As can be seen from the contour plot in Fig. (6.2) both effects can be of comparable magnitude. If one considers, for example, a perturber with a scale length of 0.01 ($\lambda_{\max}/4$), a doubling of its size has the same effect as a mass loss of 18 percent of the original mass.

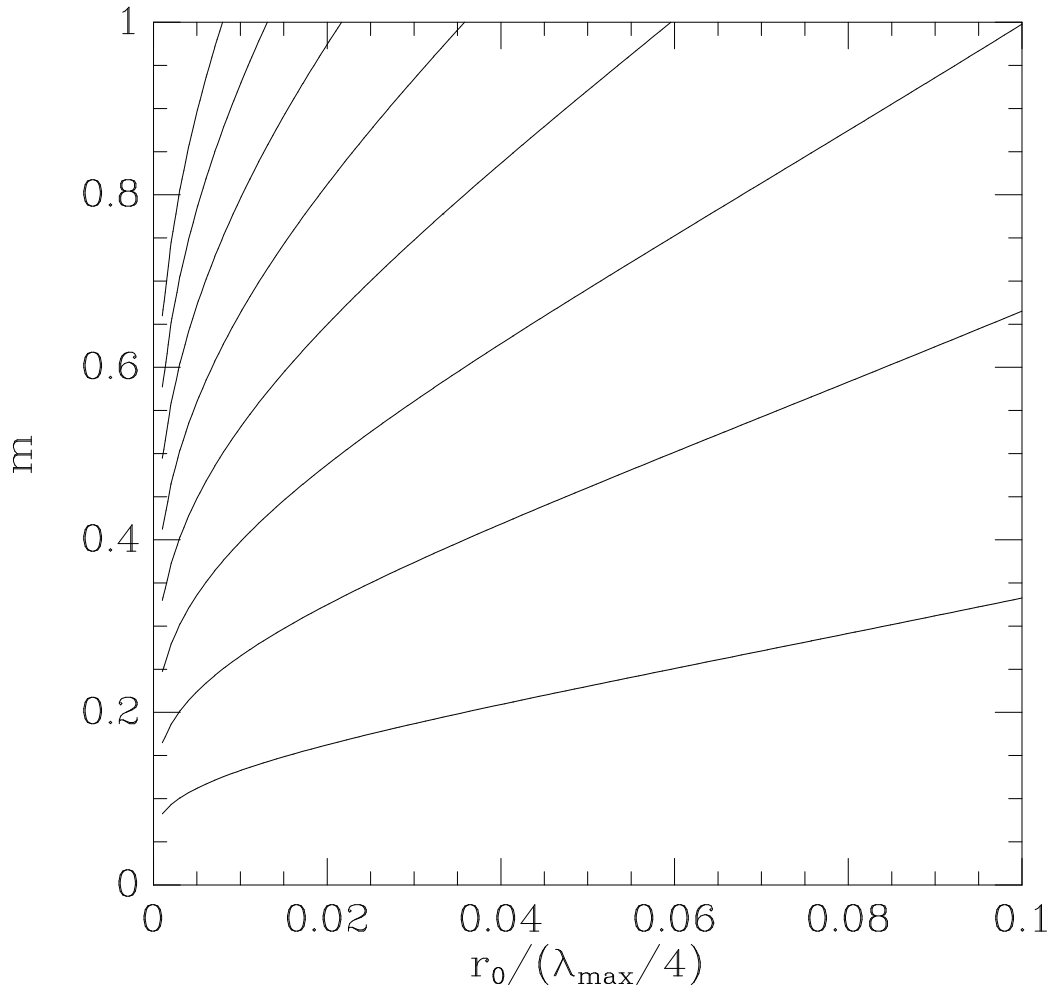


Figure 6.2: Contour plot of $m \cdot \ln\Lambda$ for a Plummer sphere. The mass m is given in arbitrary units. The contour levels span the range from 0.5 to 4 at equidistant intervals of 0.5.

Chapter 7

The role of an anisotropic velocity distribution in DF

The linear momentum exchange with DF has been studied in a vast literature on many aspects of it. However, analytical progress on the subject has been scarce ([Mar68]; [19772]; [Bin77]), with the recent calculation of the drag force exerted on extended bodies [EF07a], explained in the previous chapter.

In the beginning of chapter six it was mentioned that although the DF formula (4.40) suffers from a lot of oversimplifications such as the homogeneity of the distribution of the sea of particles and the infinite extension of the system they form, these assumptions remain valid to first order. However, since observational studies suggest that systems such as elliptical galaxies and clusters of galaxies have a non-spherical shape, it becomes important to ask what is the effect behind this non-sphericity. One physical explanation could be the rotation of the system itself, although observational and theoretical studies of many elliptical systems have shown that these systems are not supported by rotation ([BC75]; [Ill77]; [Bin78]; [Bin05]; [KBC⁺08]). An alternative explanation is due to orbital anisotropy [Bin76]. Which seems to be the correct explanation due to the recent study of lenticular galaxies conducted by the SAURON project [CEB⁺07]. The non-spherical appearance of the system is due to the flattening of the velocity ellipsoid.

Also, in the dark-matter context, it is believed from state-of-the-art numerical simulations of dark-halo formation that the velocity distribution of the particles in the halo is anisotropic [cf. KAPG08]. Actually, the degree of anisotropy could be moderate [ANS06] or significant [TB05]. Having this in mind, we explore in this chapter the role this anisotropic equilibria could have on the dynamical evolution of the satellites orbiting the system.

In this respect, Binney [Bin77] has been the only one to take one step further the treatment to have obtained an analytical expression for DF that

incorporates an anisotropic velocity distribution function for the field particles; having been tested numerically to work remarkably well in flattened systems [PJK04], although it is observed a progressive reduction of the orbit's ellipticity not found in the N-body calculations.

The mode analysis applied in the previous chapter is now used to explore the effect an anisotropic velocity distribution has on the net dynamical drag exerted on a point-mass satellite. Fuchs & Athanassoula [FA05] have shown that, if the velocity ellipsoid is either prolate or oblate, the velocity dispersion in the solution of the Boltzmann equation (6.5) is replaced by an effective velocity dispersion which depends on the semi-axes of the velocity ellipsoid and its orientation relative to the wave vector \mathbf{k} . This complicates the evaluation of the integrals with respect to the wave numbers in eq. (6.27) considerably.

7.1 The effective velocity dispersion

Let us start by writing the Gaussian velocity distribution function for the sea particles

$$f_0 = \frac{n_b}{\sqrt{2\pi}^3 \sigma^3} \exp - \left(\frac{u^2}{2\sigma^2} + \frac{v^2}{2\sigma^2} + \frac{w^2}{2\sigma^2} \right), \quad (7.1)$$

which for an anisotropy distribution will take the form (see Figs. (7.1), (7.2)),

$$f_0 = \frac{n_b}{\sqrt{2\pi}^3 \sigma_u \sigma_v \sigma_w} \exp - \left(\frac{u^2}{2\sigma_u^2} + \frac{v^2}{2\sigma_v^2} + \frac{w^2}{2\sigma_w^2} \right), \quad (7.2)$$

where v and w are the planar velocity components of the system, for example, a galaxy, cluster or halo. The velocity component perpendicular to this plane is denoted by u . We introduce again Cartesian coordinates (ξ, η, ζ) and align the ξ -axis with the wave vector \mathbf{k} of the Fourier-transformed distribution function $f_{h\mathbf{k}}$.

For technical reasons we assume $\sigma_v = \sigma_w$, which will leave Eq. (7.2) with a symmetry on v . With this choice we can now align, without loss of generality, one of the coordinates perpendicular to \mathbf{k} with the v component that is parallel to the k_y -axis along which the particle travels with velocity v_0 . Therefore, if we carry out the integration of Eq. (7.2) over v we obtain

$$\int_{-\infty}^{+\infty} f_0 dv = f_0(u, w) \frac{1}{\sqrt{2\pi}\sigma_v} \int_{-\infty}^{+\infty} \exp - \left(\frac{v^2}{2\sigma_v^2} \right) dv = f_0(u, w). \quad (7.3)$$

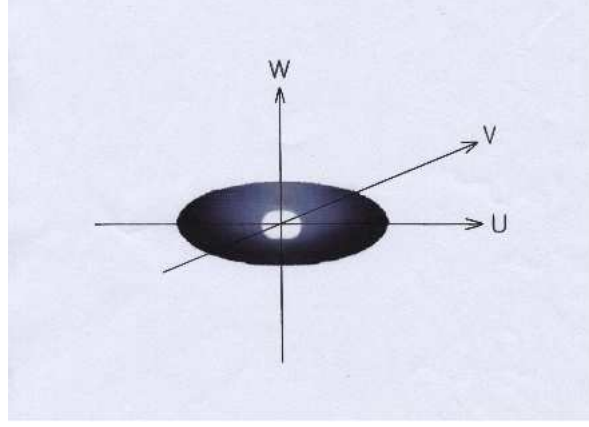


Figure 7.1: Velocity ellipsoid describing an anisotropic velocity distribution. Following the treatment developed in chapter 6, the particle is traveling with velocity v_0 along the k_y -axis which is parallel to the v -velocity component.

And so the contribution from the v component has been taken into account. Next, based on the geometry of the problem (cf. Fig. (7.2)), we express the distribution function as

$$f_0 = \frac{n_b}{2\pi\sigma_u\sigma_w} \exp - \left(\frac{(v_{\parallel} \cos \alpha + v_{\perp} \sin \alpha)^2}{2\sigma_u^2} + \frac{(v_{\parallel} \sin \alpha + v_{\perp} \cos \alpha)^2}{2\sigma_w^2} \right), \quad (7.4)$$

where v_{\perp} is the second velocity component perpendicular to the wave vector \mathbf{k} and v_{\parallel} is the velocity component parallel to it. The angle between the wave vector and the u -axis is denoted by α (Fig. (7.2)). We rewrite Eq. (7.4) as

$$f_0 = \frac{n_b}{2\pi\sigma_u\sigma_w} \exp - \left(\frac{v_{\parallel}^2 \cos^2 \alpha - 2v_{\parallel}v_{\perp} \cos \alpha \sin \alpha + v_{\perp}^2 \sin^2 \alpha}{2\sigma_u^2} \right) \\ \times \exp - \left(\frac{v_{\parallel}^2 \sin^2 \alpha + 2v_{\parallel}v_{\perp} \cos \alpha \sin \alpha + v_{\perp}^2 \cos^2 \alpha}{2\sigma_w^2} \right), \quad (7.5)$$

and we rearrange terms to carry out the integration over the second velocity component perpendicular to \mathbf{k} ,

$$f_0 = \frac{n_b}{2\pi\sigma_u\sigma_w} \exp - \left(\frac{v_{\parallel}^2 \sin^2 \alpha}{2\sigma_w^2} - \frac{v_{\parallel}^2 \cos^2 \alpha}{2\sigma_u^2} \right) \int_{-\infty}^{+\infty} dv_{\perp} \\ \times \exp - \left[v_{\perp} \left(\frac{2v_{\parallel} \cos \alpha \sin \alpha}{2\sigma_w^2} - \frac{2v_{\parallel} \cos \alpha \sin \alpha}{2\sigma_u^2} \right) + v_{\perp}^2 \left(\frac{\cos^2 \alpha}{2\sigma_w^2} + \frac{\sin^2 \alpha}{2\sigma_u^2} \right) \right] \quad (7.6)$$

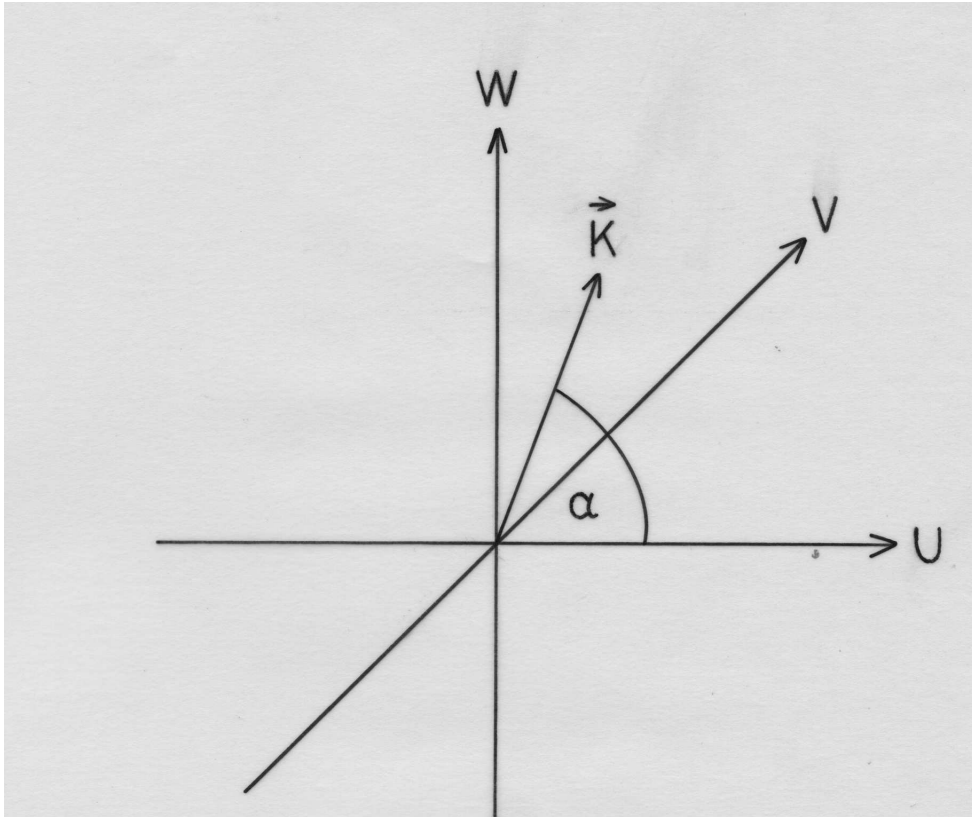


Figure 7.2: Geometry of an anisotropic velocity distribution. For simplicity, the magnitude of the velocity dispersion σ_v of the velocity component v , is equal to the velocity dispersion σ_w that corresponds to the velocity component w . α describes the angle between the wave vector \mathbf{k} and the u -axis.

With use of the formula

$$\int_{-\infty}^{+\infty} dx \exp -(px^2 \pm qx) = \exp \left(\frac{q^2}{4p} \right) \sqrt{\frac{\pi}{p}}, \quad (7.7)$$

we can carry out the integration, thus obtaining

$$f_0 = \frac{\sqrt{\pi} n_b}{2\pi \sigma_u \sigma_w} \exp - \left(\frac{v_{\parallel}^2 \sin^2 \alpha}{2\sigma_w^2} - \frac{v_{\parallel}^2 \cos^2 \alpha}{2\sigma_u^2} \right) \left(\frac{\cos^2 \alpha}{2\sigma_w^2} + \frac{\sin^2 \alpha}{2\sigma_u^2} \right)^{-\frac{1}{2}} \\ \times \exp - \left[\frac{\left(\frac{v_{\parallel} \cos \alpha \sin \alpha}{\sigma_w^2} - \frac{v_{\parallel} \cos \alpha \sin \alpha}{\sigma_u^2} \right)^2}{4 \left(\frac{\cos^2 \alpha}{2\sigma_w^2} + \frac{\sin^2 \alpha}{2\sigma_u^2} \right)} \right] \quad (7.8)$$

We rearrange the terms in the exponential function

$$\exp - \frac{v_{\parallel}^2}{2} \left[\frac{\left(\frac{\sin^2 \alpha}{\sigma_w^2} + \frac{\cos^2 \alpha}{\sigma_u^2} \right) \left(\frac{\cos^2 \alpha}{\sigma_w^2} + \frac{\sin^2 \alpha}{\sigma_u^2} \right) - \cos^2 \alpha \sin^2 \alpha \left(\frac{1}{\sigma_w^2} - \frac{1}{\sigma_u^2} \right)^2}{\frac{\cos^2 \alpha}{\sigma_w^2} + \frac{\sin^2 \alpha}{\sigma_u^2}} \right] \\ = \exp - \frac{v_{\parallel}^2}{2} \left[\frac{\frac{\sin^2 \alpha \cos^2 \alpha}{\sigma_w^4} + \frac{\cos^4 \alpha}{\sigma_u^2 \sigma_w^2} + \frac{\sin^4 \alpha}{\sigma_w^2 \sigma_u^2} + \frac{\sin^2 \alpha \cos^2 \alpha}{\sigma_u^4} - \cos^2 \alpha \sin^2 \alpha \left(\frac{1}{\sigma_w^2} - \frac{1}{\sigma_u^2} \right)^2}{\frac{\cos^2 \alpha}{\sigma_w^2} + \frac{\sin^2 \alpha}{\sigma_u^2}} \right] \\ = \exp - \frac{v_{\parallel}^2}{2} \left[\frac{(\cos^2 \alpha + \sin^2 \alpha)^2}{\sigma_u^2 \cos^2 \alpha + \sigma_w^2 \sin^2 \alpha} \right] = \exp - \frac{v_{\parallel}^2}{2} \left[\frac{1}{\sigma_u^2 \cos^2 \alpha + \sigma_w^2 \sin^2 \alpha} \right] \quad (7.9)$$

and then rewrite Eq. (7.8) as

$$f_0 = \frac{\sqrt{\pi} n_b}{2\pi \sigma_u \sigma_w} \frac{\sqrt{2} \sigma_u \sigma_w}{\sqrt{\sigma_u^2 \cos^2 \alpha + \sigma_w^2 \sin^2 \alpha}} \exp \left(\frac{v_{\parallel}^2 / 2}{\sigma_u^2 \cos^2 \alpha + \sigma_w^2 \sin^2 \alpha} \right) \\ = \frac{n_b}{\sqrt{2\pi} \sqrt{\sigma_u^2 \cos^2 \alpha + \sigma_w^2 \sin^2 \alpha}} \exp \left(\frac{v_{\parallel}^2 / 2}{\sigma_u^2 \cos^2 \alpha + \sigma_w^2 \sin^2 \alpha} \right) \quad (7.10)$$

If we compare the isothermal velocity distribution function (Eq. (7.1)) and the anisotropic distribution function (Eq. (7.10)) that has been integrated over the two velocity components perpendicular to \mathbf{k} , we can see that net the effect of the anisotropy can be associated with an *effective* velocity dispersion

$$\sigma_{eff} = \sqrt{\sigma_u^2 \cos^2 \alpha + \sigma_w^2 \sin^2 \alpha} \quad (7.11)$$

This effective velocity dispersion was first obtained by Fuchs & Athanassoula [FA05]. In the next section σ_{eff} will be inserted in the formula of dynamical friction to see what is the role played by the anisotropy of the system.

7.2 The dynamical drag

7.2.1 First case: $\sigma_v = \sigma_w \neq \sigma_u$

Taking up again the method we used previously, we calculate the DF force exerted on a point-mass particle. With the inclusion of the effective velocity anisotropy, Eq. (6.29) now takes the form

$$\langle \dot{\mathbf{v}}_{\mathbf{y}} \rangle = 2 \frac{G^2 m^2 n_b}{\sqrt{2\pi} \sigma_{\text{eff}}^3} \int_{-\infty}^{+\infty} d^3 k \, k_y^2 \frac{v_0}{k^5} \exp\left(-\frac{(k_y v_0)^2}{2k^2 \sigma_{\text{eff}}^2}\right), \quad (7.12)$$

and we recognize that the trigonometric terms in Eq. (7.11) have the form (see Fig. (7.2))

$$\cos \alpha = \frac{\mathbf{k}_x}{\mathbf{k}} \quad \text{and} \quad \sin \alpha = \frac{\sqrt{\mathbf{k}_y^2 + \mathbf{k}_z^2}}{\mathbf{k}} \quad (7.13)$$

with this at hand we explicitly cast Eq. (7.12) in the form of

$$\langle \dot{\mathbf{v}}_{\mathbf{y}} \rangle = 2 \frac{G^2 m^2 n_b}{\sqrt{2\pi}} \int_{-\infty}^{+\infty} d^3 k \frac{k_y^2}{(\sigma_u^2 k_x^2 + \sigma_v^2 k_y^2 + \sigma_v^2 k_z^2)^{3/2}} \frac{v_0}{k_x^2 + k_y^2 + k_z^2} \times \exp\left(-\frac{(k_y v_0)^2}{2(\sigma_u^2 k_x^2 + \sigma_v^2 k_y^2 + \sigma_v^2 k_z^2)}\right), \quad (7.14)$$

and we normalize the wave vector components with respect to their associated velocity dispersion components, *i. e.* $k'_{x,y,z} = k_{x,y,z} \cdot \sigma_{u,v} = k_{x,y,z}$. Eq. (7.14) now reads

$$\langle \dot{\mathbf{v}}_{\mathbf{y}} \rangle = 2 \frac{G^2 m^2 n_b}{\sqrt{2\pi} \sigma_u \sigma_v^4} \int_{-\infty}^{+\infty} d^3 k \frac{k_y^2}{(k_x^2 + k_y^2 + k_z^2)^{3/2}} \frac{v_0}{\frac{k_x^2}{\sigma_u^2} + \frac{k_y^2}{\sigma_v^2} + \frac{k_z^2}{\sigma_v^2}} \times \exp\left(-\frac{(k_y v_0)^2}{2\sigma_v^2(k_x^2 + k_y^2 + k_z^2)}\right), \quad (7.15)$$

and introduce polar coordinates (r, θ) ,

$$\langle \dot{\mathbf{v}}_{\mathbf{y}} \rangle = 2 \frac{G^2 m^2 n_b}{\sqrt{2\pi} \sigma_u \sigma_v^4} \int_{-\infty}^{+\infty} dk_y \int_0^{+\infty} dr \, r \int_0^{2\pi} d\theta \frac{k_y^2}{(k_y^2 + r^2)^{3/2}} \frac{v_0}{\frac{r^2 \cos^2 \theta}{\sigma_u^2} + \frac{k_y^2}{\sigma_v^2} + \frac{r^2 \sin^2 \theta}{\sigma_v^2}} \times \exp\left(-\frac{(k_y v_0)^2}{2\sigma_v^2(k_y^2 + r^2)}\right) \quad (7.16)$$

We now concentrate on solving the integral over the angle θ . We rewrite this integral as

$$\begin{aligned}
I &= \int_0^{2\pi} d\theta \left(\frac{r^2}{\sigma_u^2} \left(\frac{1}{2} + \frac{\cos 2\theta}{2} \right) + \frac{r^2}{\sigma_v^2} \left(\frac{1}{2} - \frac{\cos 2\theta}{2} \right) + \frac{k_y^2}{\sigma_v^2} \right)^{-1} \\
&= \int_0^{2\pi} d\theta \left(\frac{r^2}{2} \left(\frac{1}{\sigma_u^2} + \frac{1}{\sigma_v^2} \right) + \frac{k_y^2}{\sigma_v^2} + \cos 2\theta \left(\frac{r^2}{2\sigma_u^2} + \frac{r^2}{2\sigma_v^2} \right) \right)^{-1} \\
&= \int_0^{4\pi} \frac{d\theta}{2} \left(\frac{r^2}{2} \left(\frac{1}{\sigma_u^2} + \frac{1}{\sigma_v^2} \right) + \frac{k_y^2}{\sigma_v^2} + \cos \theta \left(\frac{r^2}{2\sigma_u^2} + \frac{r^2}{2\sigma_v^2} \right) \right)^{-1}, \quad (7.17)
\end{aligned}$$

and split off the limits of integration in intervals $(0, 4\pi) = (0, \pi) + (\pi, 2\pi) + (2\pi, 3\pi) + (3\pi, 4\pi)$ to be able to use formula (3.613) of Gradshteyn & Ryzhik [GR00]

$$\int_0^\pi \frac{d\theta}{2} \frac{1}{A + B \cos \theta} = \frac{\pi/2}{\sqrt{A^2 + B^2}}, \quad (7.18)$$

and find the result

$$\begin{aligned}
\langle \dot{\mathbf{v}}_y \rangle &= 4\pi \frac{G^2 m^2 n_b}{\sqrt{2\pi} \sigma_u \sigma_v^4} \int_{-\infty}^{+\infty} dk_y \int_0^{+\infty} dr \frac{r k_y^2}{(k_y^2 + r^2)^{3/2}} \frac{v_0}{\sqrt{\frac{k_y^4}{\sigma_v^4} + \frac{r^2 k_y^2}{\sigma_v^2} \left(\frac{\sigma_u^2 + \sigma_v^2}{\sigma_u^2 \sigma_v^2} \right) + \frac{r^4}{\sigma_u^2 \sigma_v^2}}} \\
&\quad \times \exp \left(-\frac{(k_y v_0)^2}{2\sigma_v^2 (k_y^2 + r^2)} \right) \quad (7.19)
\end{aligned}$$

We make the change of variables $u = \sqrt{k_y^2 + r^2}$; $r = \sqrt{u^2 - k_y^2}$; $dr = u du / \sqrt{u^2 - k_y^2}$ and bring Eq. (7.19) in the form of

$$\begin{aligned}
\langle \dot{\mathbf{v}}_y \rangle &= 4\pi \frac{G^2 m^2 n_b}{\sqrt{2\pi} \sigma_u \sigma_v^4} \int_{-\infty}^{+\infty} dk_y \int_{k_y}^{+\infty} du \frac{k_y^2}{u^2} \frac{v_0}{\sqrt{\frac{k_y^4}{\sigma_v^4} + \frac{k_y^2}{\sigma_v^2} (u^2 - k_y^2) \left(\frac{\sigma_u^2 + \sigma_v^2}{\sigma_u^2 \sigma_v^2} \right) + \frac{(u^2 - k_y^2)^2}{\sigma_u^2 \sigma_v^2}}} \\
&\quad \times \exp \left(-\frac{(k_y v_0)^2}{2\sigma_v^2 u^2} \right) \quad (7.20)
\end{aligned}$$

By choosing $k_y^* = k_y/u = k_y$, $k_y^* \in [0, 1]$, Eq. (7.20) now looks like

$$\begin{aligned}
\langle \dot{\mathbf{v}}_y \rangle &= 8\pi \frac{G^2 m^2 n_b}{\sqrt{2\pi} \sigma_u \sigma_v^4} \int_0^{+\infty} du u \int_0^1 dk_y \frac{v_0 k_y^2}{\sqrt{\frac{k_y^4 u^4}{\sigma_v^4} + \frac{k_y^2 u^2}{\sigma_v^2} (u^2 - k_y^2 u^2) \left(\frac{\sigma_u^2 + \sigma_v^2}{\sigma_u^2 \sigma_v^2} \right) + \frac{(u^2 - k_y^2 u^2)^2}{\sigma_u^2 \sigma_v^2}}} \\
&\quad \times \exp \left(-\frac{(k_y v_0)^2}{2\sigma_v^2} \right) \quad (7.21)
\end{aligned}$$

where we have used the symmetry of the integral over k_y . Next we observe that

$$\begin{aligned}
I &= \sqrt{\frac{k_y^4 u^4}{\sigma_v^4} + \frac{k_y^2 u^2}{\sigma_v^2} (u^2 - k_y^2 u^2) \left(\frac{\sigma_u^2 + \sigma_v^2}{\sigma_u^2 \sigma_v^2} \right) + \frac{(u^2 - k_y^2 u^2)^2}{\sigma_u^2 \sigma_v^2}} \\
&= u^2 \sqrt{\frac{k_y^4}{\sigma_v^4} + \frac{k_y^2}{\sigma_v^2} (1 - k_y^2) \left(\frac{\sigma_u^2 + \sigma_v^2}{\sigma_u^2 \sigma_v^2} \right) + \frac{1 - 2k_y^2 + k_y^4}{\sigma_u^2 \sigma_v^2}} \\
&= u^2 \sqrt{k_y^2 \left(\frac{1}{\sigma_v^2} + \frac{1}{\sigma_v^2} \left(\frac{\sigma_u^2 + \sigma_v^2}{\sigma_u^2 \sigma_v^2} \right) + \frac{1}{\sigma_u^2 \sigma_v^2} \right) + k_y^2 \left(\frac{\sigma_u^2 + \sigma_v^2}{\sigma_u^2 \sigma_v^2} - \frac{2}{\sigma_u^2 \sigma_v^2} \right) + \frac{1}{\sigma_u^2 \sigma_v^2}} \\
&= \frac{u^2}{\sigma_u \sigma_v} \sqrt{k_y^2 \left(\frac{\sigma_u^2 \sigma_v^2}{\sigma_v^4} - \frac{\sigma_u^2 + \sigma_v^2}{\sigma_v^2} + 1 \right) + k_y^2 \left(\frac{\sigma_u^2 + \sigma_v^2}{\sigma_v^2} - 2 \right) + 1} \\
&= \frac{u^2}{\sigma_u \sigma_v} \sqrt{k_y^2 \left(\frac{\sigma_u^2}{\sigma_v^2} - 1 \right) + 1}. \tag{7.22}
\end{aligned}$$

Inserting Eq. (7.22) into Eq. (7.21) we obtain

$$\langle \dot{\mathbf{v}}_{\mathbf{y}} \rangle = 4\sqrt{2\pi} \frac{G^2 m^2 n_b}{\sigma_v^3} \int_0^{+\infty} du \frac{1}{u} \int_0^1 dk_y \frac{v_0 k_y^2}{\sqrt{1 + \left(\frac{\sigma_u^2}{\sigma_v^2} - 1 \right) k_y^2}} \exp\left(-\frac{(k_y v_0)^2}{2\sigma_v^2}\right). \tag{7.23}$$

The integral over u diverges just as the Coulomb logarithm of Chandrasekhar's formula. We denote this integral as $\ln(\Lambda)$. Then, in order to be able to properly interpret Eq. (7.23), we introduce the total velocity dispersion $\sigma_T^2 = \sigma_u^2 + 2\sigma_v^2$, and we make the change of variables $k_y^* = k_y^2$; $k_y \in [0, \infty)$; $dk_y = dk_y^*/2\sqrt{k_y^*}$ to find from Eq. (7.23) the drag on the perturber

$$\langle \dot{\mathbf{v}} \rangle = -\frac{2\sqrt{2\pi} G^2 m^2 n_b}{\sigma_T^2} \frac{\sigma_T^3}{\sigma_v^3} \frac{v_0}{\sigma_T} \ln(\Lambda) \int_0^1 dk_y^* \frac{\sqrt{k_y^*} \exp\left(-k_y^* \frac{v_0^2}{2\sigma_T^2} \frac{\sigma_T^2}{\sigma_v^2}\right)}{\sqrt{1 + \left(\frac{\sigma_T^2}{\sigma_v^2} - 3 \right) k_y^*}} \tag{7.24}$$

7.2.2 Second case: $\sigma_v \neq \sigma_u = \sigma_w$

The velocity ellipsoid corresponding to the choice $\sigma_v \neq \sigma_u = \sigma_w$ is shown in Fig. (7.3), we follow again the trajectory of a point-mass particle that travels along the k_y -axis, but in this case the trajectory of the massive body goes along the symmetric axis of the ellipsoid. In this case, the angle α in Eq. (7.11) will be determined by (see Fig. (7.4))

$$\cos \alpha = \frac{\mathbf{k}_y}{\mathbf{k}} \quad \text{and} \quad \sin \alpha = \frac{\sqrt{\mathbf{k}_x^2 + \mathbf{k}_z^2}}{\mathbf{k}}. \tag{7.25}$$

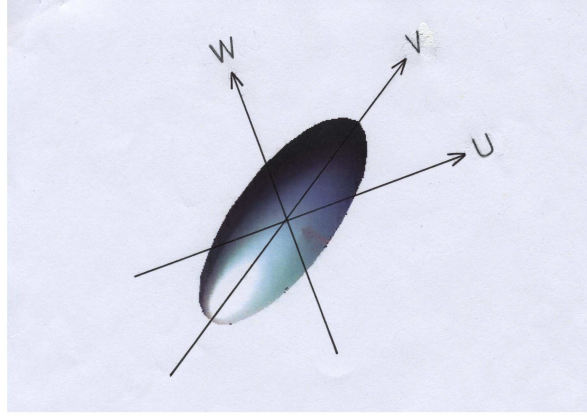


Figure 7.3: Velocity ellipsoid corresponding to the case $\sigma_v \neq \sigma_u = \sigma_w$. A particle traveling along the k_y -axis sees an anisotropic velocity distribution since the magnitude of the velocity dispersion components u, w perpendicular to the parallel component v is not the same.

With the inclusion of the trigonometric terms (7.25), Eq. (6.29) is rewritten as

$$\langle \dot{\mathbf{v}}_{\mathbf{y}} \rangle = 2 \frac{G^2 m^2 n_b}{\sqrt{2\pi}} \int_{-\infty}^{+\infty} d^3 k \frac{k_y^2}{(\sigma_u^2 k_x^2 + \sigma_v^2 k_y^2 + \sigma_u^2 k_z^2)^{3/2}} \frac{v_0}{k_x^2 + k_y^2 + k_z^2} \times \exp\left(-\frac{(k_y v_0)^2}{2(\sigma_u^2 k_x^2 + \sigma_v^2 k_y^2 + \sigma_u^2 k_z^2)}\right). \quad (7.26)$$

Considering $k'_{x,y,z} = k_{x,y,z} \cdot \sigma_{u,v,u} = k_{x,y,z}$, the equation now reads

$$\langle \dot{\mathbf{v}}_{\mathbf{y}} \rangle = 2 \frac{G^2 m^2 n_b}{\sqrt{2\pi} \sigma_u^2 \sigma_v^3} \int_{-\infty}^{+\infty} d^3 k \frac{k_y^2}{(k_x^2 + k_y^2 + k_z^2)^{3/2}} \frac{v_0}{\frac{k_x^2}{\sigma_u^2} + \frac{k_y^2}{\sigma_v^2} + \frac{k_z^2}{\sigma_u^2}} \times \exp\left(-\frac{(k_y v_0)^2}{2\sigma_v^2(k_x^2 + k_y^2 + k_z^2)}\right), \quad (7.27)$$

Using polar coordinates we get

$$\langle \dot{\mathbf{v}}_{\mathbf{y}} \rangle = 2 \frac{G^2 m^2 n_b}{\sqrt{2\pi} \sigma_u^2 \sigma_v^3} \int_{-\infty}^{+\infty} dk_y \int_0^{+\infty} dr 2\pi r \frac{k_y^2}{(k_y^2 + r^2)^{3/2}} \frac{v_0}{\frac{r^2}{\sigma_u^2} + \frac{k_y^2}{\sigma_v^2}} \times \exp\left(-\frac{(k_y v_0)^2}{2\sigma_v^2(k_y^2 + r^2)}\right), \quad (7.28)$$

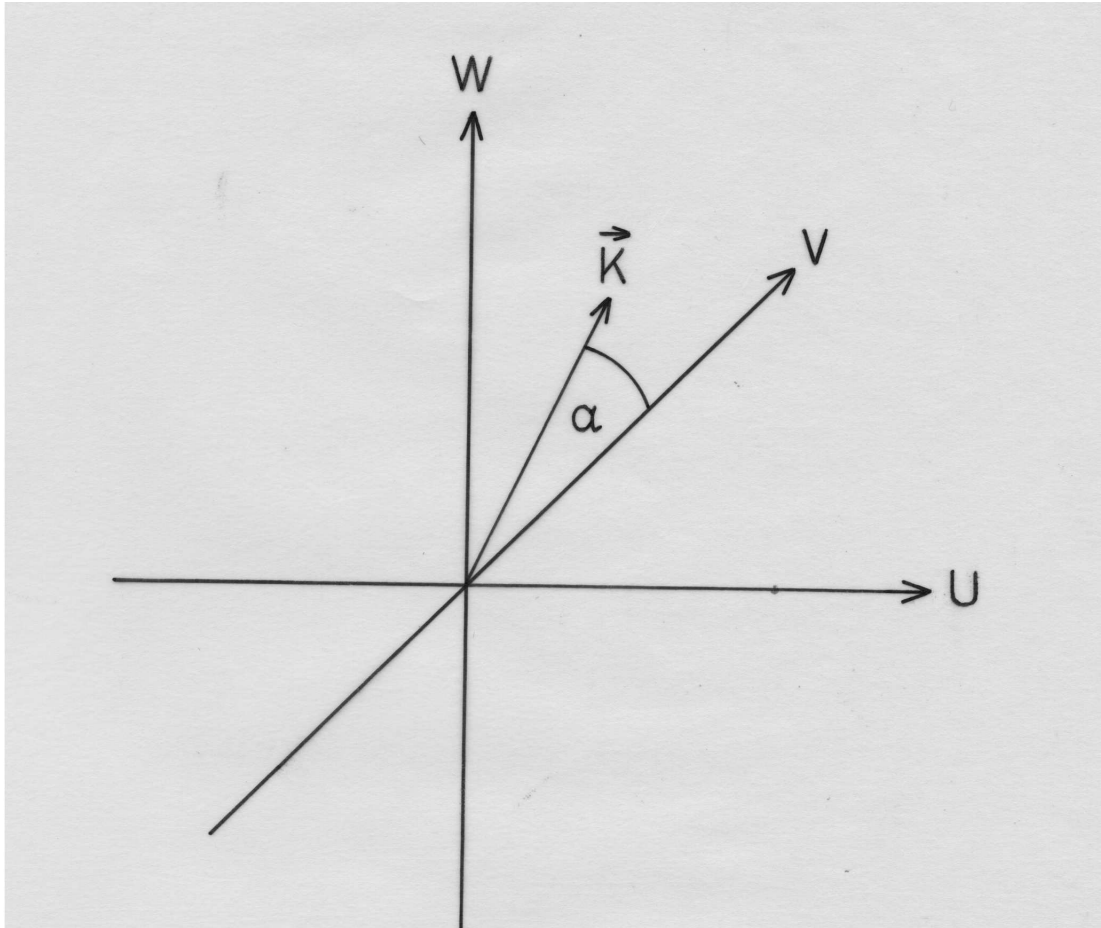


Figure 7.4: Schematic representation showing the angle between the wave vector \mathbf{k} and the component \mathbf{k}_y along which the perturber is flying.

and making the substitution $u = \sqrt{k_y^2 + r^2}$; $du = r dr / \sqrt{k_y^2 + r^2} = r dr / u$, we find

$$\begin{aligned} \langle \dot{\mathbf{v}}_{\mathbf{y}} \rangle = & 4 \frac{\sqrt{2\pi} G^2 m^2 n_b}{\sigma_u^2 \sigma_v^3} \int_0^{+\infty} dk_y \int_{|k_y|}^{+\infty} du \frac{1}{u^2} \frac{v_0 k_y^2}{\frac{u^2 - k_y^2}{\sigma_u^2} + \frac{k_y^2}{\sigma_v^2}} \\ & \times \exp\left(-\frac{(k_y v_0)^2}{2\sigma_v^2 u^2}\right). \end{aligned} \quad (7.29)$$

Changing the limits of integration we obtain

$$\begin{aligned} \langle \dot{\mathbf{v}}_{\mathbf{y}} \rangle = & 4 \frac{\sqrt{2\pi} G^2 m^2 n_b}{\sigma_u^2 \sigma_v^3} \int_0^{+\infty} du \frac{1}{u} \int_0^1 dk_y \frac{v_0 k_y^2}{\frac{1 - k_y^2}{\sigma_u^2} + \frac{k_y^2}{\sigma_v^2}} \\ & \times \exp\left(-\frac{(k_y v_0)^2}{2\sigma_v^2}\right), \end{aligned} \quad (7.30)$$

and we make the choice $k_y^* = k_y^2$; $dk_y^* = 2k_y dk_y$, obtaining

$$\begin{aligned} \langle \dot{\mathbf{v}}_{\mathbf{y}} \rangle = & 2 \frac{\sqrt{2\pi} G^2 m^2 n_b}{\sigma_u^2 \sigma_v^3} \ln(\Lambda) \int_0^1 dk_y^* \frac{v_0 \sqrt{k_y^*}}{1 + k_y^* \frac{\sigma_u^2 - \sigma_v^2}{\sigma_v^2}} \\ & \times \exp\left(-\frac{k_y^* v_0^2}{2\sigma_v^2}\right), \end{aligned} \quad (7.31)$$

where we have used the notation $\ln(\Lambda)$ for the divergent integral. Introducing the total velocity dispersion for this case $\sigma_T^2 = 2\sigma_u^2 + \sigma_v^2$, we write the dynamical drag as

$$\langle \dot{\mathbf{v}} \rangle = -\frac{2\sqrt{2\pi} G^2 m^2 n_b}{\sigma_T^2} \frac{\sigma_T^3}{\sigma_v^3} \frac{v_0}{\sigma_T} \ln(\Lambda) \int_0^1 dk_y^* \frac{\sqrt{k_y^*} \exp\left(-k_y^* \frac{v_0^2}{2\sigma_T^2} \frac{\sigma_T^2}{\sigma_v^2}\right)}{1 + \left(\frac{\sigma_T^2}{\sigma_v^2} - 3\right) \frac{k_y^*}{2}}. \quad (7.32)$$

7.3 Discussion and Conclusions

In the previous section we have carried out the formal calculation of the DF force exerted on a point-mass particle as it moves through the velocity ellipsoid of the background particles. It must be said that Binney [Bin77] has been the only one to consider such a situation, although our results are valid not only for a disk-like oblate ellipsoid, but also for a cigar-shaped prolate ellipsoid. We start the discussion by plotting the behaviour of Eq.(7.24) in Fig. (7.5). Eq.(7.24) describes the drag force on a satellite that is traveling through a velocity ellipsoid at angle α (see Fig. (7.2)). The

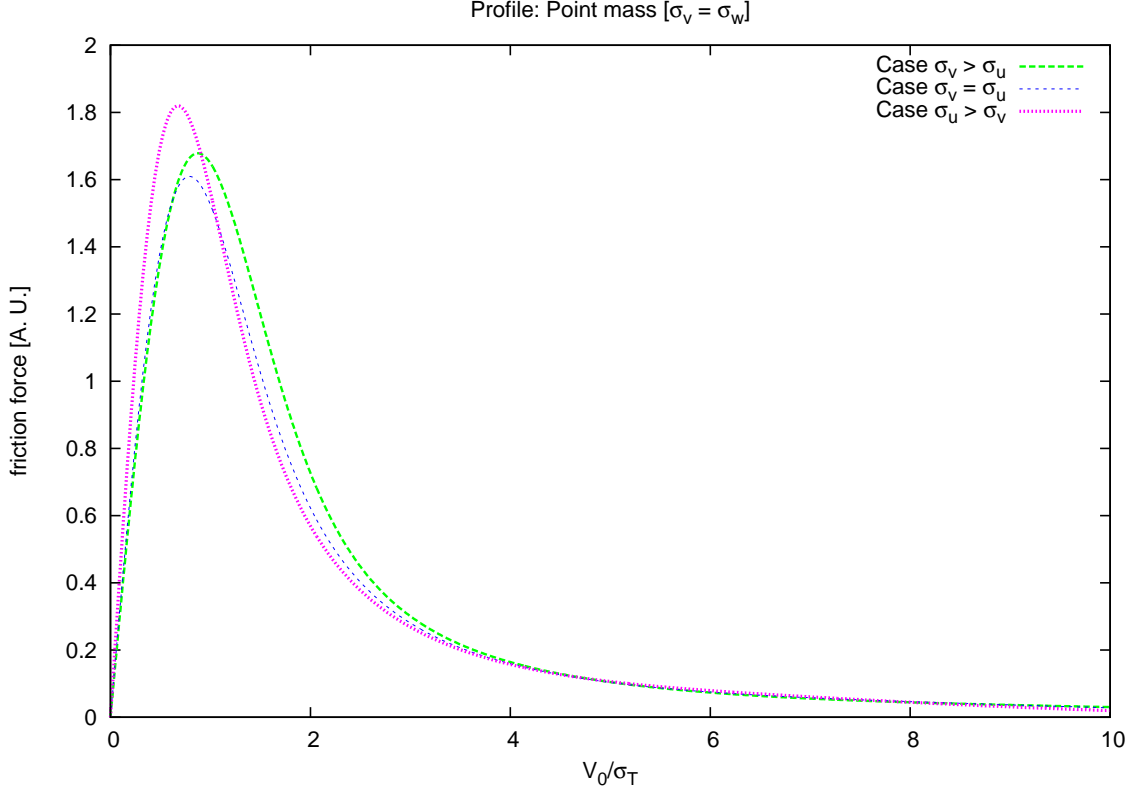


Figure 7.5: DF force's Eq. (7.24) plotted for three different choices: $\sigma_v = \sigma_w > \sigma_u$ corresponding to an oblate velocity ellipsoid, $\sigma_v = \sigma_w < \sigma_u$ gives the contribution from an prolate ellipsoid, and the isotropic velocity dispersion contribution is also included for reference.

factor $2\sqrt{2\pi}G^2m^2n_b\ln(\Lambda)/\sigma_T^2$ is not plotted. By plotting the force given by Eq.(7.24) in terms of the total velocity dispersion σ_T , we can maintain its total value constant, letting us then see directly the relative contribution of every choice of σ_v .

Let us start describing the situation corresponding to the choice $\sigma_v > \sigma_u$. One can immediately see from Fig. (7.5) the dual behaviour of DF: on the one hand, in the regime of low velocities ($v_0 < \sigma_T$), the distribution function (Eq. (7.2)) is approximately constant, which means that the force goes as v_0 and therefore the effect of the anisotropy is not present, this DF dependence on v_0 bears resemblance with the deceleration a moving body experiences inside a viscous fluid according to Stokes's formula. On the other hand, for dynamically warm particles ($v_0 > \sigma_T$), the effect of the anisotropic terms arises, resulting in a net increase of the drag force as compared with the isotropic case.

As for the prolate–spheroid case ($\sigma_v = \sigma_w < \sigma_u$), due to the interplay between the exponential and the square–root terms in Eq.(7.24), the force is always bigger than the isotropic force, although symmetric, thus resembling the behaviour of the isotropic case, regardless of the precise value of σ_v , as long as the condition $\sigma_v < \sigma_u$ is satisfied.

Following the standard procedure [cf. BT87], we can give a time unit of the process if we loosely consider that Eq.(7.24) can be written as $kv_0 = \alpha v_0$, and if we choose $v_0 = \sigma_v$ as well as $\sigma_v = 2\sigma_u$ for simplicity. We obtain from Eq.(7.24) the decay time for a satellite orbiting the system

$$\begin{aligned} \frac{1}{k} \equiv t_{dec} &= 0.289 \frac{\sigma_v^3}{G^2 m \rho_b \ln(\Lambda)} \\ &= \frac{1.53 \times 10^{10} \text{ yr}}{\ln(\Lambda)} \left(\frac{\sigma_v}{10 \text{ kms}^{-1}} \right)^3 \left(\frac{1 \text{ M}_\odot}{m} \right) \left(\frac{10^3 \text{ M}_\odot \text{ pc}^{-3}}{\rho} \right). \end{aligned} \quad (7.33)$$

Next, we show the behaviour of the DF formula (7.32) by plotting it. This again means that the factor $2\sqrt{2\pi}G^2m^2n_b\ln(\Lambda)/\sigma_T^2$ is not taken explicitly into account. We would like to highlight first that, as long as the condition $\sigma_v > \sigma_u$ is satisfied, the anisotropic terms in the force term of Eq. (7.32) will tend to *widen* (with respect to the isotropic case) the drag force for increasing values of σ_v with respect to σ_u in the $v_0 > \sigma_T$ velocity regime; in the regime $v_0 < \sigma_T$ the distribution function remains constant regardless of the value of σ_v , and it closely follows the isotropic case. In Fig. (7.6) we plot the situation for a particular choice of σ_v .

Also in Fig. (7.6), it is shown the force contribution for the case $\sigma_v < \sigma_u$. As expected, due to the exponential term in Eq. (7.32), the force will increase with decreasing σ_v in the regime $v_0 < \sigma_T$. Certainly the exponential term is the leading term in this case, since once values $v_0 > \sigma_T$ are spanned, the force will drop precipitately.

We also give an order of magnitude estimate of the decay time of the process in this case. Taking again simple assumptions $v_0 = \sigma_v$, $\sigma_u = 2\sigma_v$, we obtain find from Eq.(7.32)

$$\begin{aligned} \frac{1}{k} \equiv t_{dec} &= 0.967 \frac{\sigma_v^3}{G^2 m \rho_b \ln(\Lambda)} \\ &= \frac{5.12 \times 10^{10} \text{ yr}}{\ln(\Lambda)} \left(\frac{\sigma_v}{10 \text{ kms}^{-1}} \right)^3 \left(\frac{1 \text{ M}_\odot}{m} \right) \left(\frac{10^3 \text{ M}_\odot \text{ pc}^{-3}}{\rho} \right). \end{aligned} \quad (7.34)$$

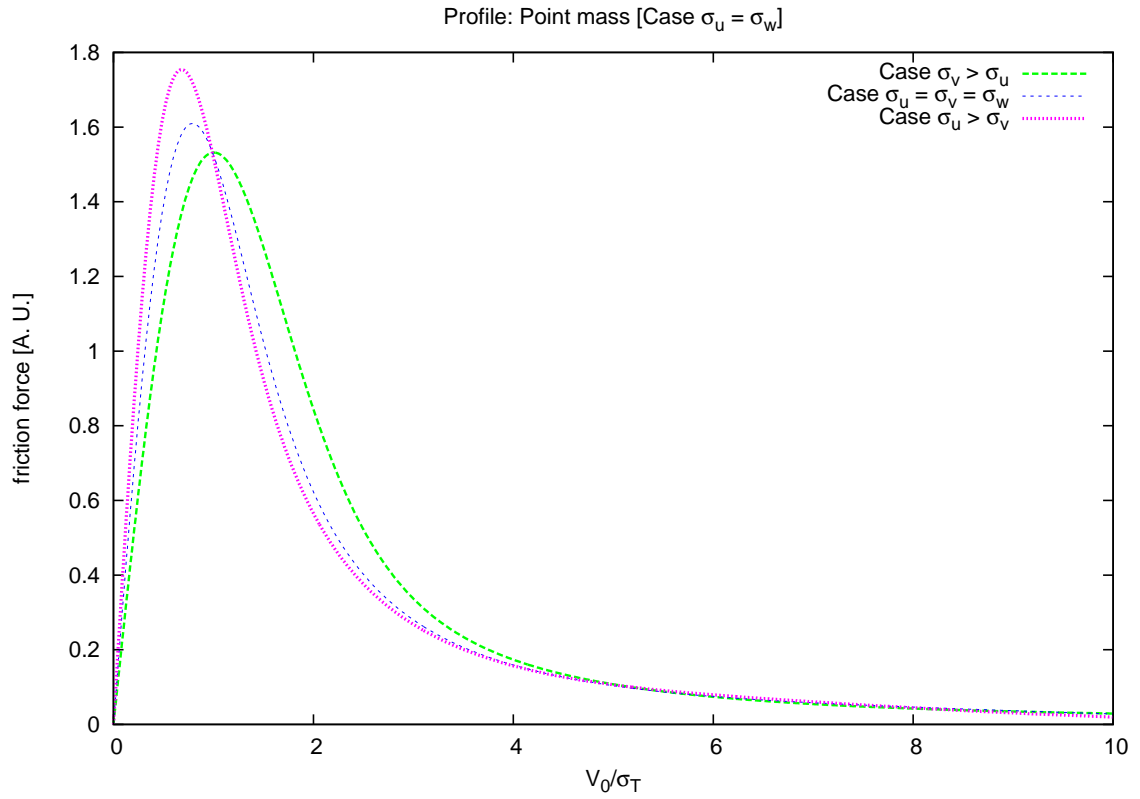


Figure 7.6: DF force for the case: $\sigma_v \neq \sigma_u = \sigma_w$. In this case the particle travels right in the middle of the velocity ellipsoid. The drag experienced by the massive body is weaker than in the previous case ($\sigma_v = \sigma_w \neq \sigma_u$).

To finish the discussion, it must be said that one could relate the force term in the case ($\sigma_v = \sigma_w > \sigma_u$), to Binney's parallel force component [F_{\parallel} of Bin77], which is the force a particle traveling along a coplanar orbit (in our more general treatment along the k_y -axis) with velocity $v_{\parallel} = v_0$ and velocity dispersion $\sigma_{\parallel} = \sigma_v$ experiences when the magnitude of the parallel velocity dispersion component is equal to the other coplanar component σ_w (cf. Fig. (7.2)). In fact, if we make the substitution of variables $k_y^* = 1/1+q$; $dk_y^* = -dq/(1+q)^2$; $q \in [\infty, 0]$, from Eq.(7.24) we recover Binney's Eq. (3) of [Bin77]

$$\begin{aligned}
\langle \dot{\mathbf{v}} \rangle &= 2\sqrt{2\pi}G^2m^2n_b\frac{v_0}{\sigma_{\parallel}^3}\ln(\Lambda)\int_{\infty}^0dq\frac{1}{\sqrt{1+q}}\frac{1}{\sqrt{1+\left(\frac{\sigma_{\perp}^2}{\sigma_{\parallel}^2}-1\right)k_y^*}} \\
&\times \exp\left(-\frac{v_0^2}{2(1+q)\sigma_{\parallel}^2}\right) \\
&= -2\sqrt{2\pi}G^2m^2n_b\sqrt{1-e^2}\frac{v_0}{\sigma_{\parallel}^2\sigma_{\perp}}\ln(\Lambda)\int_0^{\infty}dq\frac{1}{\sqrt{1-e^2+q}}\frac{1}{(1+q)^2} \\
&\times \exp\left(-\frac{v_0^2}{2(1+q)\sigma_{\parallel}^2}\right), \tag{7.35}
\end{aligned}$$

where $e = \sqrt{1 - \sigma_{\perp}^2/\sigma_{\parallel}^2}$ is the eccentricity. Eq. (7.35) differs from Eq. (3) of [Bin77] in the Coulomb logarithm which is written in terms of the wave vector and not in terms of the impact parameter, its evaluation is open to a lot of interpretation as we had already discussed in section (4.3), and in principle one could argue that $\ln(k_{max}/k_{min})$ could be similar to $\ln(b_{max}/b_{min})$. However, the major difference between our treatment and that of Binney's is the explicit dependence of the perpendicular component v_{\perp} in Eq. (3) of [Bin77], component that by construction of our model it had already been integrated over. Binney compared the contribution from the perpendicular component with the parallel component (Eq. (7.35)) to explain the flattening observed in some clusters of galaxies. Since his perpendicular force is bigger than the force exerted on a massive galaxy along the plane of the system, its trajectory will be confined to this plane, thus flattening the distribution of the massive bodies in the system. Here we have calculated the force exerted on a massive body as it moves at different angles through a velocity ellipsoid.

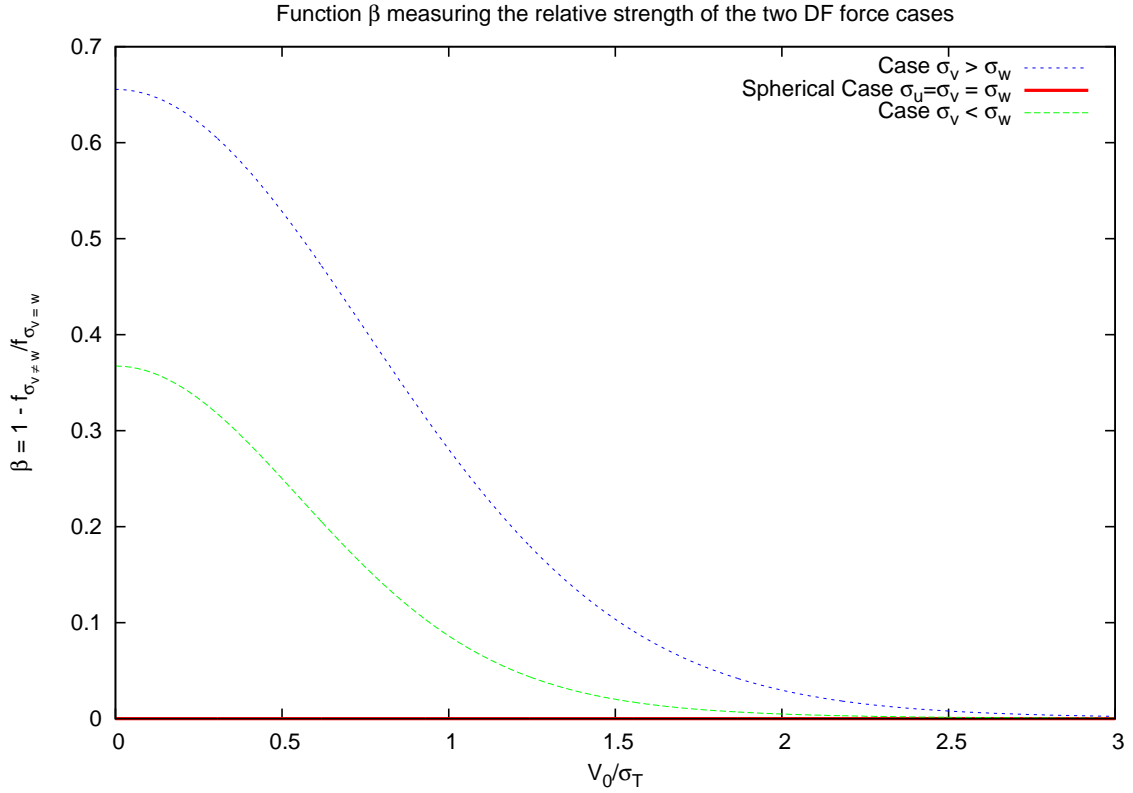


Figure 7.7: Plot of the β function showing the relative strength between the two cases considered in our treatment. The value of the DF force for the case $\sigma_v = \sigma_w \neq \sigma_u$ is considerably bigger than the relative value of the DF force in the case $\sigma_v \neq \sigma_w = \sigma_u$ for $\sigma_v < \sigma_w$. The relative strength in the isotropic case is obviously zero.

Although the situation treated here is not the same as that considered in [Bin77], for illustration purposes we compare here the contribution between the two cases $\sigma_v = \sigma_w \neq \sigma_u$ and $\sigma_v \neq \sigma_w = \sigma_u$, by plotting the function $\beta = 1 - F_{v \neq w} / F_{v=w}$ which bears resemblance to Binney's $\beta = 1 - F_{\parallel} / F_{\perp}$ function which gives the degree of the flattening. It is evident from Fig. (7.7) that the contribution from the case $\sigma_v = \sigma_w \neq \sigma_u$ ($F_{v=w}$) dominates over the contribution for the case $\sigma_v \neq \sigma_w = \sigma_u$ ($F_{v \neq w}$), for both regimes $\sigma_v > \sigma_w$ and $\sigma_v < \sigma_w$. This is intuitively expected since a particle traveling along the k_y -axis will see a *net* anisotropic component of the velocity ellipsoid in the case $\sigma_v = \sigma_w \neq \sigma_u$, whereas in the case $\sigma_v \neq \sigma_w = \sigma_u$ the particle will see a symmetric velocity ellipsoid.

7.4 The role of a *missaligned* velocity ellipsoid

7.4.1 First case: $\sigma_v = \sigma_w \neq \sigma_u$

In this section we extend our analysis to include an angle dependence in the trajectory the satellite follows as it travels through the background system. From Fig. (7.8) we can see that the velocity plane defined by the velocity components v , u , is not longer aligned with the plane defined by the wave vector components k_y , k_x . We assume there exists an opening angle β between the axis u and k_x . In this situation the angle described by Eq. (7.11) has the form

$$\cos \alpha = \frac{k_x \cos \beta + k_y \sin \beta}{k}. \quad (7.36)$$

We then introduce this equation into the effective velocity dispersion Eq. (7.11), to obtain

$$\begin{aligned}
\sigma_{eff}^2 &= \sigma_u^2 \cos^2 \alpha + \sigma_v^2 \sin^2 \alpha \\
&= \frac{\sigma_u^2}{k^2} (k_x^2 \cos^2 \beta + 2k_x k_y \sin \beta \cos \beta + k_y^2 \sin^2 \beta) \\
&\quad + \frac{\sigma_v^2}{k^2} (k^2 - k_x^2 \cos^2 \beta - 2k_x k_y \sin \beta \cos \beta - k_y^2 \sin^2 \beta) \\
&= \frac{k_x^2}{k^2} (\sigma_u^2 \cos^2 \beta + \sigma_v^2 - \sigma_v^2 \cos^2 \beta) \\
&\quad + \frac{2k_x k_y}{k^2} (\sigma_u^2 \sin \beta \cos \beta - \sigma_v^2 \sin \beta \cos \beta) \\
&\quad + \frac{k_y^2}{k^2} (\sigma_u^2 \sin^2 \beta + \sigma_v^2 - \sigma_v^2 \sin^2 \beta) + \sigma_v^2 k_z^2 \\
&= \frac{k_x^2}{k^2} (\sigma_u^2 \cos^2 \beta + \sigma_v^2 \sin^2 \beta) \\
&\quad + \frac{2k_x k_y}{k^2} (\sigma_u^2 - \sigma_v^2) \sin \beta \cos \beta \\
&\quad + \frac{k_y^2}{k^2} (\sigma_u^2 \sin^2 \beta + \sigma_v^2 \cos^2 \beta) + \sigma_v^2 k_z^2
\end{aligned} \tag{7.37}$$

It is advantageous to express Eq. (7.37) as

$$\sigma_{eff}^2 = \frac{\kappa^2 + \sigma_v^2 k_z^2}{k^2}, \tag{7.38}$$

where $\kappa^2 = k_x^2 (\sigma_u^2 \cos^2 \beta + \sigma_v^2 \sin^2 \beta) + k_x k_y (\sigma_u^2 - \sigma_v^2) \sin \beta \cos \beta + k_y^2 (\sigma_u^2 \sin^2 \beta + \sigma_v^2 \cos^2 \beta)$. Inserting Eq. (7.38) into Eq. (6.29) we find

$$\begin{aligned}
\langle \dot{\mathbf{v}}_{\mathbf{x}}, \dot{\mathbf{v}}_{\mathbf{y}} \rangle &= 4 \frac{G^2 m^2 n_b}{\sqrt{2\pi}} \int_0^{+\infty} dk_z \int_{-\infty}^{+\infty} d^2 k \frac{(k_x k_y, k_y^2)}{(\kappa^2 + \sigma_v^2 k_z^2)^{3/2}} \frac{v_0}{k_x^2 + k_y^2 + k_z^2} \\
&\quad \times \exp - \left(\frac{(k_y v_0)^2}{2(\kappa^2 + \sigma_v^2 k_z^2)} \right). \tag{7.39}
\end{aligned}$$

Note that due to the missalignment of axis the $k_x k_y$ -component of $\langle \dot{\mathbf{v}}_{\mathbf{y}} \rangle$ is present (cf. Eq. (6.29)). We continue further by taking the substitutions $\kappa^* = \kappa/\sigma_v$, and $r = 1/\sqrt{\kappa^* + k_z^2}$; $dr = -k_z/(\kappa^* + k_z^2)^{3/2}$; $r \in [1/\kappa^*, 0]$, with

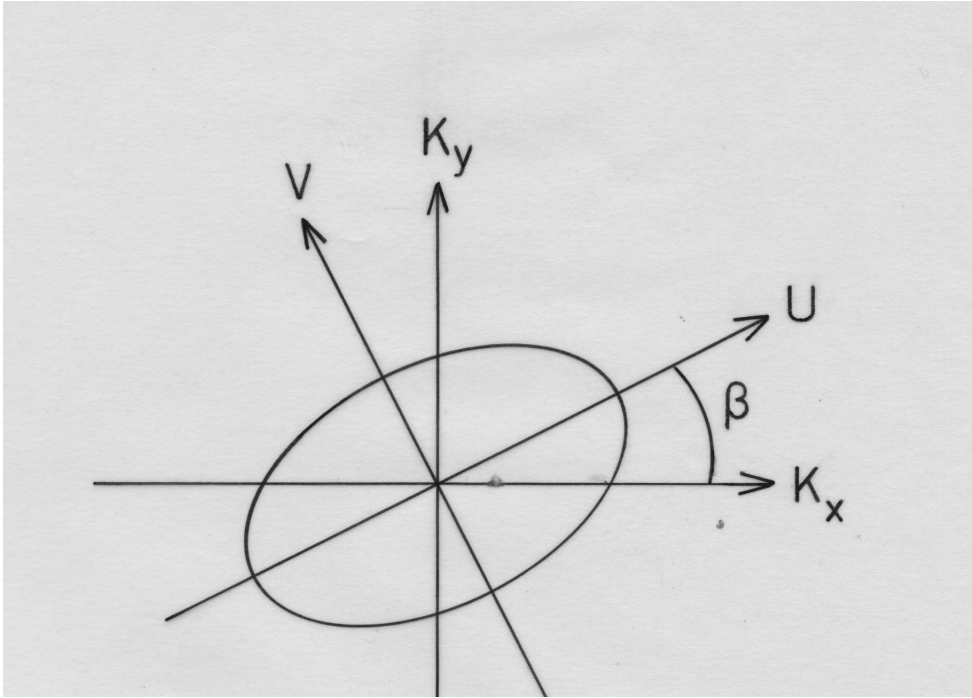


Figure 7.8: Sketch showing the angle β that accounts for the missalignment between the velocity axes u, v and the wave vector components k_x, k_y . In this situation the contribution from the component $\langle \dot{\mathbf{v}}_x \rangle$ is not longer zero.

which Eq. (7.39) takes the form

$$\begin{aligned}
\langle \dot{\mathbf{v}}_{\mathbf{x}}, \dot{\mathbf{v}}_{\mathbf{y}} \rangle &= 4 \frac{G^2 m^2 n_b}{\sqrt{2\pi} \sigma_v^3} \int_{-\infty}^{+\infty} d^2 k \int_0^{1/\kappa^*} dr \frac{v_0(k_x k_y, k_y^2)}{k_x^2 + k_y^2 + k_z^2} \frac{\exp - \left(\frac{(k_y v_0 r)^2}{2\sigma_v^2} \right)}{k_z} \\
&= 4 \frac{G^2 m^2 n_b}{\sqrt{2\pi} \sigma_v^3} \int_{-\infty}^{+\infty} d^2 k \int_0^{1/\kappa^*} dr \frac{v_0(k_x k_y, k_y^2)}{k_x^2 + k_y^2 + \frac{1}{r^2} - \kappa^{*2}} \frac{\exp - \left(\frac{(k_y v_0 r)^2}{2\sigma_v^2} \right)}{\sqrt{\frac{1}{r^2} - \kappa^{*2}}} \\
&= 4 \frac{G^2 m^2 n_b}{\sqrt{2\pi} \sigma_v^3} \int_{-\infty}^{+\infty} d^2 k \int_0^{1/\kappa^*} dr r \frac{v_0(k_x k_y, k_y^2)}{r^2(k_x^2 + k_y^2 - \kappa^{*2}) + 1} \frac{\exp - \left(\frac{(k_y v_0 r)^2}{2\sigma_v^2} \right)}{\sqrt{1 - \kappa^{*2} r^2}}.
\end{aligned} \tag{7.40}$$

We make the substitution $r = \sqrt{s}$; $dr = ds/2\sqrt{s}$; $r \in [0, 1/\kappa^{*2}]$, to get

$$\langle \dot{\mathbf{v}}_{\mathbf{x}}, \dot{\mathbf{v}}_{\mathbf{y}} \rangle = 2 \frac{G^2 m^2 n_b}{\sqrt{2\pi} \sigma_v^3} \int_{-\infty}^{+\infty} d^2 k \int_0^{1/\kappa^{*2}} ds s \frac{v_0(k_x k_y, k_y^2)}{s(k_x^2 + k_y^2 - \kappa^{*2}) + 1} \frac{\exp - \left(\frac{(k_y v_0)^2 s}{2\sigma_v^2} \right)}{\sqrt{1 - \kappa^{*2} s}}. \tag{7.41}$$

To proceed further we consider the change of variables $t = \kappa^{*2} s$; $dt = \kappa^{*2} ds$; $t \in [0, 1]$, and obtain

$$\langle \dot{\mathbf{v}}_{\mathbf{x}}, \dot{\mathbf{v}}_{\mathbf{y}} \rangle = 2 \frac{G^2 m^2 n_b}{\sqrt{2\pi} \sigma_v^3} \int_{-\infty}^{+\infty} d^2 k \int_0^1 dt \frac{t}{\kappa^{*4}} \frac{v_0(k_x k_y, k_y^2)}{1 + t \left(\frac{k_x^2 + k_y^2 - \kappa^{*2}}{\kappa^{*2}} \right)} \frac{\exp - \left(\frac{(k_y v_0)^2 t}{2\sigma_v^2 \kappa^{*2}} \right)}{\sqrt{1 - t}}. \tag{7.42}$$

One of the two remaining integrals can be solved by taking the substitution $k_x^* = k_x/k_y$; $dk_x^* = dk_x/k_y$. κ^* will now read $1/\kappa^{*2} = \sigma_v^2/k_y^2 [k_x^2 (\sigma_u^2 \cos^2 \beta + \sigma_v^2 \sin^2 \beta) + 2k_x^* (\sigma_u^2 - \sigma_v^2) \sin \beta \cos \beta + \sigma_u^2 \sin^2 \beta + \sigma_v^2 \cos^2 \beta]$.

From Eq. (7.42) we find

$$\begin{aligned}
\langle \dot{\mathbf{v}}_{\mathbf{x}}, \dot{\mathbf{v}}_{\mathbf{y}} \rangle &= 2 \sqrt{\frac{2}{\pi}} G^2 m^2 n_b \sigma_v \int_0^{+\infty} dk_y \frac{1}{k_y} \int_{-\infty}^{+\infty} dk_x^* \int_0^1 dt \frac{v_0(k_x^*, 1)}{(A k_x^{*2} + B k_x^* + C)^2} \\
&\quad \times \frac{t}{\sqrt{1 - t}} \frac{\exp - \left(\frac{v_0^2 t}{2(A k_x^{*2} + B k_x^* + C)} \right)}{1 + t \left(\frac{\sigma_v^2 (1 + k_x^{*2})}{(A k_x^{*2} + B k_x^* + C)^2} - 1 \right)} \tag{7.43}
\end{aligned}$$

where $A = \sigma_u^2 \cos^2 \beta + \sigma_v^2 \sin^2 \beta$, $B = 2(\sigma_u^2 - \sigma_v^2) \sin \beta \cos \beta$, and $C = \sigma_u^2 \sin^2 \beta + \sigma_v^2 \cos^2 \beta$. Using again the notation $\ln(\Lambda)$ for the integral that diverges and introducing the total velocity dispersion $\sigma_T^2 = \sigma_u^2 + 2\sigma_v^2$, we obtain the DF

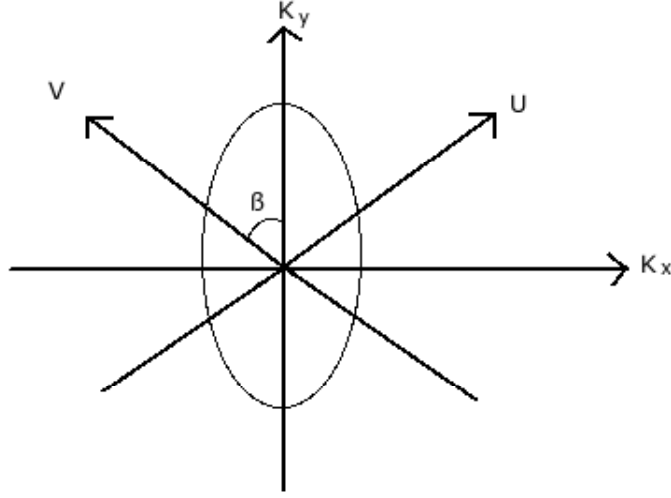


Figure 7.9: Now we consider the missalignment between the plane described by the u, v components and the k_x, k_y axes in the case $\sigma_v \neq \sigma_w = \sigma_u$.

formula

$$\begin{aligned} \langle \dot{\mathbf{v}}(x, y, 0) \rangle = & -2\sqrt{\frac{2}{\pi}} \frac{G^2 m^2 n_b}{\sigma_T^2} \frac{\sigma_v}{\sigma_T} \frac{v_0}{\sigma_T} \ln(\Lambda) \int_{-\infty}^{+\infty} dk_x^* \int_0^1 dt \frac{v_0(k_x^*, 1)}{(A'k_x^{*2} + B'k_x^* + C')^2} \\ & \times \frac{t}{\sqrt{1-t}} \frac{\exp\left(-\frac{t(v_0^2/\sigma_T^2)}{2(A'k_x^{*2} + B'k_x^* + C')}\right)}{1+t\left(\frac{(\sigma_v^2/\sigma_T^2)(1+k_x^{*2})}{(A'k_x^{*2} + B'k_x^* + C')^2} - 1\right)} \end{aligned} \quad (7.44)$$

where now $A' = (1 - 3\frac{\sigma_v^2}{\sigma_T^2}) \cos^2 \beta + \frac{\sigma_v^2}{\sigma_T^2}$, $B' = 2(1 - 3\frac{\sigma_v^2}{\sigma_T^2}) \sin \beta \cos \beta$, and $C' = (1 - 3\frac{\sigma_v^2}{\sigma_T^2}) \sin^2 \beta + \frac{\sigma_v^2}{\sigma_T^2}$.

7.4.2 Second case: $\sigma_v \neq \sigma_w = \sigma_u$

In this case the missalignment between the the velocity components u, v , and the wave vector components k_x, k_y is described in Fig. (7.9). In this situation the angle in Eq. (7.25) is modified and replace by the term

$$\cos \alpha = \frac{k_y \cos \beta + k_x \sin \beta}{k}. \quad (7.45)$$

And put this equation into the effective velocity dispersion Eq. (7.11), to get

$$\begin{aligned}
\sigma_{eff}^2 &= \sigma_v^2 \cos^2 \alpha + \sigma_w^2 \sin^2 \alpha \\
&= \frac{\sigma_v^2}{k^2} (k_y^2 \cos^2 \beta + 2k_x k_y \sin \beta \cos \beta + k_x^2 \sin^2 \beta) \\
&+ \frac{\sigma_w^2}{k^2} (k^2 - k_y^2 \cos^2 \beta - 2k_x k_y \sin \beta \cos \beta - k_x^2 \sin^2 \beta) \\
&= \frac{k_y^2}{k^2} (\sigma_v^2 \cos^2 \beta + \sigma_w^2 - \sigma_w^2 \cos^2 \beta) \\
&+ \frac{2k_x k_y}{k^2} (\sigma_v^2 \sin \beta \cos \beta - \sigma_w^2 \sin \beta \cos \beta) \\
&+ \frac{k_x^2}{k^2} (\sigma_v^2 \sin^2 \beta + \sigma_w^2 - \sigma_w^2 \sin^2 \beta) + \sigma_w^2 k_z^2 \\
&= \frac{k_y^2}{k^2} (\sigma_v^2 \cos^2 \beta + \sigma_w^2 \sin^2 \beta) \\
&+ \frac{2k_x k_y}{k^2} (\sigma_v^2 - \sigma_w^2) \sin \beta \cos \beta \\
&+ \frac{k_x^2}{k^2} (\sigma_v^2 \sin^2 \beta + \sigma_w^2 \cos^2 \beta) + \sigma_w^2 k_z^2
\end{aligned} \tag{7.46}$$

Following the method explained in the previous subsection, we rewrite Eq. (7.46) as

$$\sigma_{eff}^2 = \frac{\kappa^2 + \sigma_w^2 k_z^2}{k^2}, \tag{7.47}$$

where $\kappa^2 = k_y^2 (\sigma_v^2 \cos^2 \beta + \sigma_w^2 \sin^2 \beta) + k_x k_y (\sigma_v^2 - \sigma_w^2) \sin \beta \cos \beta + k_x^2 (\sigma_v^2 \sin^2 \beta + \sigma_w^2 \cos^2 \beta)$. Now we insert this equation into the general formula (6.29) and obtain

$$\begin{aligned}
\langle \dot{\mathbf{v}}_{\mathbf{x}}, \dot{\mathbf{v}}_{\mathbf{y}} \rangle &= 4 \frac{G^2 m^2 n_b}{\sqrt{2\pi}} \int_0^{+\infty} dk_z \int_{-\infty}^{+\infty} d^2 k \frac{(k_x k_y, k_y^2)}{(\kappa^2 + \sigma_w^2 k_z^2)^{3/2}} \frac{v_0}{k_x^2 + k_y^2 + k_z^2} \\
&\quad \times \exp - \left(\frac{(k_y v_0)^2}{2(\kappa^2 + \sigma_w^2 k_z^2)} \right)
\end{aligned} \tag{7.48}$$

We make the substitutions $\kappa^* = \kappa/\sigma_w$, and $r = 1/\sqrt{\kappa^* + k_z^2}$; $dr = -k_z/(\kappa^* + k_z^2)^{3/2}$; $r \in [1/\kappa^*, 0]$, and rewrite Eq. (7.48) as

$$\begin{aligned}
\langle \dot{\mathbf{v}}_{\mathbf{x}}, \dot{\mathbf{v}}_{\mathbf{y}} \rangle &= 4 \frac{G^2 m^2 n_b}{\sqrt{2\pi} \sigma_w^3} \int_{-\infty}^{+\infty} d^2 k \int_0^{1/\kappa^*} dr \frac{v_0 (k_x k_y, k_y^2)}{k_x^2 + k_y^2 + k_z^2} \frac{\exp - \left(\frac{(k_y v_0 r)^2}{2\sigma_w^2} \right)}{k_z} \\
&= 4 \frac{G^2 m^2 n_b}{\sqrt{2\pi} \sigma_w^3} \int_{-\infty}^{+\infty} d^2 k \int_0^{1/\kappa^*} dr r \frac{v_0 (k_x k_y, k_y^2)}{r^2 (k_x^2 + k_y^2 - \kappa^{*2}) + 1} \frac{\exp - \left(\frac{(k_y v_0 r)^2}{2\sigma_w^2} \right)}{\sqrt{1 - \kappa^{*2} r^2}},
\end{aligned} \tag{7.49}$$

and with the change of variables $s = r^2$; $ds = 2rdr$; $r \in [0, 1/\kappa^{*2}]$, to get

$$\langle \dot{\mathbf{v}}_{\mathbf{x}}, \dot{\mathbf{v}}_{\mathbf{y}} \rangle = 2 \frac{G^2 m^2 n_b}{\sqrt{2\pi} \sigma_w^3} \int_{-\infty}^{+\infty} d^2 k \int_0^{1/\kappa^{*2}} ds s \frac{v_0(k_x k_y, k_y^2)}{s(k_x^2 + k_y^2 - \kappa^{*2}) + 1} \frac{\exp - \left(\frac{(k_y v_0)^2 s}{2\sigma_w^2} \right)}{\sqrt{1 - \kappa^{*2} s}}. \quad (7.50)$$

Next, from the substitution $t = \kappa^{*2} s$; $dt = \kappa^{*2} ds$; $t \in [0, 1]$, we find

$$\langle \dot{\mathbf{v}}_{\mathbf{x}}, \dot{\mathbf{v}}_{\mathbf{y}} \rangle = 2 \frac{G^2 m^2 n_b}{\sqrt{2\pi} \sigma_w^3} \int_{-\infty}^{+\infty} d^2 k \int_0^1 dt \frac{t}{\kappa^{*4}} \frac{v_0(k_x k_y, k_y^2)}{1 + t \left(\frac{k_x^2 + k_y^2 - \kappa^{*2}}{\kappa^{*2}} \right)} \frac{\exp - \left(\frac{(k_y v_0)^2 t}{2\sigma_w^2 \kappa^{*2}} \right)}{\sqrt{1 - t}}. \quad (7.51)$$

As before, with the substitution $k_x^* = k_x/k_y$; $dk_x^* = dk_x/k_y$, we rewrite κ^* as

$$1/\kappa^{*2} = \frac{\sigma_w^2}{k_y^2} [k_x^{*2} (\sigma_v^2 \sin^2 \beta + \sigma_w^2 \cos^2 \beta) + 2k_x^* (\sigma_v^2 - \sigma_w^2) \sin \beta \cos \beta + \sigma_v^2 \cos^2 \beta + \sigma_w^2 \sin^2 \beta] \quad (7.52)$$

And Eq. (7.51) will look like

$$\langle \dot{\mathbf{v}}_{\mathbf{x}}, \dot{\mathbf{v}}_{\mathbf{y}} \rangle = 2 \sqrt{\frac{2}{\pi}} G^2 m^2 n_b \sigma_w \ln(\Lambda) \int_{-\infty}^{+\infty} dk_x^* \int_0^1 dt \frac{v_0(k_x^*, 1)}{(A k_x^{*2} + B k_x^* + C)^2} \times \frac{t}{\sqrt{1-t}} \frac{\exp - \left(\frac{v_0^2 t}{2(A k_x^{*2} + B k_x^* + C)} \right)}{1 + t \left(\frac{\sigma_w^2 (1 + k_x^{*2})}{(A k_x^{*2} + B k_x^* + C)^2} - 1 \right)} \quad (7.53)$$

where in this case $A = \sigma_v^2 \sin^2 \beta + \sigma_w^2 \cos^2 \beta$, $B = 2(\sigma_v^2 - \sigma_w^2) \sin \beta \cos \beta$, and $C = \sigma_v^2 \cos^2 \beta + \sigma_w^2 \sin^2 \beta$, and where $\ln(\Lambda)$ is the Coulomb logarithm. A total velocity dispersion of the form $\sigma_T^2 = 2\sigma_w^2 + \sigma_v^2$ is considered when writing the DF formula

$$\langle \dot{\mathbf{v}}(x, y, 0) \rangle = -2 \sqrt{\frac{2}{\pi}} \frac{G^2 m^2 n_b}{\sigma_T^2} \frac{\sqrt{\sigma_T^2 - \sigma_w^2}}{\sqrt{2\sigma_T}} \frac{v_0}{\sigma_T} \ln(\Lambda) \int_{-\infty}^{+\infty} dk_x^* \int_0^1 dt \frac{v_0(k_x^*, 1)}{(A' k_x^{*2} + B' k_x^* + C')^2} \times \frac{t}{\sqrt{1-t}} \frac{\exp - \left(\frac{t(v_0^2/\sigma_T^2)}{2(A' k_x^{*2} + B' k_x^* + C')} \right)}{1 + t \left(\frac{\left(\frac{\sigma_T^2 - \sigma_w^2}{2\sigma_T^2} \right) (1 + k_x^{*2})}{(A' k_x^{*2} + B' k_x^* + C')^2} - 1 \right)} \quad (7.54)$$

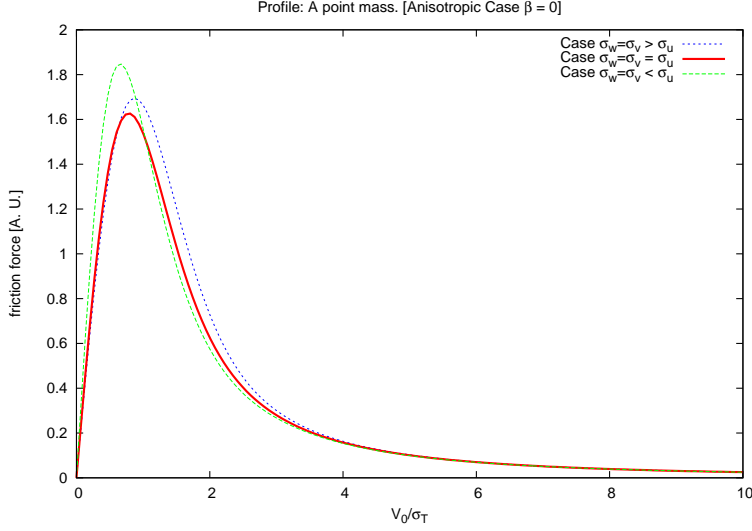


Figure 7.10: Plot of Eq. (7.44) for $\beta = 0$. This choice reproduces exactly the behaviour of Eq. (7.24).

where now

$$\begin{aligned}
 A' &= \left(\frac{\sigma_v^2}{\sigma_T^2} \right) \sin^2 \beta - \left(\frac{\sigma_T^2 - \sigma_v^2}{2\sigma_T^2} \right) \cos^2 \beta \\
 B' &= \left(3 \frac{\sigma_v^2}{\sigma_T^2} - 1 \right) \sin \beta \cos \beta \\
 C' &= \left(\frac{\sigma_v^2}{\sigma_T^2} \right) \cos^2 \beta + \left(\frac{\sigma_T^2 - \sigma_v^2}{2\sigma_T^2} \right) \sin^2 \beta.
 \end{aligned} \tag{7.55}$$

7.5 Discussion and Conclusions

We now present a series of plots showing the behaviour of the inner part of Eq. (7.44) for different choices of the angle β . The factor $2\sqrt{2/\pi}G^2m^2n_b/\sigma_T^2\ln(\Lambda)$ is not plotted. As expected, the case $\beta = 0$ is nothing but the case described by Eq. (7.24) (see Fig. (7.5)).

As one starts to look at the plots corresponding to different choices of the misalignment-angle $\beta = \pi/4, \pi/3, \pi/2$ (Figs. (7.11), (7.12), (7.13)), one can see the progressive increase of the DF force for increasing values of β in the case $\sigma_v > \sigma_u$. The increment in the force when $\beta = \pi/2$ can be as high as 30% with respect to the choice $\beta = 0$. When $\beta = \pi/2$ is chosen the massive body will find itself traveling with velocity v_0 along the k_y -axis that is oriented with the velocity ellipsoid-component u . In such a situation the *degree*

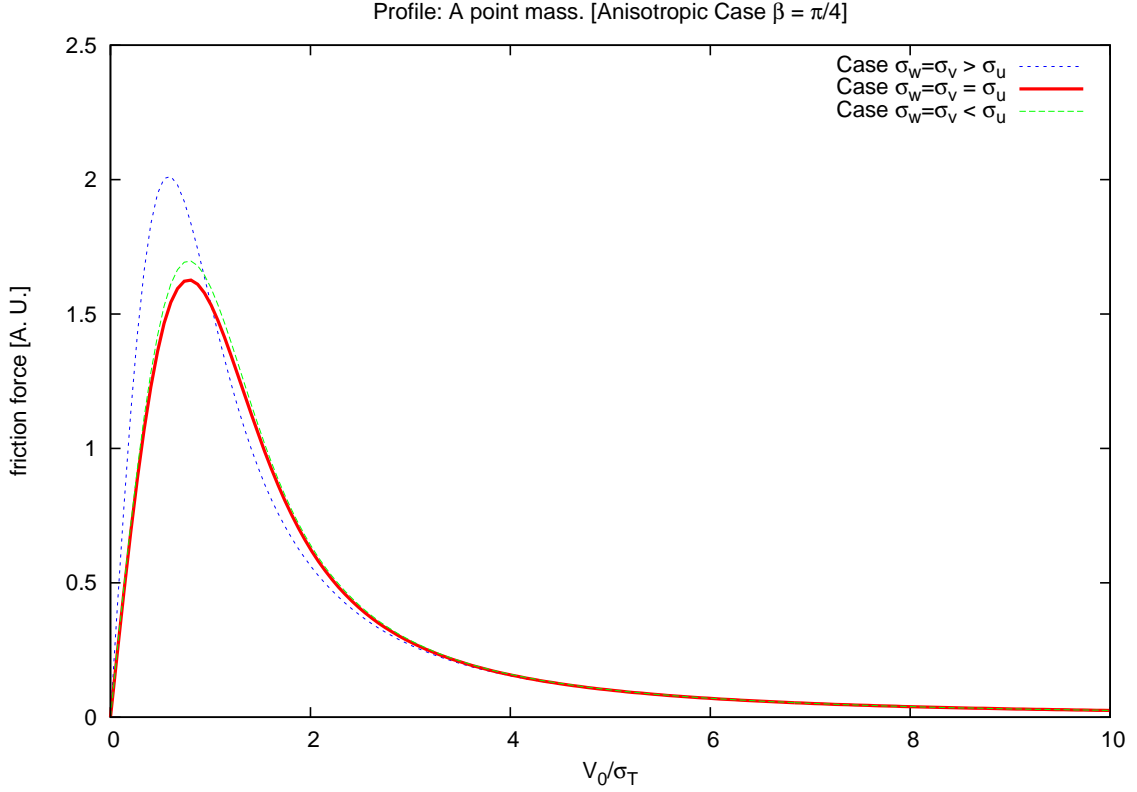


Figure 7.11: Plot of the kernel of Eq. (7.44) for the choice $\beta = \pi/4$. Even for this modest non-zero value of the misalignment-angle β , the increment in the force is considerable when an oblate-ellipsoid is considered ($\sigma_v > \sigma_u$). For a prolate spheroid ($\sigma_v < \sigma_u$) the value of the force also starts to drop drastically.

of anisotropy of the distribution function is maximum and the value of the force changes drastically for relative values of σ_v and σ_u . When $\sigma_v < \sigma_u$, the force drops considerably for the choice $\beta = \pi/4$ with respect to the aligned case $\beta = 0$. For $\beta = \pi/3$ the situation is pretty similar to the isotropic case and for $\beta = \pi/2$ the force will be weaker than the isotropic force although it will not fall off so fast as in this case.

Contrary to previous cases, there will be a second contribution from Eq. (7.44) to the drag, since the velocity component $\langle \dot{\mathbf{v}}_{\mathbf{x}} \rangle$ is not longer zero. In Figs. (7.14) and (7.15) we show the most interesting cases, one can note first that the isotropic case is zero as expected due to symmetry (cf. Eq.(7.44)). Although the contribution to the drag is not as important as it is for the $\langle \dot{\mathbf{v}}_{\mathbf{y}} \rangle$ component, we can see the opposite contributions from the cases

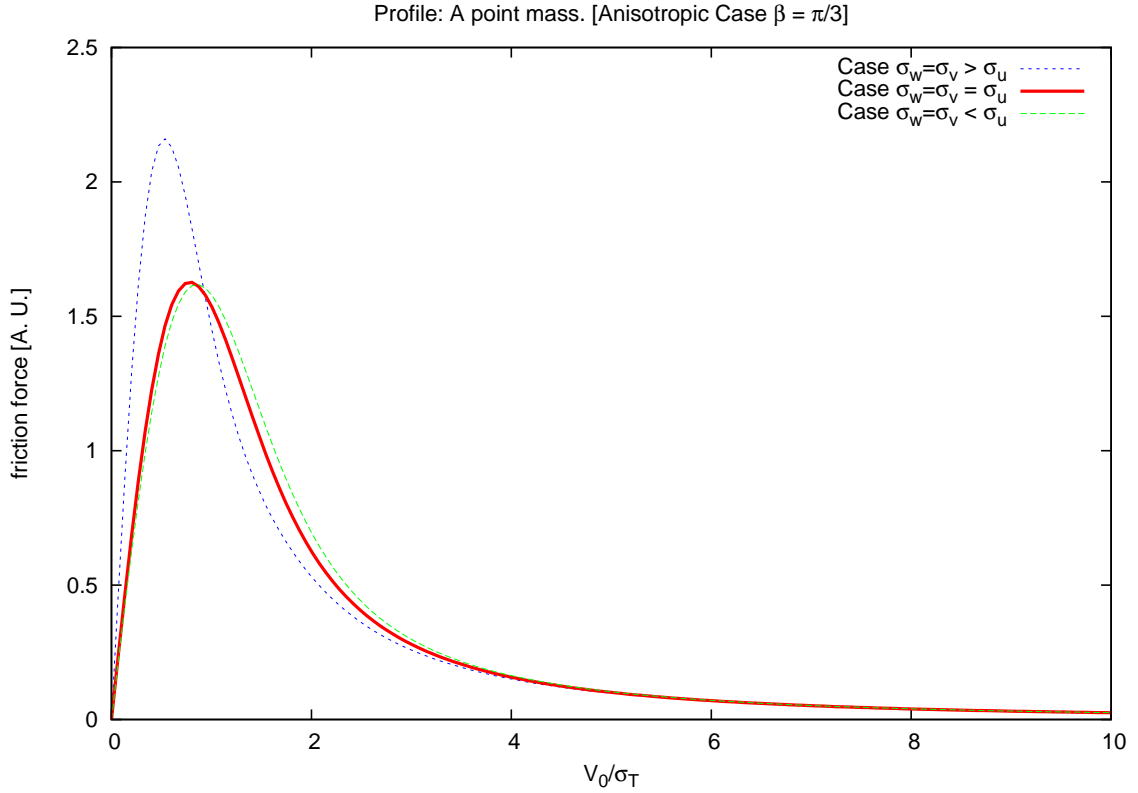


Figure 7.12: Behaviour of Eq. (7.44) for the choice $\beta = \pi/3$. A particle traveling at this angle through a prolate ellipsoid ($\sigma_v < \sigma_u$) will experience a drag very similar to the force exerted by a sea of particles with an isotropic velocity distribution. On the other hand, when an oblate ellipsoid is included ($\sigma_v > \sigma_u$), the force exerted on the perturber continues to rise with respect to the case when the angle is zero.

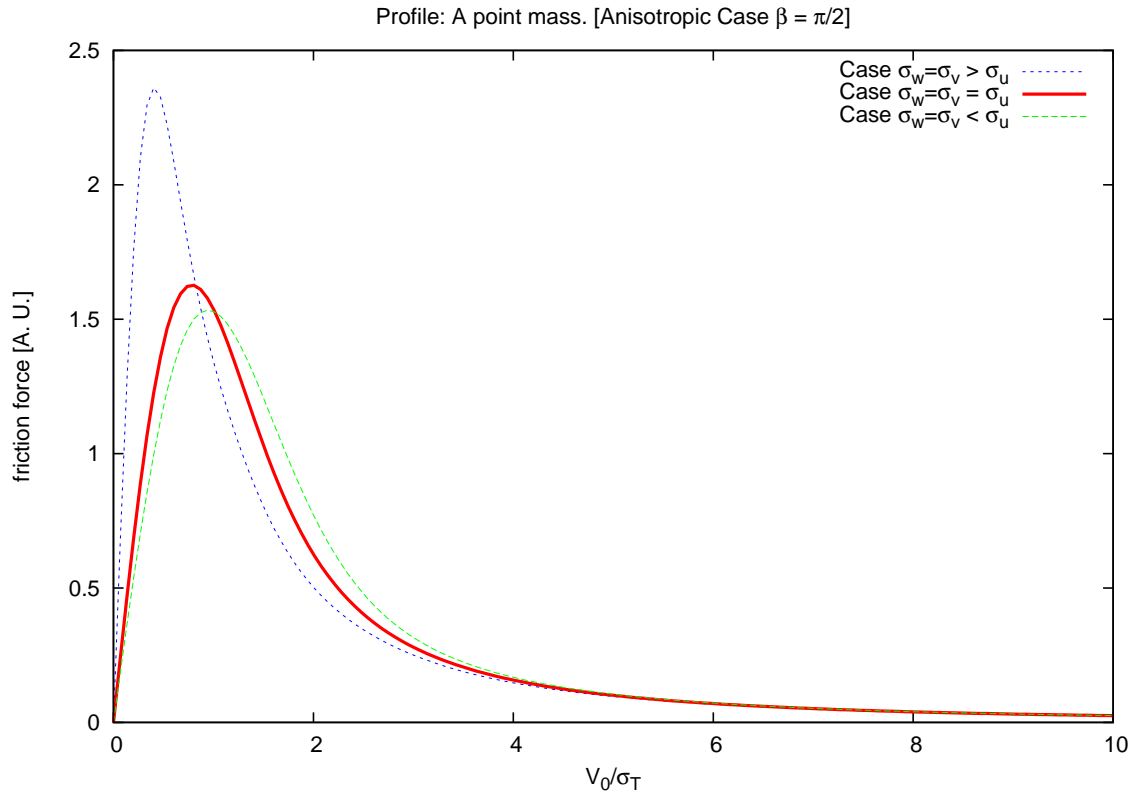


Figure 7.13: Behaviour of Eq. (7.44) for the choice $\beta = \pi/2$. The force exerted by an oblate-ellipsoid ($\sigma_v = \sigma_w > \sigma_u$) is highest in this case. The opposite effect arises for the $\sigma_v = \sigma_w < \sigma_u$.

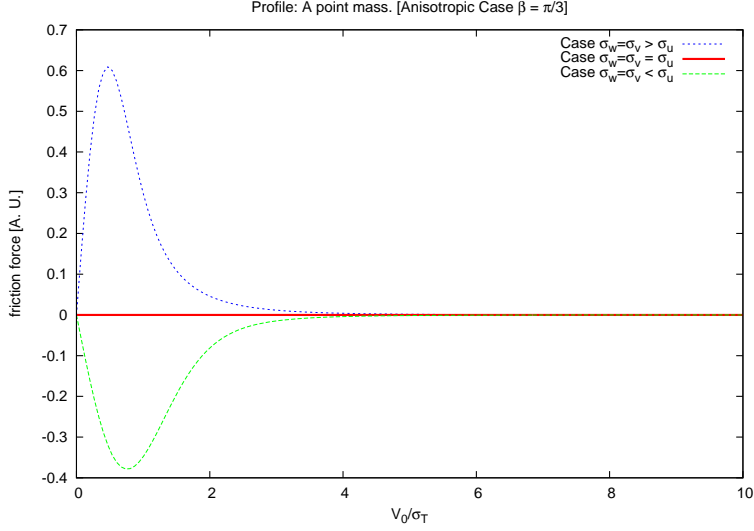


Figure 7.14: Behaviour of the velocity component $\langle \dot{\mathbf{v}}_{\mathbf{x}} \rangle$ of Eq. (7.44) for the choice $\beta = \pi/3$. Due to the changing sign of the formula, two opposite contributions will appear. Whether an oblate or an prolate ellipsoid is considered the net contribution from this component will be much smaller than the contribution from the term $\langle \dot{\mathbf{v}}_{\mathbf{y}} \rangle$.

$\sigma_v > \sigma_u$ and $\sigma_v < \sigma_u$; due to the fact that the $\langle \dot{\mathbf{v}}_{\mathbf{x}} \rangle$ term depends on the mixed term $k_x k_y$ (see the general formula (6.29)), the change of sign in Eq. (7.44) will make both a negative and a positive drag force to appear, meaning that the particle will experience a net acceleration and deceleration depending upon the sign of the terms. In any case, the contribution from the $\langle \dot{\mathbf{v}}_{\mathbf{y}} \rangle$ component to the force is at least two times bigger than that from $\langle \dot{\mathbf{v}}_{\mathbf{x}} \rangle$ and could even be bigger for different values of the velocity–dispersion components.

For comparison with Eq. (7.33), we give an estimate of the time it would take a satellite to decay for the case $\beta = \pi/2$ and by taking into account the simplifications $v_0 = \sigma_v$, $\sigma_v = 2\sigma_w$, and choosing $\beta = \pi/2$. We find

$$\begin{aligned} \frac{1}{k} \equiv t_{dec} &= 0.118 \frac{\sigma_v^3}{G^2 m \rho_b \ln(\Lambda)} \\ &= \frac{6.24 \times 10^9 \text{ yr}}{\ln(\Lambda)} \left(\frac{\sigma_v}{10 \text{ kms}^{-1}} \right)^3 \left(\frac{1 \text{ M}_{\odot}}{m} \right) \left(\frac{10^3 \text{ M}_{\odot} \text{ pc}^{-3}}{\rho} \right). \end{aligned} \quad (7.56)$$

Now we turn our attention to Eq. (7.54) that describes the DF exerted on a particle as this makes its way through a velocity–ellipsoid such that

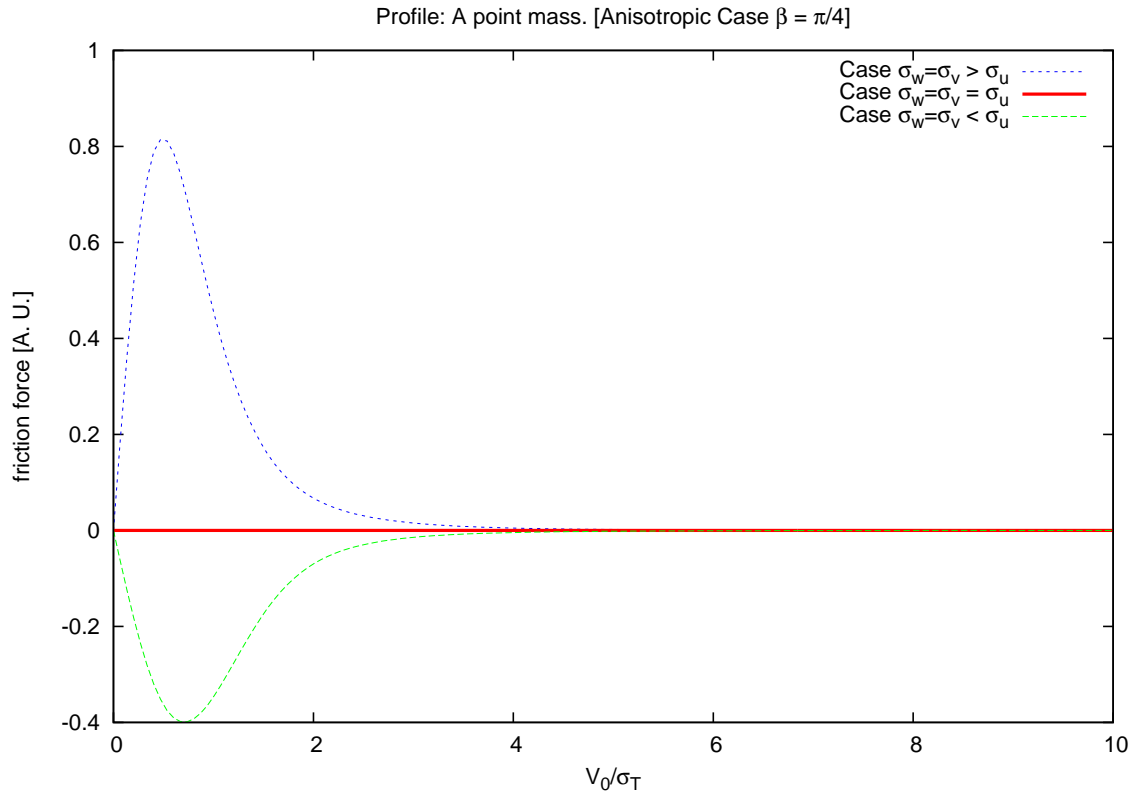


Figure 7.15: Plot of the force term $\langle \dot{\mathbf{v}}_{\mathbf{x}} \rangle$ of Eq. (7.44) for the choice $\beta = \pi/4$. The force exerted by an oblate-ellipsoid ($\sigma_v = \sigma_w > \sigma_u$) is two times bigger, but of opposite sign, than the $\sigma_v = \sigma_w < \sigma_u$ case.

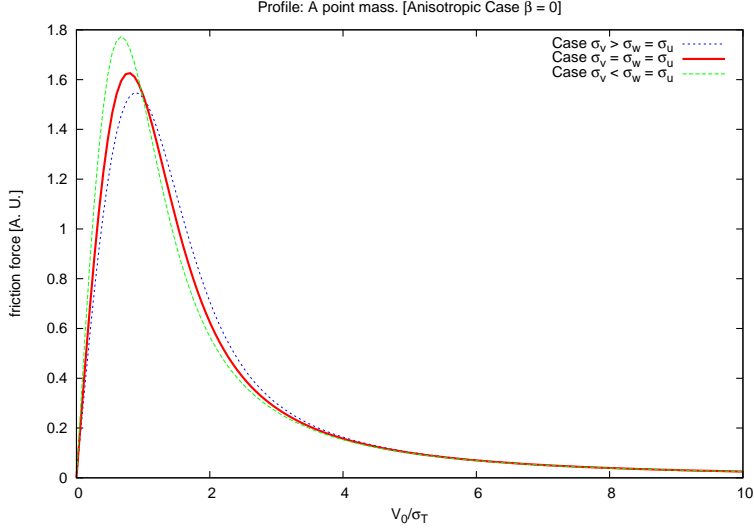


Figure 7.16: For the choice $\beta = 0$, Eq. (7.54) will reproduce the situation described in Fig. (7.6).

($\sigma_v \neq \sigma_w = \sigma_u$). Its behaviour can be understood by looking at Figs. (7.16), (7.17), and (7.18). As expected, the choice $\beta = 0$ (Fig. (7.16)) reproduces the case plotted in Fig. (7.6). Although in this case the changes in the force are not so notorious as in the previous situation ($\sigma_v = \sigma_w \neq \sigma_u$), the anisotropy also plays an important role here. For $\beta = 0$, due to the fact that $\sigma_w = \sigma_u$ the difference in the distribution function (with respect to the isotropic case) will be maximum when $\sigma_w > \sigma_v$, however, if $\beta = \pi/2$ is chosen, the satellite will travel with velocity v_0 along the k_y -axis which is oriented with the velocity component u of the ellipsoid, and so for $\sigma_u > \sigma_v$ the force felt by the particle will not be so different than that produced by an isotropic velocity spheroid. The change between the isotropic case and the cases with $\beta = \pi/4, \pi/3$ are minimum.

For comparison with Eq. (7.33), which was derived for the case $\beta = 0$, we give an estimate of the time it would take a satellite to decay for the case $\beta = \pi/2$ and by taking into account the simplifications $v_0 = \sigma_v, \sigma_v = 2\sigma_w$. We find

$$\begin{aligned} \frac{1}{k} \equiv t_{dec} &= 1.4 \frac{\sigma_v^3}{G^2 m \rho_b \ln(\Lambda)} \\ &= \frac{7.4 \times 10^{10} \text{yr}}{\ln(\Lambda)} \left(\frac{\sigma_v}{10 \text{ km s}^{-1}} \right)^3 \left(\frac{1 \text{ M}_\odot}{m} \right) \left(\frac{10^3 \text{ M}_\odot \text{pc}^{-3}}{\rho} \right). \end{aligned} \quad (7.57)$$

By comparing Eqs. (7.33), (7.34), (7.56), and (7.57), one can see how big

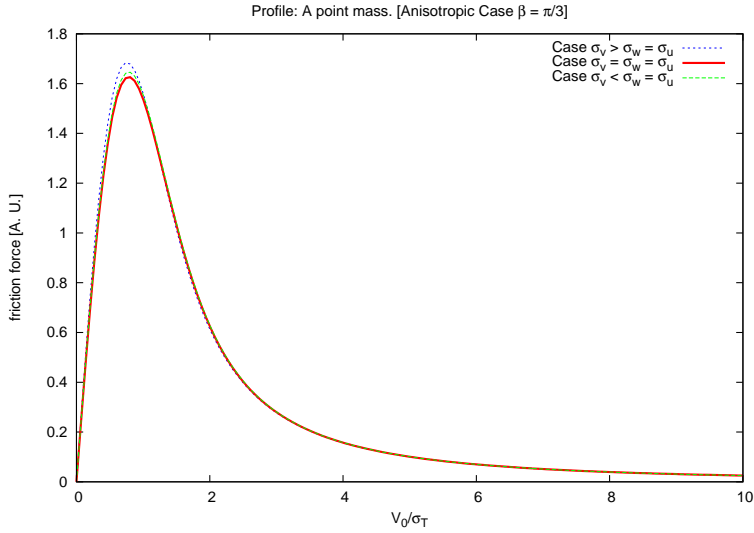


Figure 7.17: Behaviour of Eq. (7.54) for the choice $\beta = \pi/3$. Due to the fact that the particle's trajectory is no longer aligned with the velocity component v of the velocity ellipsoid, the effect of the anisotropy will be reduced and the force contribution will be similar to that given by the isotropic term

the differences in the decay time can be depending on the situation considered. We conclude that the anisotropy of the host system can considerably alter the value of the drag exerted on a body flying through it. Therefore the equations derived here should be helpful in determining better estimates of the DF process.

The contribution from the velocity component $\langle \dot{\mathbf{v}}_{\mathbf{x}} \rangle$ is plotted in Figs. (7.19) and (7.20). The behaviour of this component will be similar to the previous case described by Eq. (7.44): there is a deceleration and acceleration of the particle depending on the value of the effective velocity dispersion. However, the net contribution in both cases will be smaller than the contribution from the term $\langle \dot{\mathbf{v}}_{\mathbf{y}} \rangle$. Due to symmetry, the contribution from the isotropic case vanishes.

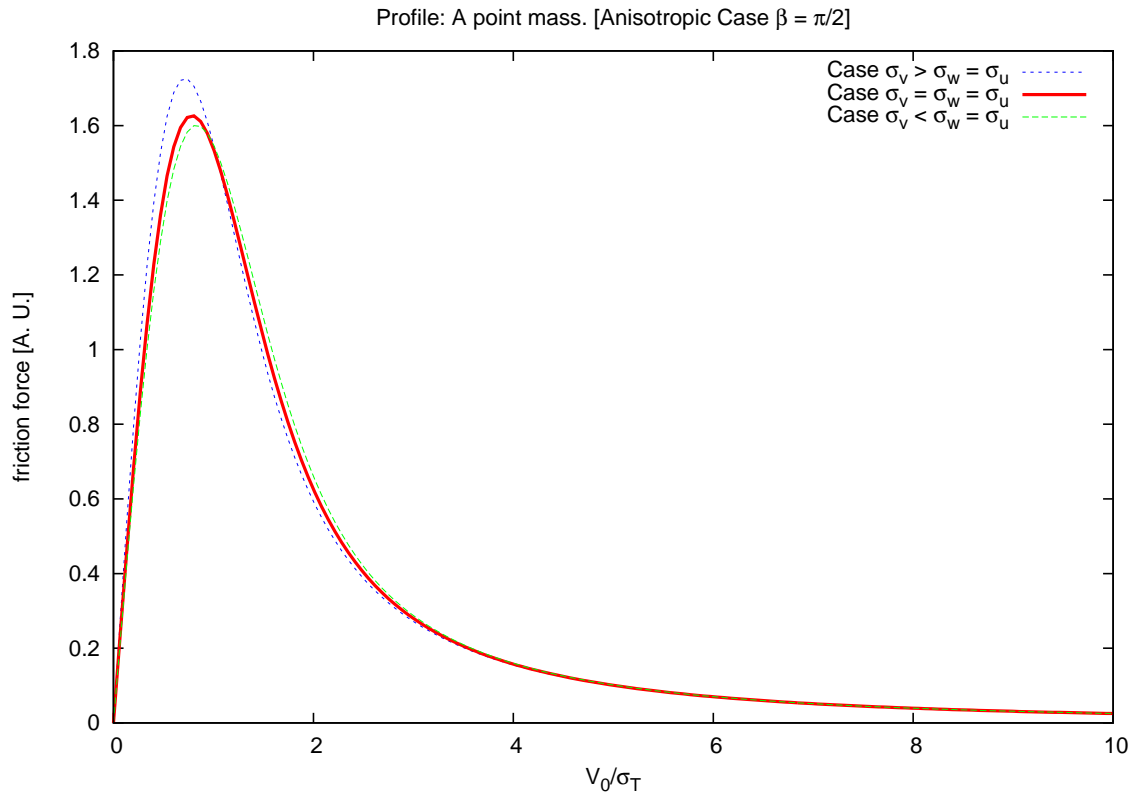


Figure 7.18: Eq. (7.54) for $\beta = \pi/2$. In this situation the k_y -axis is oriented with the velocity-ellipsoid component w and $\sigma_T^2 = 2\sigma_w^2 + \sigma_v^2$. The distribution function will remain almost constant in the range $\sigma_v < \sigma_w$ and will have its maximum change when $\sigma_v > \sigma_w$.

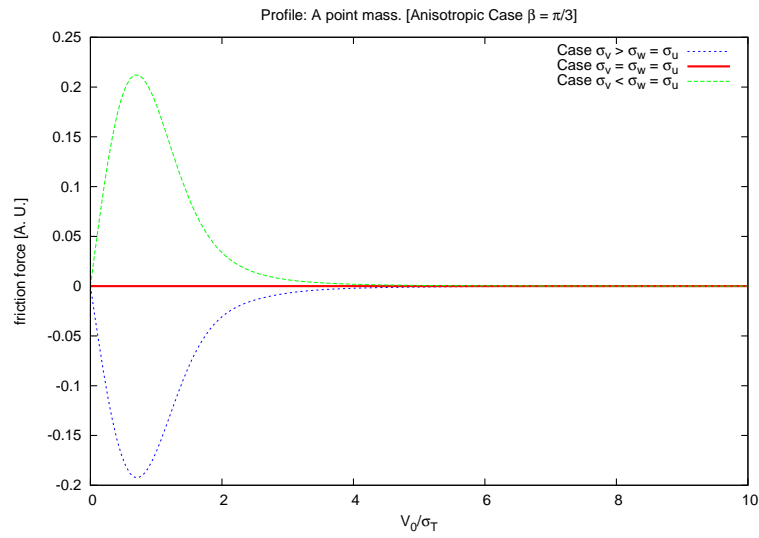


Figure 7.19: Behaviour of the velocity component $\langle \dot{\mathbf{v}}_{\mathbf{x}} \rangle$ of Eq. (7.54) for the choice $\beta = \pi/3$. The force exerted by an oblate-ellipsoid ($\sigma_v > \sigma_w = \sigma_u$) is positive. The opposite effect arises for the case of a prolate ellipsoid ($\sigma_v < \sigma_w = \sigma_u$). The isotropic case is zero due to the symmetry in Eq. (7.54).

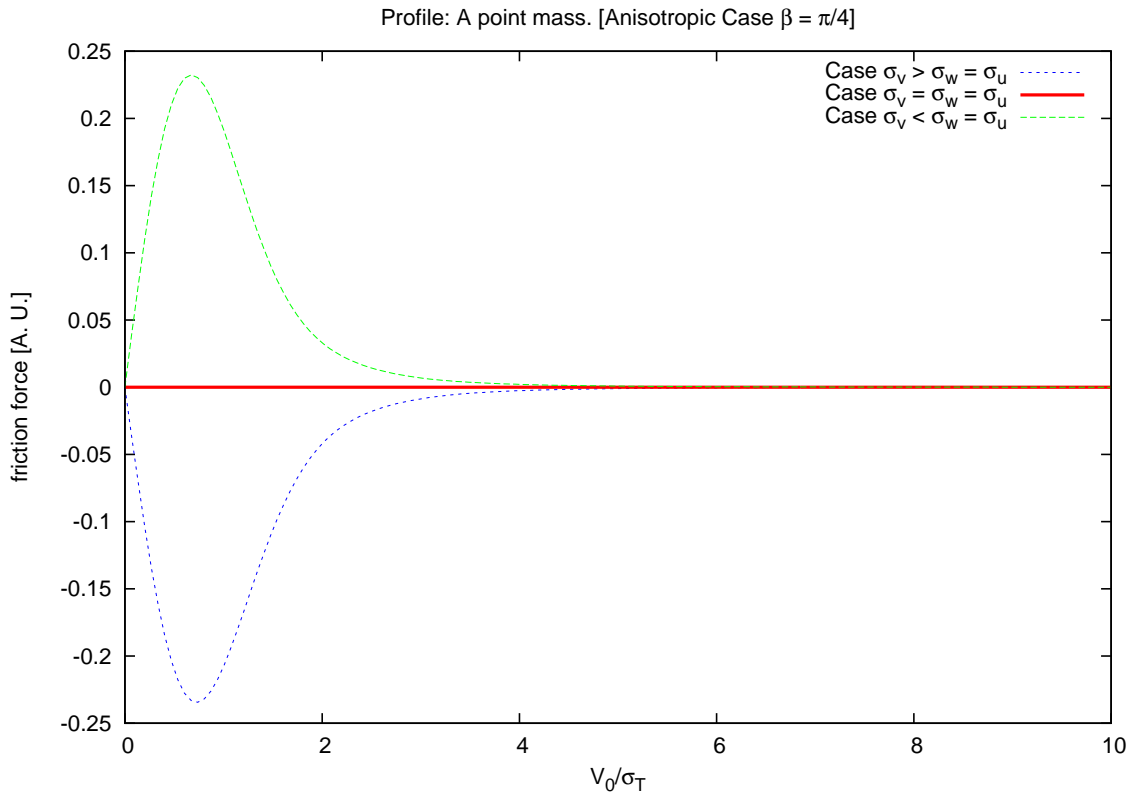


Figure 7.20: When the choice $\beta = \pi/4$ is made the velocity component $\langle \dot{\mathbf{v}}_x \rangle$ of Eq. (7.54) will have two contributions of opposite sign but of the same magnitude. The force exerted by an oblate-ellipsoid ($\sigma_v = \sigma_w > \sigma_u$) represents a deceleration of the particle and in the case $\sigma_v = \sigma_w < \sigma_u$ there will be an acceleration although these contributions will be smaller than that from the $\langle \dot{\mathbf{v}}_y \rangle$ case.

Chapter 8

Conclusions

We started this work by investigating the Jeans instability of a galactic disk embedded in a dynamically responsive dark halo [EF07b]. This became recently important as physical reasoning was that the self-gravity of the disk, which has a destabilizing effect, was reduced by the surrounding halo. Similarly the onset of non-axisymmetric coherent large-scale instabilities of the entire disk such as the bar-instability was thought to be damped by a surrounding halo.

However, modern high-resolution simulations in which the surrounding halo is treated as a dynamically responsive system, have shown that actually the opposite is true.

We studied then the dynamical stability of an infinitesimally thin galactic disk using the model of a patch of the galactic disk developed by Toomre [Too64], Goldreich & Lynden-Bell [GL65], Julian & Toomre [JT66] and Fuchs [Fuc01]. The patch is assumed to rotate around the galactic center and the differential rotation of the stars is approximated as a linear shear flow. The surface density is assumed to be constant over the patch. Polar coordinates are approximated by pseudo Cartesian coordinates (x, y) with x pointing in the radial direction and y in the direction of rotation, respectively. We calculated the dynamical response of the disk to a small 'ring-like' perturbations of the gravitational disk potential by solving the linearized Boltzmann equation. In deriving the induced density perturbation we considered a Gaussian velocity distribution of the stars with a velocity. By assuming the disk to be self-gravitating, we consider a self-consistent treatment that satisfies Poisson equation.

After this standard procedure, we included then a *living* halo by considering dark matter particles to follow straight-line orbits with an isotropic velocity distribution modelled also by a Gaussian distribution and by ne-

glecting all density gradients in the halo so that the halo density distribution is assumed to be homogeneous.

We apply directly the results of Fuchs [Fuc04] who extended the model of a local patch of a galactic disk by embedding it into a dark halo. The dark-matter halo responds to the potential perturbation in the disk and develops potential perturbations which have the same radial structure $\exp(ikx)$ as in the disk. In this way we calculated the induced perturbation of the gravitational potential of the dark halo, which means that the halo supports the perturbation in the disk and therefore the density perturbation in the disk is stronger than in an isolated disk.

We get an equation that describes the line of neutrally stable ($\omega = 0$) perturbations in the space spanned by Q_T and $\lambda/\lambda_{\text{crit}}$ as in the case of an isolated disk, but now modified by an extra term. It is shown that the disk-halo system becomes nominally Jeans unstable. On small scales the instability is suppressed, if the Toomre stability index Q_T is higher than a certain threshold, but on large scales the Jeans instability sets invariably in.

However, by using this simple self-consistent disk-halo model it is demonstrated that this occurs on scales which are much larger than the system so that this is indeed only a nominal effect. From a practical point of view the dynamical stability of galactic disks is not affected by a live dark halo.

Since the determination of the dynamical friction force exerted by a gravitating system of background stars on a test star moving through the system is one of the classical problems of stellar dynamics, as part of the second project of this doctoral thesis, we followed a wave-mechanical treatment to calculate the drag force exerted by an infinite homogeneous background of stars on a perturber as this makes its way through the system. This is an alternative approach as that developed in Chandrasekhar's seminal paper of dynamical friction [Cha43], where he envisaged the scenario of a sequence of consecutive gravitational two-body encounters of test and field stars. We calculate the drag force exerted on a Plummer sphere and a sphere with the density distribution of a Hernquist profile.

We rigorously calculated the drag force exerted on these bodies following the approach of both Marochnik [Mar68] and Kalnajs [19772] who determined the polarization cloud created in the background medium as a massive object was making its way through the system. This mode analysis can be simply understood as linear and angular momentum exchange in stellar systems ([TW84]; [Fuc04]), and has been extensively used in plasma physics [Sti62].

We assume an infinite homogenous distribution of field stars on isotropic

straight-line orbits. The response of the system of background stars to the perturbation due to a massive perturber is determined by solving the linearized Boltzmann equation. Then, by Fourier-transforming both the perturbations of the distribution function and the potential we solved Boltzmann's equation in an easier way. In the process of doing so, we consider, without loss of generality, the spatial coordinates x_i and the corresponding velocity components v_i to be oriented with one axis parallel to the direction of the wave vector. We integrate over the two velocity components perpendicular to \mathbf{k} , and we assume for the field stars always a Gaussian velocity distribution function.

Once the general solution is found, we moved onto calculating the corresponding Fourier-transform potentials of different perturbing bodies, such as a extended body having a density profile of the Hernquist type, a Plummer sphere, and a point mass (for comparison with the other two). It is worth saying that Plummer spheres have constant density cores, whereas numerical simulations of the formation of galactic haloes in cold dark matter cosmology show that dark haloes may have a central density cusp. Thus models of a Plummer or a Hernquist sphere should encompass the range of plausible models for satellite galaxies.

Because only in the direction of motion of the perturber there is a net effect, we carry out our development making use of all possible symmetries to compute all integrals over phase space and we get a general DF formula in terms of an error function and on a Coulomb logarithm that depends on the specific potential of the perturber under consideration.

Next, we computed the exact form of the Coulomb logarithm associated to a Herquist, Plummer and a point mass profile. In this way it is shown that the shape of the perturber affects only the exact form of the Coulomb logarithm. The latter converges on small scales, because encounters of the test and field stars with impact parameters less than the size of the massive perturber become inefficient. We confirm this way earlier results based on the impulse approximation of small angle scatterings.

Also worth noting is the fact that we also discuss, first, on the more realistic escenario where perturbers can be deformed by tidal fields. One source of the tidal field is the induced polarization cloud itself. However, we found that this effect is expected to be small. And second, we also discuss on effect present if the perturbers were gravitationally bound systems themselves like globular clusters or dwarf satellite galaxies. Such objects can and do loose mass due to tidal shocking, and such effect both effects could be of comparable magnitude as the one caused by DF.

Finally, as part of the third and final PhD thesis' project, we extended our analysis of DF, in a straightforward way, to include anisotropic velocity distributions of the field stars. Based on the fact that Fuchs & Athanassoula [FA05] showed that if the velocity ellipsoid is either prolate or oblate, the velocity dispersion in the solution of the Boltzmann equation is replaced by an effective velocity dispersion which depends on the semi-axes of the velocity ellipsoid and its orientation relative to the wave vector \mathbf{k} . This complicated the evaluation of the integrals with respect to the wave numbers considerably. Nonetheless, we managed to get handy, easy-to-use formulae of DF for a point mass for different orientations of the trajectory of the massive body with respect to the velocity ellipsoid. Whether the ellipsoid was prolate or oblate, the value of the force could change drastically from the isotropic case. Although in this last case there will be a non-zero contribution from the $\langle \dot{\mathbf{v}}_{\mathbf{x}} \rangle$ component of the force, its contribution will in general be smaller than the contribution from the $\langle \dot{\mathbf{v}}_{\mathbf{y}} \rangle$ component.

The ability of satellites to alter the phase space distribution of the background system in such a situation is of great importance for its dynamical evolution and the DF force formulae derived here could be a useful tool to constraint on physical grounds the evolution of such systems.

Bibliography

- [19772] in Gravitational N-Body Problem. page 13. Reidel Publ. Comp, 1912., 1972.
- [Abt99] H. A. Abt, editor. *The Astrophysical Journal, American Astronomical Society Centennial Issue*, volume 525. Univ. of Chicago Press, 1999, 1999.
- [ANS06] M. G. Abadi, J. F. Navarro, and M. Steinmetz. Stars beyond galaxies: the origin of extended luminous haloes around galaxies. *MNRAS*, 365:747–758, January 2006.
- [AS72] M. Abramowitz and I. A. Stegun. *Handbook of Mathematical Functions*. Handbook of Mathematical Functions, New York: Dover, 1972, 1972.
- [Ath02] E. Athanassoula. Bar-Halo Interaction and Bar Growth. *ApJL*, 569:L83–L86, April 2002.
- [Ath03] E. Athanassoula. What determines the strength and the slowdown rate of bars? *MNRAS*, 341:1179–1198, June 2003.
- [BC75] F. Bertola and M. Capaccioli. Dynamics of early type galaxies. I - The rotation curve of the elliptical galaxy NGC 4697. *ApJ*, 200:439–445, September 1975.
- [Bin76] J. Binney. Is the flattening of elliptical galaxies necessarily due to rotation. *MNRAS*, 177:19–29, October 1976.
- [Bin77] J. Binney. Dynamical friction in aspherical clusters. *MNRAS*, 181:735–746, December 1977.
- [Bin78] J. Binney. On the rotation of elliptical galaxies. *MNRAS*, 183:501–514, May 1978.

- [Bin05] J. Binney. Rotation and anisotropy of galaxies revisited. *MNRAS*, 363:937–942, November 2005.
- [Bos97] A. P. Boss. Giant planet formation by gravitational instability. *Science*, 276:1836–1839, 1997.
- [Bos03] A. P. Boss. Rapid Formation of Outer Giant Planets by Disk Instability. *ApJ*, 599:577–581, December 2003.
- [BS80] J. N. Bahcall and R. M. Soneira. The universe at faint magnitudes. I - Models for the galaxy and the predicted star counts. *ApJS*, 44:73–110, September 1980.
- [BT87] J. Binney and S. Tremaine. *Galactic dynamics*. Princeton, NJ, Princeton University Press, 1987, 747 p., 1987.
- [Bv87] T. R. Bontekoe and T. S. van Albada. Decay of galaxy satellite orbits by dynamical friction. *MNRAS*, 224:349–366, January 1987.
- [CEB⁺07] M. Cappellari, E. Emsellem, R. Bacon, M. Bureau, R. L. Davies, P. T. de Zeeuw, J. Falcón-Barroso, D. Krajnović, H. Kuntschner, R. M. McDermid, R. F. Peletier, M. Sarzi, R. C. E. van den Bosch, and G. van de Ven. The SAURON project - X. The orbital anisotropy of elliptical and lenticular galaxies: revisiting the $(V/\sigma, \epsilon)$ diagram with integral-field stellar kinematics. *MNRAS*, 379:418–444, August 2007.
- [Cha42] S. Chandrasekhar. *Principles of stellar dynamics*. Physical Sciences Data, 1942.
- [Cha43] S. Chandrasekhar. Dynamical Friction. I. General Considerations: the Coefficient of Dynamical Friction. *ApJ*, 97:255–+, March 1943.
- [CMG99] M. Colpi, L. Mayer, and F. Governato. Dynamical Friction and the Evolution of Satellites in Virialized Halos: The Theory of Linear Response. *ApJ*, 525:720–733, November 1999.
- [CVM01] S. A. Cora, M. M. Vergne, and J. C. Muzzio. On the Effect of Chaotic Orbits on Dynamical Friction. *ApJ*, 546:165–175, January 2001.
- [Dam93] T. M. Dame. The Distribution of Neutral Gas in the Milky Way. In S. S. Holt and F. Verter, editors, *Back to the Galaxy*, volume 278 of *American Institute of Physics Conference Series*, pages 267–278, 1993.

- [de 48] G. de Vaucouleurs. Recherches sur les Nebuleuses Extragalactiques. *Annales d'Astrophysique*, 11:247–+, January 1948.
- [Dek76] E. Dekker. Spiral structure and the dynamics of galaxies. *Phys. Rep.*, 24:315–389, 1976.
- [dMR01] W. J. G. de Blok, S. S. McGaugh, and V. C. Rubin. High-Resolution Rotation Curves of Low Surface Brightness Galaxies. II. Mass Models. *AJ*, 122:2396–2427, November 2001.
- [EF07a] O. Esquivel and B. Fuchs. Dynamical friction force exerted on spherical bodies. *MNRAS*, 378:1191–1195, July 2007.
- [EF07b] O. Esquivel and B. Fuchs. Jeans instability of a galactic disk embedded in a live dark halo. *A&A*, 468:803–805, June 2007.
- [EL08] A. Escala and R. B. Larson. Stability of Galactic Gas Disks and the Formation of Massive Clusters. *ArXiv e-prints*, 806, June 2008.
- [FA05] B. Fuchs and E. Athanassoula. Interaction between a galactic disk and a live dark halo with an anisotropic velocity distribution. *A&A*, 444:455–459, December 2005.
- [FCT08] K. Foyle, S. Courteau, and R. J. Thacker. An N-body/SPH study of isolated galaxy mass density profiles. *MNRAS*, 386:1821–1844, June 2008.
- [FFT79] R. Frahm, B. Fuchs, and K. O. Thielheim. Spiral density waves illustrated by the superposition of periodic stellar orbits. *A&SS*, 63:185–191, June 1979.
- [Fuc01] B. Fuchs. Density waves in the shearing sheet. I. Swing amplification. *A&A*, 368:107–121, March 2001.
- [Fuc04] B. Fuchs. Density waves in the shearing sheet. IV. Interaction with a live dark halo. *A&A*, 419:941–948, June 2004.
- [GG03] E. Griv and M. Gedalin. The fine-scale spiral structure of low and moderately high optical depth regions of Saturn's main rings: A review. *Planet. Space Sci.*, 51:899–927, December 2003.
- [GHO99] O. Y. Gnedin, L. Hernquist, and J. P. Ostriker. Tidal Shocking by Extended Mass Distributions. *ApJ*, 514:109–118, March 1999.

- [GL65] P. Goldreich and D. Lynden-Bell. II. Spiral arms as sheared gravitational instabilities. *MNRAS*, 130:125–+, 1965.
- [GO97] O. Y. Gnedin and J. P. Ostriker. Destruction of the Galactic Globular Cluster System. *ApJ*, 474:223–+, January 1997.
- [GR00] I. S. Gradshteyn and I. M. Ryzhik. *Table of integrals, series and products*. New York: Academic Press, —c2000, 5th ed. completely reset, edited by Jeffrey, Alan, 2000.
- [Her90] L. Hernquist. An analytical model for spherical galaxies and bulges. *ApJ*, 356:359–364, June 1990.
- [HF04] J. Holmberg and C. Flynn. The local surface density of disc matter mapped by Hipparcos. *MNRAS*, 352:440–446, August 2004.
- [HFM03] Y. Hashimoto, Y. Funato, and J. Makino. To Circularize or Not To Circularize?-Orbital Evolution of Satellite Galaxies. *ApJ*, 582:196–201, January 2003.
- [HWdZ99] A. Helmi, S. D. M. White, P. T. de Zeeuw, and H. Zhao. Debris streams in the solar neighbourhood as relicts from the formation of the Milky Way. *Nature*, 402:53–55, November 1999.
- [Ill77] G. Illingworth. Rotation in 13 elliptical galaxies. *ApJL*, 218:L43–L47, December 1977.
- [Jaf83] W. Jaffe. A simple model for the distribution of light in spherical galaxies. *MNRAS*, 202:995–999, March 1983.
- [JB00] I.-G. Jiang and J. Binney. The orbit and mass of the Sagittarius dwarf galaxy. *MNRAS*, 314:468–474, May 2000.
- [Jea19] J. H. Jeans. *Problems of cosmogony and stellar dynamics*. Cambridge, University press, 1919., 1919.
- [JSH95] K. V. Johnston, D. N. Spergel, and L. Hernquist. The Disruption of the Sagittarius Dwarf Galaxy. *ApJ*, 451:598–+, October 1995.
- [JT66] W. H. Julian and A. Toomre. Non-Axisymmetric Responses of Differentially Rotating Disks of Stars. *ApJ*, 146:810–+, December 1966.

- [JW97] H. Jahreiß and R. Wielen. The impact of HIPPARCOS on the Catalogue of Nearby Stars. The stellar luminosity function and local kinematics. In *Hipparcos - Venice '97*, volume 402 of *ESA Special Publication*, pages 675–680, August 1997.
- [KAPG08] A. Knebe, B. Arnold, C. Power, and B. K. Gibson. The dynamics of subhaloes in warm dark matter models. *MNRAS*, 386:1029–1037, May 2008.
- [KBC⁺08] D. Krajnovic, R. Bacon, M. Cappellari, R. L. Davies, P. T. de Zeeuw, E. Emsellem, J. Falcon-Barroso, H. Kuntschner, R. M. McDermid, R. F. Peletier, M. Sarzi, R. C. E. van den Bosch, and G. van de Ven. The SAURON project - XII. Kinematic substructures in early-type galaxies: evidence for disks in fast rotators. *ArXiv e-prints*, 807, July 2008.
- [Keg98] W. H. Kegel. *Plasmaphysik*. Plasmaphysik. Eine Einführung. Kegel, Wilhelm H., pp. 320. ISBN 3-540-63701-X. Springer-Verlag Berlin Heidelberg 1998, 1998.
- [KKBP98] A. V. Kravtsov, A. A. Klypin, J. S. Bullock, and J. R. Primack. The Cores of Dark Matter-dominated Galaxies: Theory versus Observations. *ApJ*, 502:48–+, July 1998.
- [Lin59] B. Lindblad. Galactic Dynamics. *Handbuch der Physik*, 53:21–+, 1959.
- [LK72] D. Lynden-Bell and A. J. Kalnajs. On the generating mechanism of spiral structure. *MNRAS*, 157:1–+, 1972.
- [Mar68] L. S. Marochnik. A Test Star in a Stellar System. *Soviet Astronomy*, 11:873–+, April 1968.
- [NFW97] J. F. Navarro, C. S. Frenk, and S. D. M. White. A Universal Density Profile from Hierarchical Clustering. *ApJ*, 490:493–+, December 1997.
- [OP73] J. P. Ostriker and P. J. E. Peebles. A Numerical Study of the Stability of Flattened Galaxies: or, can Cold Galaxies Survive? *ApJ*, 186:467–480, December 1973.
- [PJK04] J. Peñarrubia, A. Just, and P. Kroupa. Dynamical friction in flattened systems: a numerical test of Binney’s approach. *MNRAS*, 349:747–756, April 2004.

- [Plu15] H. C. Plummer. The distribution of stars in globular clusters. *MNRAS*, 76:107–121, December 1915.
- [PS91] J. C. Papaloizou and G. J. Savonije. Instabilities in self-gravitating gaseous discs. *MNRAS*, 248:353–369, February 1991.
- [Ros50] W. P. Rosse. Observations on the Nebulae. *Phil. Trans. R. Soc. London*, 140:499, 1850.
- [Sti62] T. H. Stix. *The Theory of Plasma Waves*. The Theory of Plasma Waves, New York: McGraw-Hill, 1962, 1962.
- [TB05] M. Trenti and G. Bertin. A family of models of partially relaxed stellar systems. I. Dynamical properties. *A&A*, 429:161–172, January 2005.
- [TC08] O. Tiret and F. Combes. Evolution of spiral galaxies in modified gravity. II. Gas dynamics. *A&A*, 483:719–726, June 2008.
- [Too64] A. Toomre. On the gravitational stability of a disk of stars. *ApJ*, 139:1217–1238, May 1964.
- [Too77] A. Toomre. Theories of spiral structure. *ARAA*, 15:437–478, 1977.
- [TW84] S. Tremaine and M. D. Weinberg. Dynamical friction in spherical systems. *MNRAS*, 209:729–757, August 1984.
- [Van75] P. O. Vandervoort. Resonant Stellar Orbits in Spiral Galaxies. II. a General Epicyclic Theory. *ApJ*, 201:50–62, October 1975.
- [VB05] E. I. Vorobyov and S. Basu. The effect of non-isothermality on the gravitational collapse of spherical clouds and the evolution of protostellar accretion. *MNRAS*, 363:1361–1368, November 2005.
- [VW99] H. Velazquez and S. D. M. White. Sinking satellites and the heating of galaxy discs. *MNRAS*, 304:254–270, April 1999.
- [Whi76] S. D. M. White. Dynamical friction in spherical clusters. *MNRAS*, 174:19–28, January 1976.
- [ZMKS08] A. V. Zasov, A. V. Moiseev, A. V. Khoperskov, and E. A. Sidorova. Early-type disk galaxies: Structure and kinematics. *Astronomy Reports*, 52:79–93, February 2008.
- [ZW88] D. Zaritsky and S. D. M. White. Simulations of sinking satellites revisited. *MNRAS*, 235:289–296, November 1988.